

THESIS

THERMAL ASPECTS OF SUSTAINABLE THERMALLY ENHANCED
LNAPL ATTENUATION (STELA)

Submitted by

Daria Akhbari

Department of Civil and Environmental Engineering

In partial fulfillment of the requirements

For the Degree of Master of Science

Colorado State University

Fort Collins, Colorado

Fall 2013

Master's Committee:

Advisor: Tom Sale

Domenico Bau
Michael Ronayne

ABSTRACT

THERMAL ASPECTS OF SUSTAINABLE THERMALLY ENHANCED LNAPL ATTENUATION (STELA)

Extensive bodies of light non-aqueous phase liquids (LNAPLs) are commonly found beneath petroleum facilities. Related concerns include lateral spreading of LNAPL, impacts to groundwater, and impacts to indoor air. Recent studies have shown that natural losses of LNAPL can be on the order of thousands of gallons per acre per year and temperature is a primary factor controlling rates of natural losses. Results of the laboratory and field experiments suggest that LNAPL impacted media in the range of 18-30°C can have loss rates that are an order of magnitude greater than media at temperatures less than 18°C. The vision that has emerged from recent work is that passive thermal management strategies could enhance natural losses of LNAPL and significantly reduce the longevity of LNAPL.

Owing to this new understanding, plans were developed for a small-scale field demonstration of sustainable thermally enhanced LNAPL attenuation (STELA) at a former refinery in Wyoming, located adjacent to the North Platte River. The overarching objective of the STELA initiative is to develop a new technology for LNAPLs that is more effective, faster, more sustainable, and/or lower cost than current options.

The primary objective of the field demonstration is to collect data needed to evaluate cost and performance at field sites. In November 2011, seventeen multilevel sampling systems were installed in a 10m by 10m area. Preheating temperature and water quality data were collected through the multilevel samplers over a period of 10 months. In August 2012, ten heating elements, including submersible heat trace wires wrapped around 7.6 cm ID PVC pipe with

thermostat controls, were installed upgradient of the sampling network to deliver heat to sustain subsurface temperature in an LNAPL body. The heating elements were energized in September 2012. Subsequently, effects of the heating elements on the subsurface temperature were monitored using 17 multilevel sampling systems equipped with 6 thermocouples for 10 months.

Preheating data indicates that in the absence of heating, subsurface temperatures are in the range of 18-30°C for 40 days per year. Data collected from September 2012 to July 2013 indicates that with heating, conditions can be maintained in the target range for 60 to 200 days per year depending upon proximity to the heat source. A principle challenge is heat loss to the surface in the winter. Minimum and maximum power inputs have been 15 kw-hr/day and 30 kw-hr/day occurring, respectively in October and May. Assuming an energy cost of 0.10 kw-hr, this equates to costs of 1.5 \$/day to 3 \$/day. An independent experiment using Geo-net layer showed that using Gas Permeable Insulation/Heat Sink (GPIHS) system has the potential to enhance the ability of the heating system to sustain temperature beneath the ground surface, and, potentially decrease the power costs.

A primary challenge with evaluation and design of STELA systems is anticipating the appropriate spacing of heating elements and necessary energy inputs. Herein this challenge is met by developing a model, calibrated to field data, which can be used to design a full-scale STELA remedies.

The overarching objective of the modeling is to demonstrate methods that can be employed to evaluate and/or design full-scale STELA systems. At 5m downgradient of the heating elements, the developed model, accurately, predicted 60 days of the effective season in 2012. Also, the simulation results anticipate that by keeping the heating system activated for three

years, the effective season will increase each year. At 5m downgradient of the heating elements, model results suggested 120 days and 150 days of effective season for 2013 and 2014, respectively as compared to 60 days in the first year. The ability of the model to anticipate the effective season for the next years makes the model a useful tool to design and evaluate the future STELA systems.

Calibration of the model to the field data shows that exothermic reactions associated with LNAPL losses can change the heat distribution at the system. In addition, the simulation results indicate that the losses at the subsurface are in the range of 5,000 to 10,000gal/acre/yr. These anticipated loss rates are consistent with the previous values reported by McCoy (2012) in 2012 (~900-11,000gal/acre/yr.)

A conceptual STELA design is developed in the last chapter to explore the cost of a STELA system at a 1-hectare site. The design is based on condition at the former refinery in Wyoming where the STELA field demonstration was conducted. The cost analysis study indicated that the primary cost is the heating elements installation. The second significant cost is the operation costs, and the third significant cost that can be reduced is the energy source. The cost estimates normalized to common units indicated that the total cost ranges between \$590,000 to \$720,000 per hectare, \$11.9 to \$14.4 per cubic meter of treated soil, and \$1.3 to \$1.5 liter of LNAPL removed depends on the energy source, heating system and the degradation rate. Cost of this magnitude support the hypothesis that STELA has the potential to have cost that is lower than other options employed for LNAPL remediation.

ACKNOWLEDGEMENTS

The success of this study required the help of many individuals. Without them, I might not meet my objectives in doing this study. I want to give gratitude to the following people for their invaluable help and support:

I would like to express my deepest gratitude to my advisor, Dr. Tom Sale, for his excellent guidance, caring, patience, and providing me with an excellent atmosphere for doing research. Tom, I hope that I could be as lively, enthusiastic, and energetic. Without your guidance and persistent help this thesis would not have been possible.

I would also like to thank Dr. Bau and Dr. Ronayne for their interest in my topic and willingness to provide assistance. Discussions with you have been illuminating in developing my background in groundwater modeling.

I also have to thank Dr. De Long for her helpful advice and suggestions in general.

I would like to offer my special thanks to CCH people. In my daily work I have been blessed with a friendly and cheerful group of students. In many ways I have learnt much from and because of them.

I am particularly grateful for the assistance given by Maria Irianni Renno and Adam Byrne. Without you this study would not be possible.

Gary Dick, thank you for your technical insights.

Furthermore, I would also like to acknowledge with much appreciation the crucial role of the staff of Trihydro, for their field support. A special thanks goes to Alysha Anderson and Tom Gardner for your hospitality and guidance.

Thank you, Chevron for the technical and financial support.

Baba, Maman, and Bardia have given me their unequivocal support throughout, as always, for which my mere expression of thanks likewise does not suffice.

Masih, thank you for being the best friend in the world and always being there for me! I really appreciate your career advice and suggestions in general.

My friends in US, Iran and other parts of the World were sources of laughter, joy, and support. Special thanks go to Pooria, Saeed, Azadeh, Saleh, Khatoon, Ramin, Soheil, Saman, Mehrdad and Farnaz. I am very happy that, in many cases, my friendships with you have extended well beyond our shared time in Fort Collins. A very heartfelt thank you goes to Hannah. You were my first American friend and will remain always the best one.

Thank you God for all the incredible blessings you have always given me through my whole life and especially during these years. Thank you for providing the opportunity to make this possible.

TABLE OF CONTENTS

ABSTRACT.....	ii
ACKNOWLEDGEMENTS.....	v
LIST OF TABLES.....	xi
LIST OF FIGURES.....	xii
1. INTRODUCTION.....	1
1.1 Research Objectives.....	1
1.2 Thesis Overview.....	2
2. THERMAL ASPECTS OF A FIELD DEMONSTRATION OF STELA.....	3
2.1 Synopsis.....	3
2.2 Introduction.....	4
2.3 Methods.....	7
2.3.1 Field Description.....	7
2.3.2 Soil Core Collection.....	10
2.3.3 Multilevel Sampling (MLS) System Installation.....	10
2.3.4 Multilevel Sampling System Design.....	11
2.3.5 Temperature Measurements.....	13
2.3.6 Heating Elements Design and Installation.....	14
2.3.7 Gas Permeable Insulation/Heat Sink (GPIHS).....	15

2.3.8	Groundwater Flow Direction	17
2.4	Results	17
2.4.1	Hydrogeology	17
2.4.2	Preheating Temperature Envelope	22
2.4.3	Effective Season.....	24
2.4.4	Heating System Effects on the Subsurface Heat Movement	27
2.4.5	Opportunities to Enhance the Heating System Design	28
2.5	Conclusions	32
3.	HEAT TRANSPORT MODEL IN SUPPORT OF STELA FIELD DEMONSTRATION..	35
3.1	Synopsis	35
3.2	Introduction	36
3.3	Background	37
3.3.1	Review of Numerical Models for Subsurface Heat Transport.....	38
3.3.2	Solute and Heat Transport Analogy.....	39
3.3.3	MT3DMS limitations for the heat transport simulation	46
3.4	Methods.....	49
3.4.1	Field/Site Description	49
3.4.2	Hydrogeology	53
3.4.3	Natural LNAPL loss rate and energy production correlation	55
3.4.4	Model Setup.....	57

3.4.5	Quantifying the effects of exothermic biodegradation	65
3.5	Results	67
3.5.1	Evaluation of the LNAPL Losses and Related Effects on the Subsurface Temperature.....	67
3.5.2	Addressing of temporal temperature variations	71
3.5.3	Anticipation the long-term performance of the STELA field demonstration.....	74
3.6	Conclusions	76
4.	CONCEPTUAL DESIGN AND COSTS FOR A 1-HECTARE STELA SYSTEM	78
4.1	Introduction	78
4.2	Cost components	79
4.2.1	Site characterization.....	79
4.2.2	Laboratory testing	80
4.2.3	Numerical Simulations.....	80
4.2.4	Field demonstration	81
4.2.5	Facility design.....	81
4.2.6	Construction	82
4.2.7	Operations, maintenance, and monitoring	84
4.3	Results of Cost Analysis	86
4.3.1	Most Significant Cost Components	86
4.3.2	Cost Reduction Options	89

4.4. Range of Cost Estimates	91
4.5 Comparison of STELA costs and other LNAPL Remedial Technologies.....	94
5. THESIS CONCLUSIONS.....	95
6. FUTURE WORKS	97
REFERENCES.....	99
APPENDIX A: HYPOTHICAL SITE COST STUDIES/ COST WORKSHEET.....	109

LIST OF TABLES

Table 3.1: LNAPL loss rates and corresponding energy releases for each scenario	56
Table 3.2: Input parameters for the groundwater flow model (MODFLOW).....	59
Table 3.3: Input parameters for the heat transport model (MT3DMS).....	62
Table 3.4: General performance ratings for statistics (Moriassi et al. 2007)	67
Table 4.1: Site characteristics and system designs for base case.....	79
Table 4.2: Summary of the degradation rates at the hypothetical example site.	88
Table 4.3: Cost analysis summery-Base Case (Case 1).....	89
Table 4.4: Summery of sensitivity analysis.....	91
Table 4.5: Cost estimate summary (Unit Costs)	92

LIST OF FIGURES

Figure 2.1: STELA installation and monitoring timeline.	7
Figure 2.2: Google Earth photos.....	9
Figure 2.3: Multilevel sampler schematic (Zeman 2012).....	11
Figure 2.4: STELA field demonstration layout..	13
Figure 2.5: Heating element schematic.....	16
Figure 2.6: Field demonstration 3D frame with observed soils.....	18
Figure 2.7: Groundwater flow direction variation based on three points method.	19
Figure 2.8: Representative groundwater contour map based on collected water levels in November 2012.....	20
Figure 2.9: Annual temperature envelope.....	23
Figure 2.10: Temperature lags through the subsurface.....	24
Figure 2.11: Length of the effective season depending up on the position to the heating elements.	26
Figure 2.12: Effective season contour map.....	29
Figure 2.13: Main cross-section temperature isotherms.	30
Figure 2.14: Power consumption and power cost for the heating system.	31
Figure 2.15: Testing an insulation layer.	32
Figure 3.1: Google Earth photo.	50
Figure 3.2: STELA field demonstration.	52
Figure 3.3: STELA Installation and monitoring timeline.....	52
Figure 3.4: Representative Groundwater Contour Map.....	54
Figure 3.5: Field demonstration reference frame with observed soils.....	55

Figure 3.6: Model gridding plan view.	58
Figure 3.7: MODFLOW boundary conditions.....	60
Figure 3.8: MT3DMS boundary conditions.....	64
Figure 3.9: Casper ambient air temperature.....	65
Figure 3.10: Summary of the statistical quantifications	70
Figure 3.11: Comparison of observed temperature contours and simulation temperature contours.	72
Figure 3.12: MT3DMS simulation results at Well C3-14ft bgs	75
Figure 4.1: Base case design layout.....	85
Figure 4.2: Base case most significant costs.....	87
Figure 4.3: Summary of the cost normalized to volume of soil treated, volume of LNAPL removed, and area treated.	93
Figure 4.4: Comparison of STELA and other LNAPL remedial technologies.....	94

1. INTRODUCTION

Extensive bodies of light non aqueous phase liquids (LNAPLs) are commonly found beneath petroleum facilities. Related concerns include lateral spreading of LNAPL, impacts to groundwater, and impacts to indoor air. Fortunately, natural processes often deplete petroleum hydrocarbons in the subsurface; however, this depletion occurs at slow rates (Cozzarelli et al. 2001, Johnson et al. 2006, McCoy 2012).

When natural processes are insufficient relative to cleanup expectations, active remedial measures need to be employed. Temperature appears to be a key factor affecting the rate of natural losses of LNAPL (Mulkin-Phillips and Stewart 1974, Perfumo et al. 2007, Zeman 2012). Building on the work of Zeman (2012), a hypothesis has emerged that sustaining temperatures in the range of 18-30 °C can dramatically enhance rate of natural attenuation of subsurface LNAPLs. The vision that has emerged from recent work is that sustainable thermal management strategies (e.g. use of waste heat, solar energy, or insulation) could enhance natural losses of LNAPL and significantly reduce the longevity of LNAPL.

To test the hypothesis, a field demonstration was initiated at a former refinery in Wyoming. The site is underlain by the sandy alluvium of the North Platte River. The overarching objective of the STELA initiative is to develop a new technology for LNAPLs that is more effective, faster, more sustainable, and/or lower cost than current options.

1.1 Research Objectives

The vision that has emerged from recent work is that passive thermal management strategies could enhance natural losses of LNAPL and significantly reduce the longevity of

LNAPL. To advance this vision, information is needed to assess the cost and performance of STELA.

A primary challenge with evaluation and design of STELA systems is anticipating the necessary energy inputs. Herein this challenge is met by developing a model, calibrated to field data, which can be used to design a full-scale STELA remediation. Specifically, heat transport is evaluated by coupling MODFLOW (Harbaugh 2005) and MT3DMS (Zheng et al. 2010). Also, since the cost of a remedial technology is one of the key factors in determining its applicability, a hypothetical example was presented to illustrate the cost of a STELA system at a typical 1-hectare site in a former refinery in Wyoming.

1.2 Thesis Overview

This thesis includes three main chapters. Chapter 2 and 3 are written in the format of journal articles. Chapter 2 presents data from the STELA field demonstration. Chapter 3 presents a heat transport model that supports STELA field demonstration. Chapter 4 develops a cost estimate for STELA considering a conceptual 1-hectare site at a former refinery in Wyoming. Chapter 5 presents thesis conclusions. Finally, chapter 6 provides suggestions for the future works.

2. THERMAL ASPECTS OF A FIELD DEMONSTRATION OF STELA

2.1 Synopsis

Extensive bodies of light non-aqueous phase liquids (LNAPLs) are commonly found beneath petroleum facilities. Related concerns include lateral spreading of LNAPL, impacts to groundwater, and impacts to indoor air. Recent studies have shown that natural losses of LNAPL can be on the order of thousands of gallons per acre per year and temperature is a primary factor controlling rates of natural losses. Results of the laboratory and field experiments suggest that LNAPL impacted media in the range of 18-30⁰C can have loss rates that are an order of magnitude greater than media at temperatures less than 18°C. The vision that has emerged from recent work is that passive thermal management strategies could enhance natural losses of LNAPL and significantly reduce the longevity of LNAPL.

Owing to this new understanding, plans were developed for a small-scale field demonstration of sustainable thermally enhanced LNAPL attenuation (STELA) at a former refinery in Wyoming. The overarching objective of the STELA initiative is to develop a new technology for LNAPLs that is more effective, faster, more sustainable, and/or at lower cost than current options.

The primary objective of the field demonstration is to collect data needed to evaluate cost and performance at field sites. In November 2011, seventeen multilevel sampling systems were installed in a 10m by 10m area. Preheating temperature and water quality data were collected through the multilevel samplers over a period of 10 months. In August 2012, ten heating elements, including submersible heat trace wires wrapped around 7.6 cm ID PVC pipe with thermostat controls, were installed upgradient of the sampling network to deliver heat to sustain

subsurface temperature in an LNAPL body. The heating elements were energized in September 2012. Subsequently, effects of the heating elements on the subsurface temperature were monitored using 17 multilevel sampling systems equipped with 6 thermocouples for 10 months.

Baseline data indicates that in the absence of heating, subsurface temperatures are in the range of 18-30°C for 40 days per year. Data collected from September 2012 to July 2013 indicates that with heating, conditions can be maintained in the target range for 60 to 200 days per year depending upon proximity to the heat source.

A principle challenge is heat loss to the surface in the winter. Minimum and maximum power inputs have been 15 kw-hr/day and 30 kw-hr/day occurring, respectively in October and May. Assuming an energy cost of 0.10 kw-hr, this equates to costs of 1.5 \$/day to 3 \$/day. An independent experiment using Geo-net layer showed that using Gas Permeable Insulation/Heat Sink (GPIHS) system has the potential to enhance the ability of the heating system to sustain temperature beneath the ground surface, and, potentially decrease the power costs.

2.2 Introduction

Extensive bodies of light non aqueous phase liquids (LNAPLs) are commonly found beneath large petroleum facilities (Newell et al. 1995, Fels 1999, Sale 2003, Amos and Mayer 2005). Related concerns include lateral spreading LNAPL, impacts to groundwater, and impacts to indoor air. (Mercer and Cohen 1990, Charbeneau and Chiang 1995, Kim and Corapcioglu 2002, Huntley and Beckett 2002). Fortunately, natural processes (e.g. biological natural attenuation) often deplete petroleum hydrocarbons in the subsurface; however, at slow rates (Siegel and Bennett 1993, Cozzarelli et al. 2001, Witt et al. 2002, Johnson et al. 2006, Lundegard and Johnson 2006, Cozzarelli et al. 2009, Baedeker et al. 2011, Mahler et al. 2012).

When natural processes are insufficient relative to cleanup expectations, active remedial measures need to be employed and temperature is a primary factor controlling rates of natural losses. For instance, Perfumo et al. (2007) reported a twofold increased removal of hexadecane by increasing the temperature from 18°C to 60°C. Moreover, Mulkin-Phillips and Stewart (1974) confirmed that the rate of natural biodegradation of oil in marine temperate-to-polar zone is limited by low temperature and phosphorus concentrations.

A prospective but not widely used biological treatment is thermally enhanced natural attenuation. Higher temperature leads to lower viscosity, higher solubility and faster diffusion of hydrophobic contaminants, which lead to faster biodegradation (Leahy and Colwell 1990, Margesin and Schinner 2001, Perfumo et al. 2006, Coulon et al. 2007). Furthermore, higher temperature can lead to consequential changes in the microbial ecology (Zeman 2012).

The optimal temperature depends on the indigenous microbial community present (Mohn and Stewart 1999). Based on the Zeman's (2012) microcosm experiment results, the optimal temperature for biodegradation of the former refinery is likely between 22-40°C. GRO, DRO and BTEX compounds degraded more readily within the microcosms that held at the temperatures of 18-40°C, which suggests that the microbial community present was capable of degrading a broad range of petroleum hydrocarbons at elevated temperatures (Zeman 2012).

The vision that has emerged from recent work is that passive thermal management strategies (e.g. use of waste heat, solar energy, or insulation) could enhance natural losses of LNAPL and significantly reduce the longevity of LNAPL. Using the heating system strategies in cold regions have been previously done by the research groups in Alaska and sub-Antarctica.

Dellile et al. (2004) initiate a controlled field study in December 2000 at sub-Antarctic to evaluate the effects of a small temperature increases on the removal of crude oil and diesel fuel contaminations. Two series of enclosures were settled. In the first row of enclosures, the soil was in direct contact with the atmosphere. In contrast, in the second row, the soil of the enclosures was protected by a double plastic coating. The results of the experiment show that the annual mean temperature enhancement was 2 C at the covered enclosure. They claimed nearly complete biodegradation of alkanes after two years in all covered soils while, it could take at least 1 year more of bio attenuation to reach the same results in non-covered soils. Finally, they concluded that a further reduction of bioremediation time would be achieved using higher temperatures. Coulon et al. (2005) research group examined the effects of temperature increases on the biological degradation of the petroleum hydrocarbons at the same area, and reached to the conclusion that at the temperature of 10°C the maximum degradation of the hydrocarbons happens in a cost effective manner. Furthermore, Filler et al. (2005) conducted a research on the thermal insulation systems (TIS) for bioremediation applications in 1994 at a site in Fairbanks, Alaska. By employing the TIS, during the project life time, approximately 6000 cubic yard of the vadose zone, contaminated to 2400 mg/kg soil with gasoline and diesel fuel, was remediated within 22 months. Also, Filler et al. (2001) examined the TIS in Prudhoe Bay, AK and observed an extension of the effective season (the period of enhanced bioremediation treatment due to suitable thermal conditions) from 2.5 to 6 months during the first year of bioremediation.

Owing to these new understandings, plans were developed for a small-scale demonstration of sustainable thermally enhanced LNAPL attenuation (STELA) at a former refinery, located along the North Platte River in Wyoming. The overarching objective of the

STELA initiative was to develop a new technology for LNAPLs that is more effective, faster, more sustainable, and/or at lower costs than current options.

The primary objective of this paper is to present and analyze thermal data collected from the STELA field demonstration. This includes data collected prior to and after initiation of heating. Content includes methods, results, conclusions and recommendations for future works.

2.3 Methods

This section presents methods associated with thermal aspects of the demonstration. This includes a description of the field site, installation of Multilevel Sampling systems (MLSs), MLS data collection, heating systems, and a preliminary effort to access a GPIHS layer. The project timeline is shown in Figure 2.1.

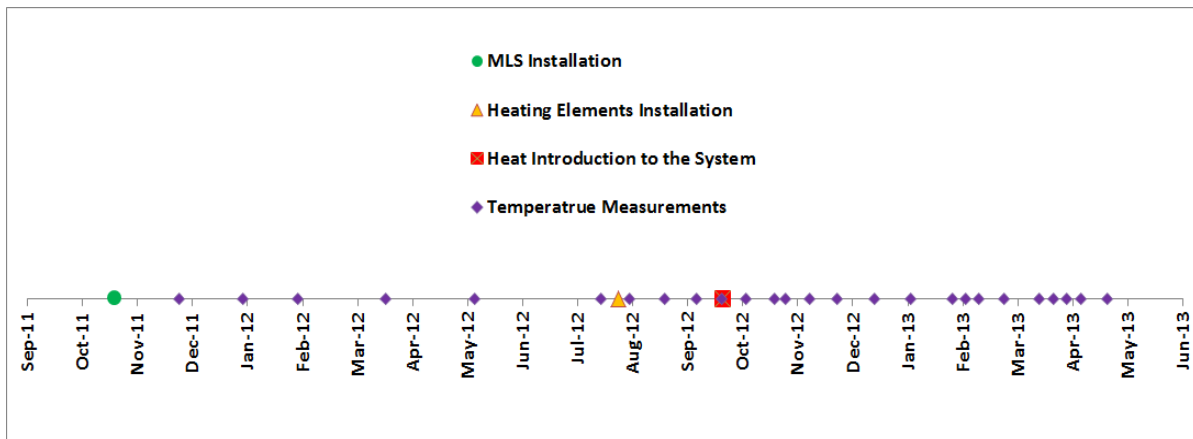


Figure 2.1: STELA installation and monitoring timeline.

2.3.1 Field Description

In the following section, a brief description of the former refinery is provided. This is based on the RCRA facility fact sheet which prepared by Chevron Environmental Services

Company (2009). The former refinery was operational from 1923 to 1982. The refinery processed crude oil from local sources into gasoline and diesel. The refineries capacity was 21,000 barrels per day when it closed in 1982. The northern border of the 200-acre refinery is formed by North Platte River. The current configuration of the refinery is shown in Figure 2.2.

The refinery was decommissioned in the mid 1990's. This included removal of processes equipment, grading of the site to provide proper drainage and seeding the property with a mix of native grasses. During the demolition and following removal of piping and subsurface structures, open excavations and exposed piping corridors were visually inspected for the presence of petroleum contaminated soils. Approximately 135,000 tons (90,000 cubic yards) of petroleum contaminated soils were excavated, removed and treated.

Historically, the owner has recovered approximately 17 million gallons of hydrocarbon from beneath the refinery and has treated and removed contaminants from approximately 2 billion gallons of groundwater. Also, sheet pile well is deployed along the river with hydraulic control to limit releases to the North Platte River. Currently, a site wide remedy is being developed through effort lead by Chevron and the Wyoming Department of Environmental Quality.

Since 2003, Colorado State University (CSU) has been conducted field research at the refinery with the goal of advancing innovative remediation methods. As part of this goal, seventeen multilevel samplers were installed in November 2011 to collect background data for the evaluation of the STELA as an innovative remedial method.

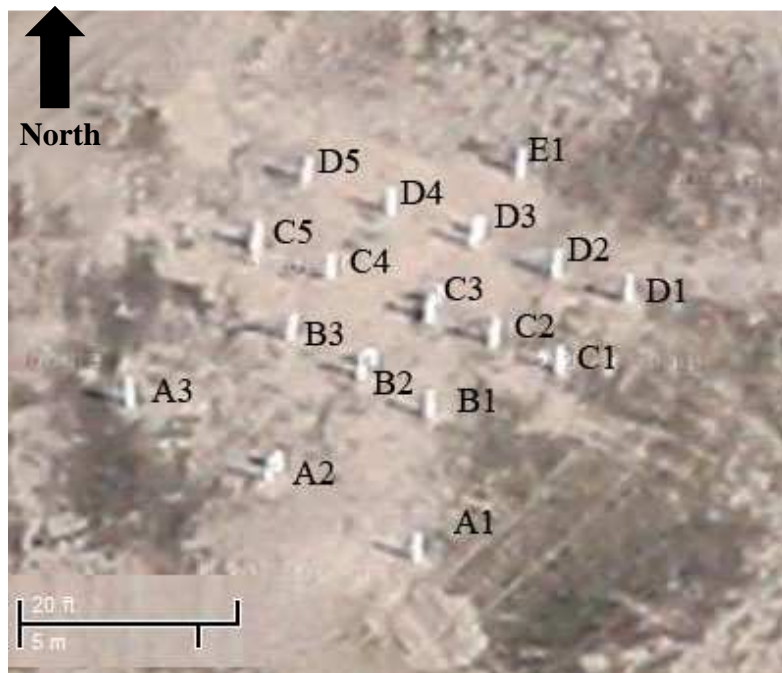


Figure 2.2: Google Earth photos. Top: Current configuration of the refinery. Bottom: Field demonstration (Before heating element installation).

2.3.2 Soil Core Collection

In November 2011, a combination of direct push and hollow stem auger drilling techniques were used to collect soil cores at the locations shown in Figure 2.2. Both methods allowed for the recovery of the soil sample cores inside 1.5m long acetate sleeves so that no direct handling of the sample took place. Approximately 4-5 m (14ft) of material was extracted at each of the seventeen MLS locations. Soil cores were flash frozen on site using dry ice and transported back to Colorado State University for analysis of hydrocarbon content, microbial ecology, and mineralogy to establish baseline data for the area (Zeman 2012, Irianni Renno 2013).

2.3.3 Multilevel Sampling (MLS) System Installation

After soil core collection, seventeen MLSs were installed at the locations where soil cores were taken. Direct push drilling was followed up by the hollow stem auger drilling to increase the diameter of the excavation. Once drilling had reached 4.2m (14ft) below ground surface, three inch ID slotted PVC pipe was lowered to the bottom of the bore hole. The MLSs were then placed inside the slotted PVC pipes down the bottom of the bore hole (~14 feet below ground surface). The area between the MLS and slotted PVC pipe was then backfilled with the sand to act as a filter pack. Figure 2.3 shows a schematic of an installed MLS (Zeman 2012).

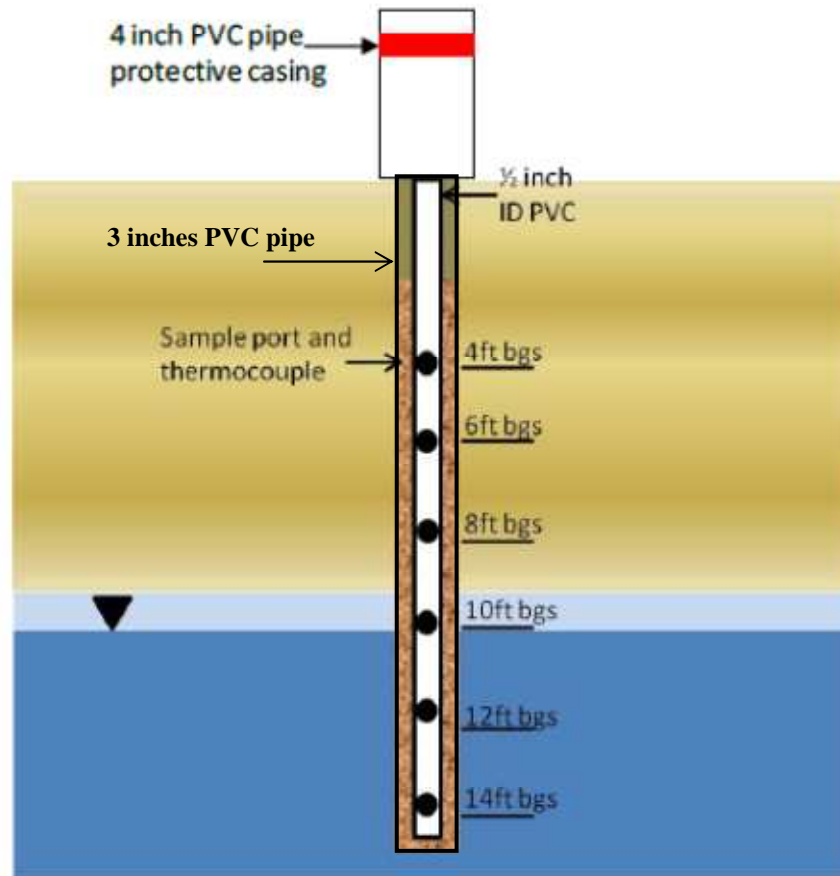


Figure 2.3: Multilevel sampler schematic (Zeman 2012). Each multilevel sampler includes six ports, three in the vadose zone and three in the saturated zone to collect Water samples, gas samples, and temperature data.

2.3.4 Multilevel Sampling System Design

Multilevel samplers (that provide water samples from depth-discrete ports in a single monitoring hole) as described by Cherry (1983) and Chapman and Parker (2004) have been used to determine the contaminant distribution in the aquifer. In the past few decades, multilevel samplers have come to popularity owing to advantage of high resolution data which are more representative of vertical transects compared to sampling with conventional wells (Macfarlane et al. 1983, Reinahrd et al. 1984, Robertson et al. 1991, Kamp et al. 1994, Pitkin et al. 1999,

Einarson and Cherry 2002, Nielsen 2006). Using the multilevel monitoring, each sample was drawn from a small volume of the aquifer so that the resulting concentration distributions are depth specific, rather than blended (Guilbeault et al. 2005).

Depth-discrete groundwater sampling along a cross-section perpendicular to groundwater flow has been employed using seventeen multilevel samplers. The vertical interval for each multilevel sampler is 4.2m (14ft). This allows for depth discrete gas (CO₂, CH₄) and water sampling with a total of six ports; three gas sampling in the vadose zone and three groundwater sampling ports. The Multilevel samplers were made at the Center for Contaminant Hydrology (CCH) at Colorado State University (CSU). Each MLS consists of a 1.27cm (1/2 inch) inner diameter (ID) schedule 40 PVC pipe (RNR supply) 1/8 inch ID Fluorinated Ethylene Propylene (FEP) tubing secured at different intervals along the PVC pipe for gas and water sample ports (US Plastic). Six individual pieces of FEP tubing is spaced at 60cm (2ft) intervals to allow three gas sample ports and 3 water sample ports. The end of the tubing is covered with nynetex screen (153 μm) to filter out silt and sand particles (Wildlife Supply CO.) (Zeman 2012). The MLS system layout is shown in the Figure 2.4.

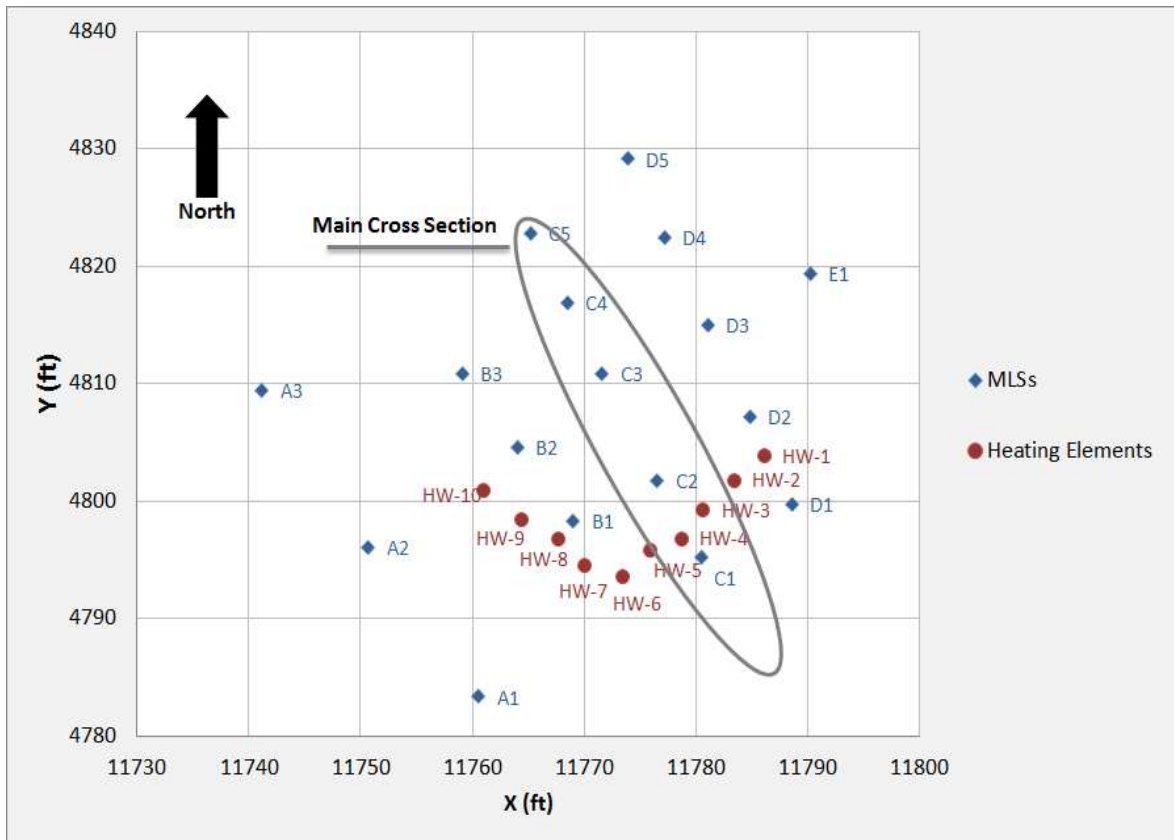


Figure 2.4: STELA field demonstration layout. In November 2011, seventeen multilevel samplers were installed to monitor the pilot. In September 2012, ten heating elements were employed in two orthogonal lines to deliver heat to the system. The pilot area is 50ft by 50ft.

2.3.5 Temperature Measurements

To evaluate the temperature changes spatially and seasonally, six thermocouples were attached to each multilevel sampler adjacent to each of the sample ports. Temperature was measured at the depths of 1.2, 1.8, 2.4, 3, 3.6, and 4.2m (4, 6, 8, 10, 12, 14ft) below the grade. The thermocouples are made with Type K parallel construction thermocouple wire (TC Direct, 24 AWG) and Type K miniature thermocouple connectors. The sensing end was spot welded to create the Type K thermocouple. In order to protect the thermocouple, a glass casing was fabricated from 4mm OD soft glass tubing. The fabricated glass cup was filled with epoxy

(Henkel, Tra-Bond Bipax) and the spot welded end of the thermocouple wire was inserted into the cup.

During the project, temperature was measured both continuously by using temperature data loggers (Lascar Electronic, EL-USB-TC) and periodically with a hand held instrument (TC direct, 305p). Starting April 2012, temperature data was collected in half hour intervals at the multilevel sampler (C3) at 4, 6, 8, 10, 12, 14ft below the ground surface (bgs). Furthermore, 30 minutes temperature data was collected since June 2012 in the saturated zone at 10, 12, 14ft bgs at the background multilevel sampler (A2), and since October 2012 at the closest multilevel samplers to the heating elements (B1 and C1). Also, periodic temperature data was collected once a month during the baseline characterization. After the activation of the heating elements in September 2012, periodic temperature data collected twice a month to evaluate the heating elements effects accurately at the entire field demonstration (using Digital Thermometers). Mining Visualization System (MVS) software (C Tech Development Corporation, MVS) was used to create the temperature isotherms. The 3D and 2D images and videos created by this software allowed high resolution analysis of the temperature responses to the heating elements through the time.

2.3.6 Heating Elements Design and Installation

In August 2012, ten heating elements were installed along the upgradient edge of the MLS system. Each heating system had a maximum energy input of 200W. The heating elements were distributed in a “Vee” due to the temporal variations in the ground water flow direction (shown in Figure 2.4). The heating elements are spaced 1m (3.28ft) apart (Figure 2.4 demonstrates the location of the heating elements). Each heating element consists of a 6m (20ft) of 16.4w/m (5w/ft) submersible heat trace (du Alaska Incorporated, Arctic Trace) wrapped

around a 7.62cm (3-inches) PVC pipe. The heating elements cover 1.82m (6ft) of the saturated zone (8-14ft) The PVC pipes were deployed in the ground using hollow stem auger drilling method. The soil was allowed to be in direct contact with the heating elements by allowing the soil to fall on the pipes. Each heating element is thermostatically controlled by electronic temperature controller (du Alaska Incorporated, NEMA 4X watertight enclosure). The temperature sensor mounted in PVC pipe's interior. To control the real temperature outside of the pipe, screen PVC pipe was used, so the sensor is in direct touch with the groundwater flow. The schematic picture of the heating elements is shown in the Figure 2.5. The heating elements were energized in September 2012. All thermostatic controls were set to 30⁰C. The energy consumption of the heating system was measured by using a standard power meter solely dedicated to the field demonstration. The power usages were manually read on a daily basis throughout the project.

2.3.7 Gas Permeable Insulation/Heat Sink (GPIHS)

To test the idea of deploying insulation as a mean to enhance the heating system design, a 1m by 1m geo-net with the thickness of 2.54cm was anchored to the ground at the Foothills Campus, Colorado State University. A thermocouple equipped with continuous data deployed 30cm below this mat. A second thermocouple equipped with a continuous temperature data logger was deployed 2m away from the geo-net at the same depth below the grade. The geo-net has been chosen as the insulation material for several reasons: It is affordable, readily available, gas permeable and the black color of the material is helpful in adsorbing solar radiation.

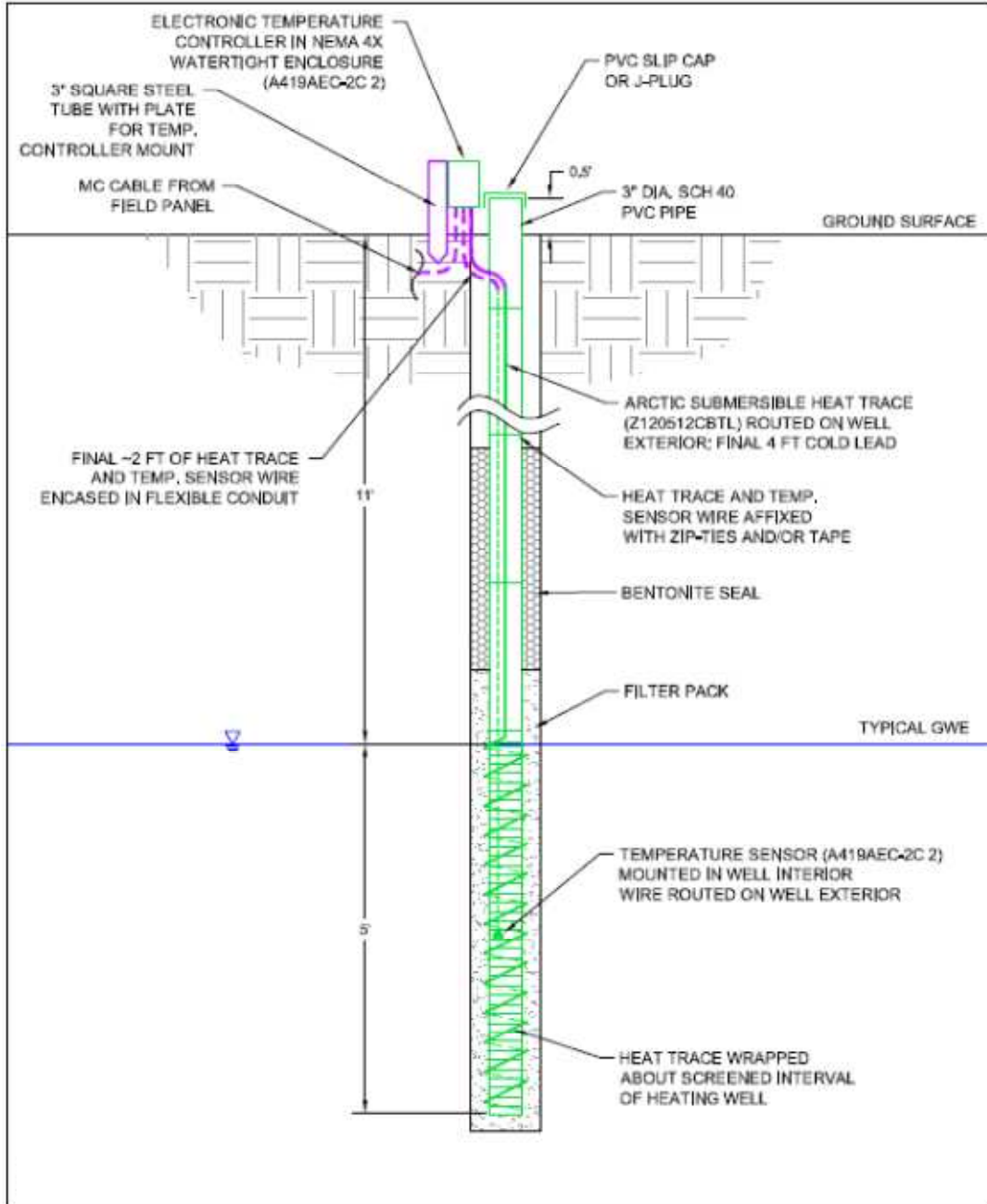


Figure 2.5: Heating element schematic. Each heating element consists of a 3 inches PVC pipe wrapping with heat traces that are thermostatically controlled at 30C. (Original drawing by Justin Prius, Trihydro Co.)

2.3.8 Groundwater Flow Direction

Water levels were measured every two weeks by using conventional groundwater interphase probes. A three points method was used to evaluate groundwater directions. Three points method is based on a simple principle of geometry: three points define a plane. If you can define the position of a plane in space you can also determine the dip (inclination) of the plane. Both the direction of ground-water movement and the hydraulic gradient can be determined if the following data are available for three wells located in any triangular arrangement (Heath, 1983):

1. The relative geographic position of the wells.
2. The distance between the wells.
3. The head at each well.

2.4 Results

This section presents the results. This includes hydrogeology, pre-heating temperature envelope, effects of the heating, and lastly opportunities to enhance the performance of the heating system.

2.4.1 Hydrogeology

Soil types beneath the former refinery range from silt to coarse-sand. At the surface, the soil mainly comprise of silty-sands and silts. At the deeper points, the soil grades to a combination of fine-sand, medium-sand, and coarse-sand. Figure 2.6 shows the observed soil types in a 3D frame.

During the two year study, groundwater level varied by up to 0.5m (1.6ft) and groundwater flow direction varied by 75 degrees. The groundwater direction varied between the north-northeast and northwest. Figure 2.7 presents the seasonal variations in the flow direction

and magnitude based on the three points method. Each arrow in the figure demonstrates the groundwater direction in a specific month calculated and the length of the arrows show the magnitude of the gradient. Furthermore, water table was 3m (9ft) below the ground surface with a variation of 50cm (1.6ft). Figure 2.8 portrays the groundwater contour map developed using MVS based on the water level data of November 2012.

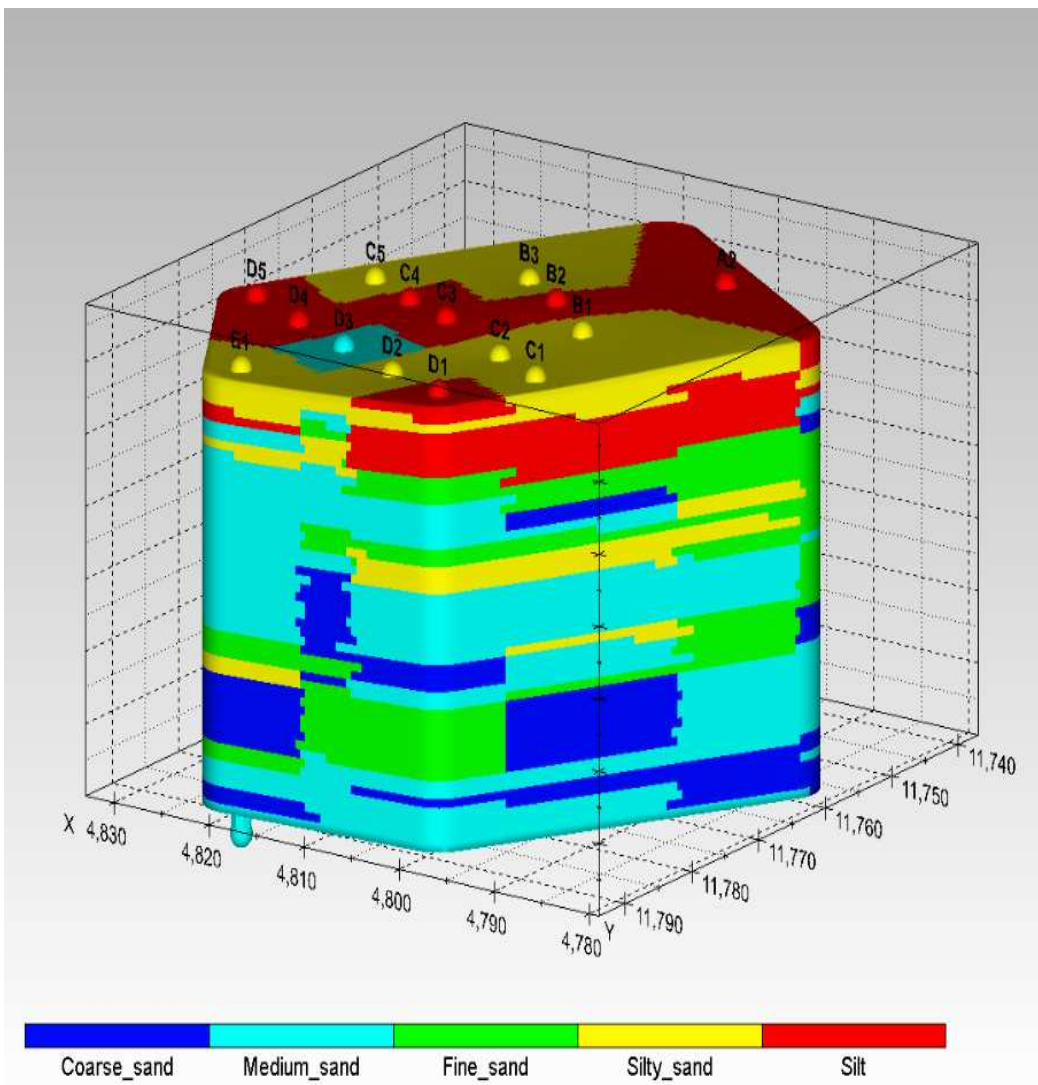


Figure 2.6: Field demonstration 3D frame with observed soils.

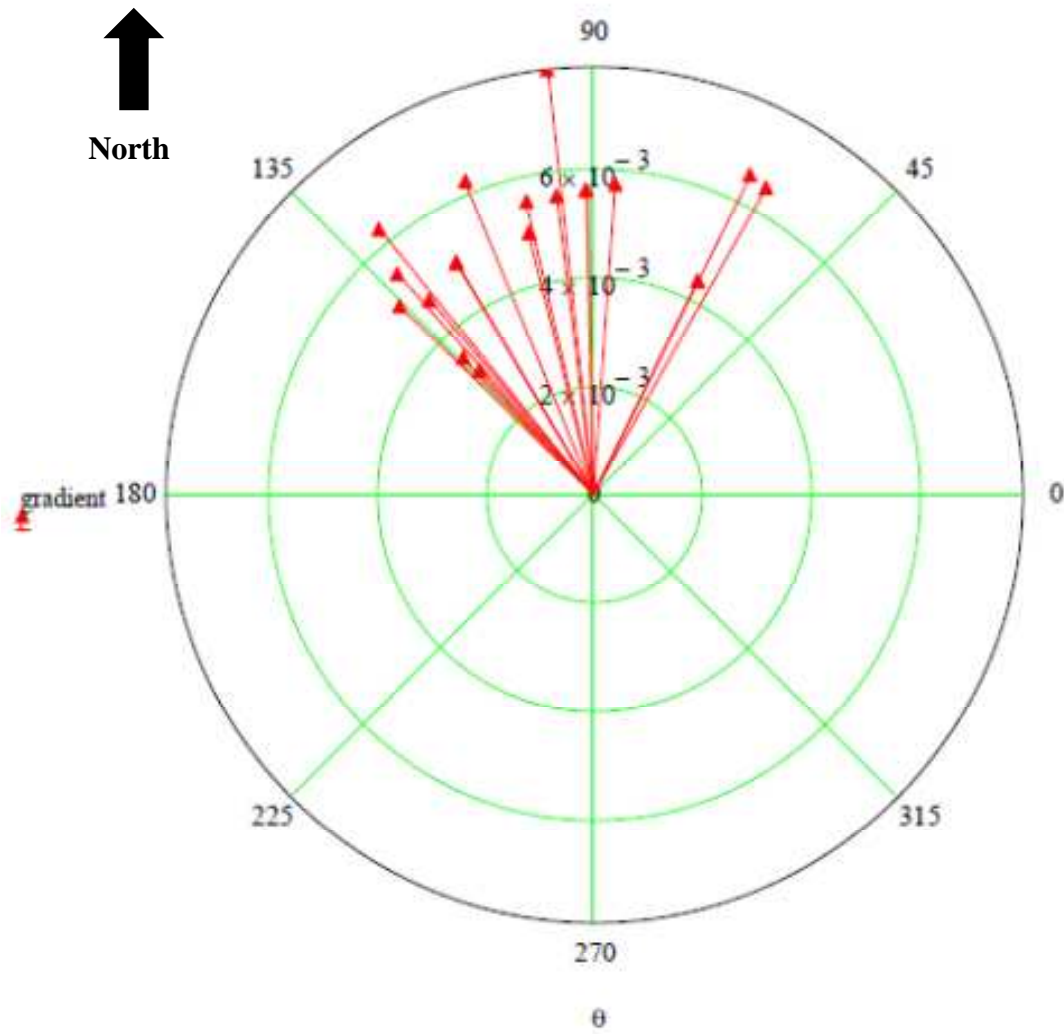


Figure 2.7: Groundwater flow direction variation based on three points method. Red arrows show the groundwater flow direction in specific months. The green circles show the magnitude of the head gradient.

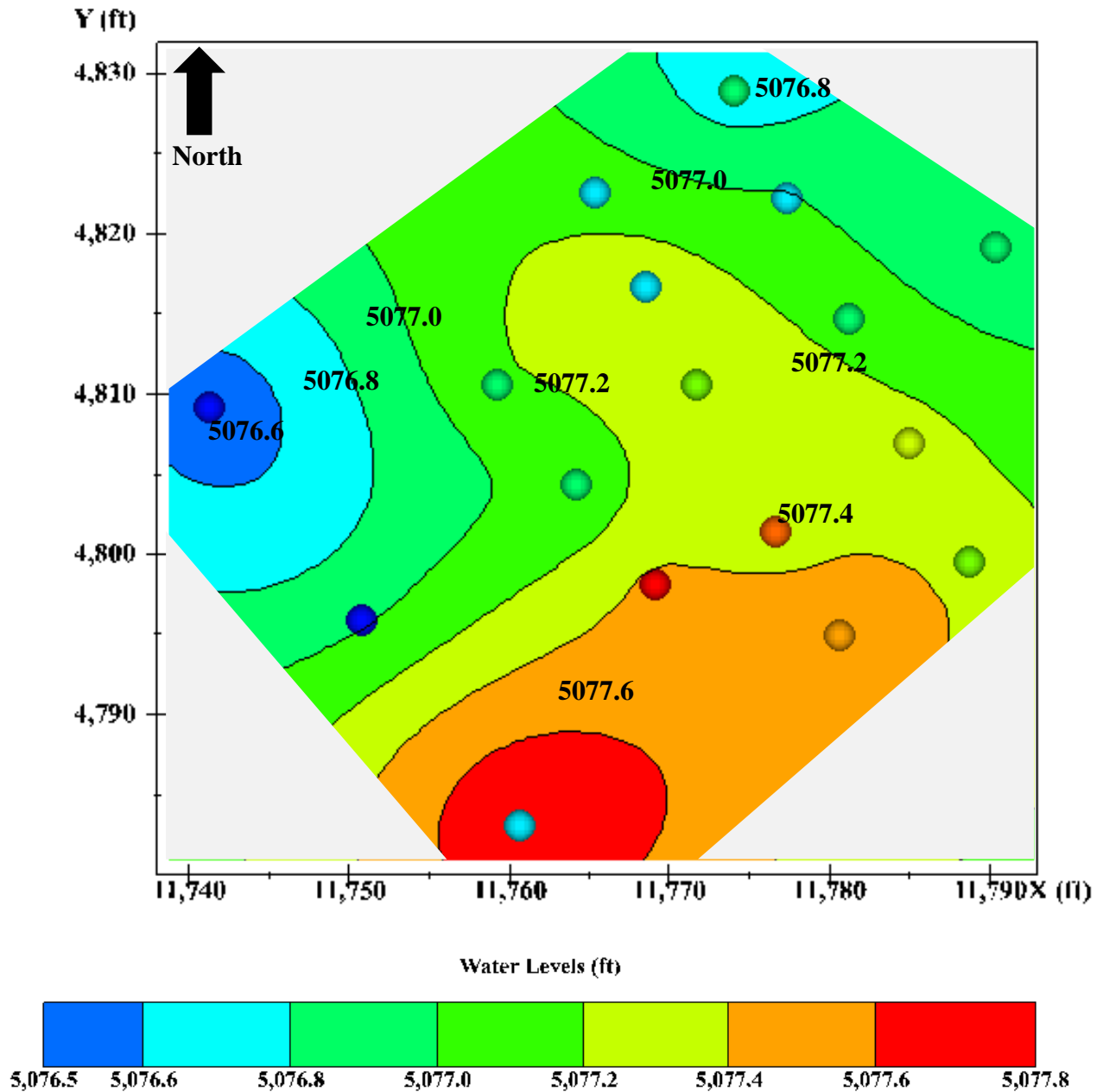


Figure 2.8: Representative groundwater contour map based on collected water levels in November 2012.

An important concern about the groundwater flow is that if temperature variation can affect the ground water movement. Temperature has an influence on several physical parameters such as density and viscosity of water. Temperature plays a role in two main ways:

Due to the following equation, the hydraulic conductivity depends on density and viscosity of water which are both temperature dependent (Anderson 2005):

Equation 2.1
$$K = kg \frac{\rho}{\mu}$$

Where, $k[L^2]$ is the intrinsic permeability of the soil, $g \left[\frac{L}{t^2} \right]$ is the gravitational acceleration, $\rho \left[\frac{M}{L^3} \right]$ is density, and $\mu \left[\frac{M}{L t} \right]$ is viscosity.

However, temperature variations in the shallow subsurface are commonly small, so simulation errors produced from using constant viscosity and density often are small and acceptable (Mendez et al. 2009).

Temperature variations can also promote free convection. Free convection refers to the heat which transfers in response to flow driven by temperature-induced density differences, while forced convection refers to the heat which transfers by the flow driven by any other mechanism. Free convection is thought to occur in areas of high heat flow such as near spreading centers in the ocean but rarely in sedimentary basins. Typically, hydrogeological studies assume that the variation of density and viscosity due to temperature is negligible. Under such circumstances, small thermal gradients in the aquifer can allow for the decoupling of the flow and heat transport equations. However, in some cases that include strong thermal variations, temperature plays an important role in the groundwater flow system (Ma and Zheng 2009), in instance, in the cases of the leachate plumes from landfills or tracer tests, variable density effects should be considered (Simmons 2005).

Ma and Zheng (2010) simulated a heat transport model to evaluate the effects of the density and viscosity changes due to the introduction of thermal energy to the subsurface systems. They clarified that the effects of fluid density and viscosity are negligible when the maximum temperature difference across the flow domain is within 15C. Since the temperature changes due to the heating elements in current STELA design is less 15⁰C, variations in fluid density and viscosity are not expected to influence the groundwater flow.

2.4.2 Preheating Temperature Envelope

An annual temperature envelope was drawn by collecting continuous temperature data at six different depths underneath the ground surface. Data that collected in the period of November 2011 to November 2012 at the background well demonstrated that the temperature is changing between 9°C to 21°C in the saturated zone. Figure 2.9 presents the temperature envelope. The annual temperature envelope consists of two curves. One curve is constructed by connecting the minimum temperature that occurs during the year at each depth at the subsurface. The other curve is constructed by connecting the maximum temperature that occurs during the year at each depth at the subsurface (Lapham 1989). The figure indicates that the magnitude of temperature fluctuation decreases as the depth increases. Lapham (1989) demonstrated that a temperature fluctuation appears to be constant below a depth of about 35ft in a sedimentary soil beneath a stream in New England. Also, in the warm seasons, the shallower points are warmer than the deeper points. On the other hand, in the winter time, the warmer temperature happens at the deeper points. It stems from the fact that the shallower points are impacted by the ambient atmosphere temperature more than that for the deeper points.

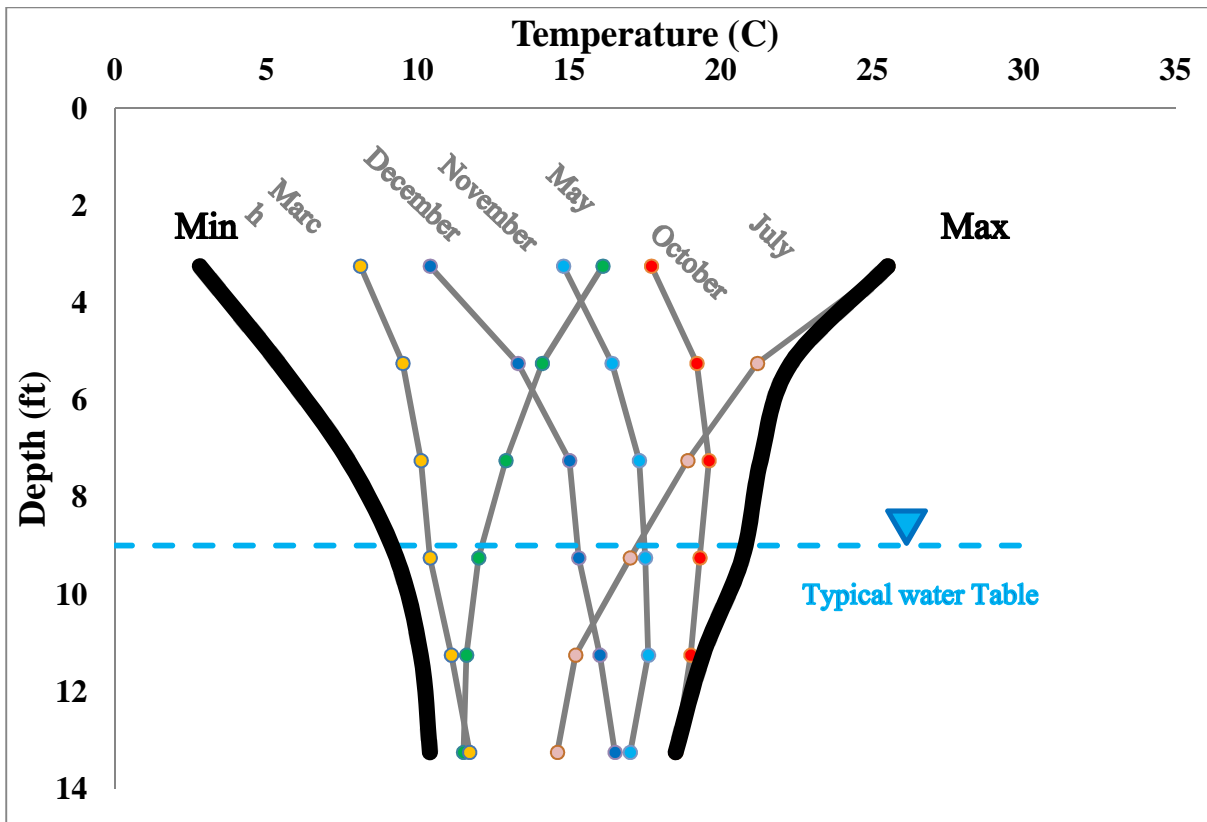


Figure 2.9: Annual temperature envelope. The annual temperature envelope consists of two curves. One curve is constructed by connecting the minimum temperature that occurs during the year at each depth at the subsurface. The other curve is constructed by connecting the maximum temperature that occurs during the year at each depth at the subsurface. The collected temperature during the year are changing in the range between the two curves.

Moreover, Lapham discussed that the monthly temperature profiles indicate that temperature at the depth beneath the stream lags behind the stream temperature. This lag occurs because of the low thermal diffusivity of the saturated sediments. The collected data at this field demonstration showed that the same lag occurs. As shown in Figure 2.10, at 4ft below the ground surface, the highest temperature was observed in July. While at 10ft and 14ft below the ground surface, the highest temperature observed in September and October, respectively. It should be noted that the heat propagates mostly through thermal conduction in the vertical

direction. The lag in highest temperatures that happens at each depth is because of the conductive component of the heat transport in the vertical direction.

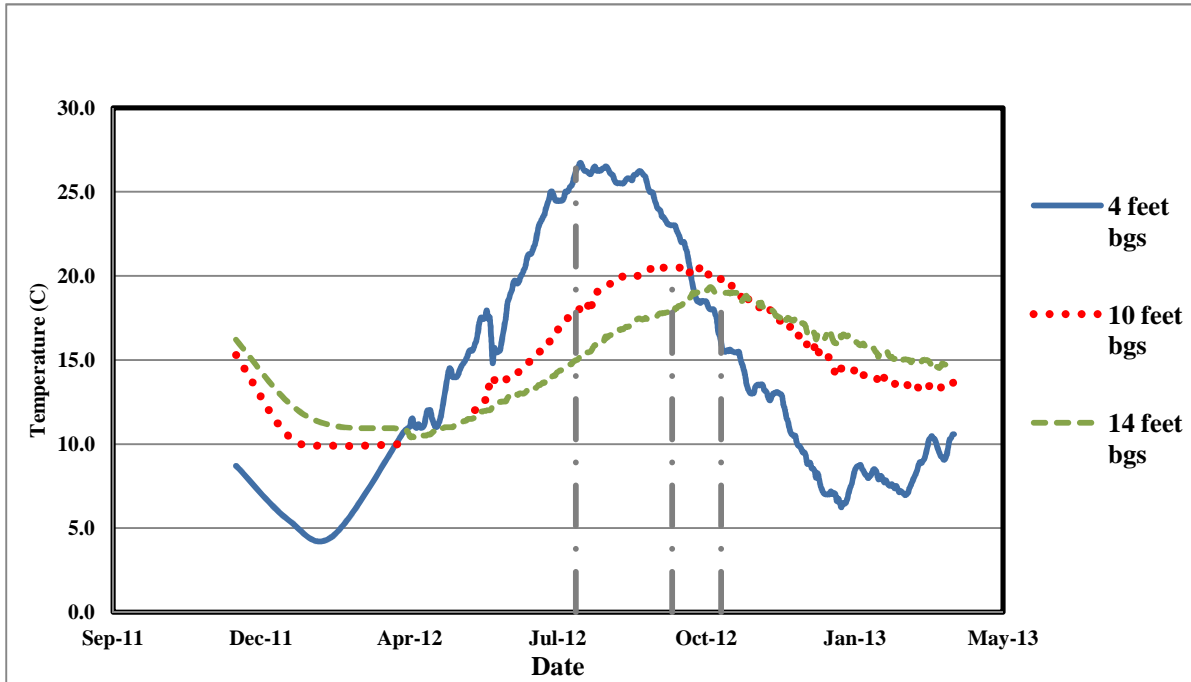


Figure 2.10: Temperature lags through the subsurface. At 4ft below the ground surface, the highest temperature was observed in July. While at 10ft and 14ft below the ground surface, the highest temperature observed in September and October, respectively. This lag in the vertical direction occurs due to the thermal diffusion.

2.4.3 Effective Season

Temperature data collected at the field demonstrated that the temperature could be as low as 10C in the saturated zone, in the coldest seasons. Zeman’s microcosm studies (2012) on the same field show that the biodegradation rate of the LNAPL, dramatically, increases at the temperatures in the range of 22°C and 30°C which leads to the enhancement of natural attenuation. Also, McCoy’s studies demonstrated the critical temperature can be 18°C. Due to this new understanding a new term, effective season, was defined related to this research. The effective season is defined as the period of the year that the temperature is above 18°C in the

saturated zone. The effective season, for this field site in natural conditions, only happens from late Septembers to the late Octobers (a month). Hence the heating elements were deployed in the site and started to work on September 27, 2012 to extend the length of the effective season. The impact of the heating elements was quick and obvious on the closest observation wells (Figure 2.11).

The length of the effective season changes depending upon the distance from the heating elements as shown in Figure 2.11. The temperature changes through time in five MLSs in the main cross-section (see Figure 2.4) are presented in this figure. The top graph shows C1 which is immediately upgradient of the heating elements. The other four graphs belong to C2, C3, C4, and C5 that are sequentially downgradient of the heating elements. The gray box in each graph shows the length of the effective season. After eight months of running the heating elements, the nearest MLS at the downgradient of the heating elements (panel b) presents the effective season of five months starting from mid-September and ending in mid-February. The length of the effective season at nearest MLS (C2-panel c) at the upgradient of the heating elements is slightly shorter (four months). The effective season at this well started in October and ended by the end of January (panel a). At MLS C3, 5m downgradient of the heating elements, the observed effective season was two months (panel c). Panels d and e present the lengths of the effective season at 7m and 10m downgradient of the heating elements, respectively. The lengths of the effective season at these monitoring wells remained unchanged at one month per year. The results of this figure demonstrates that this heating elements design affect the temperature in the field demonstration up to 5m downgradient of the heating elements.

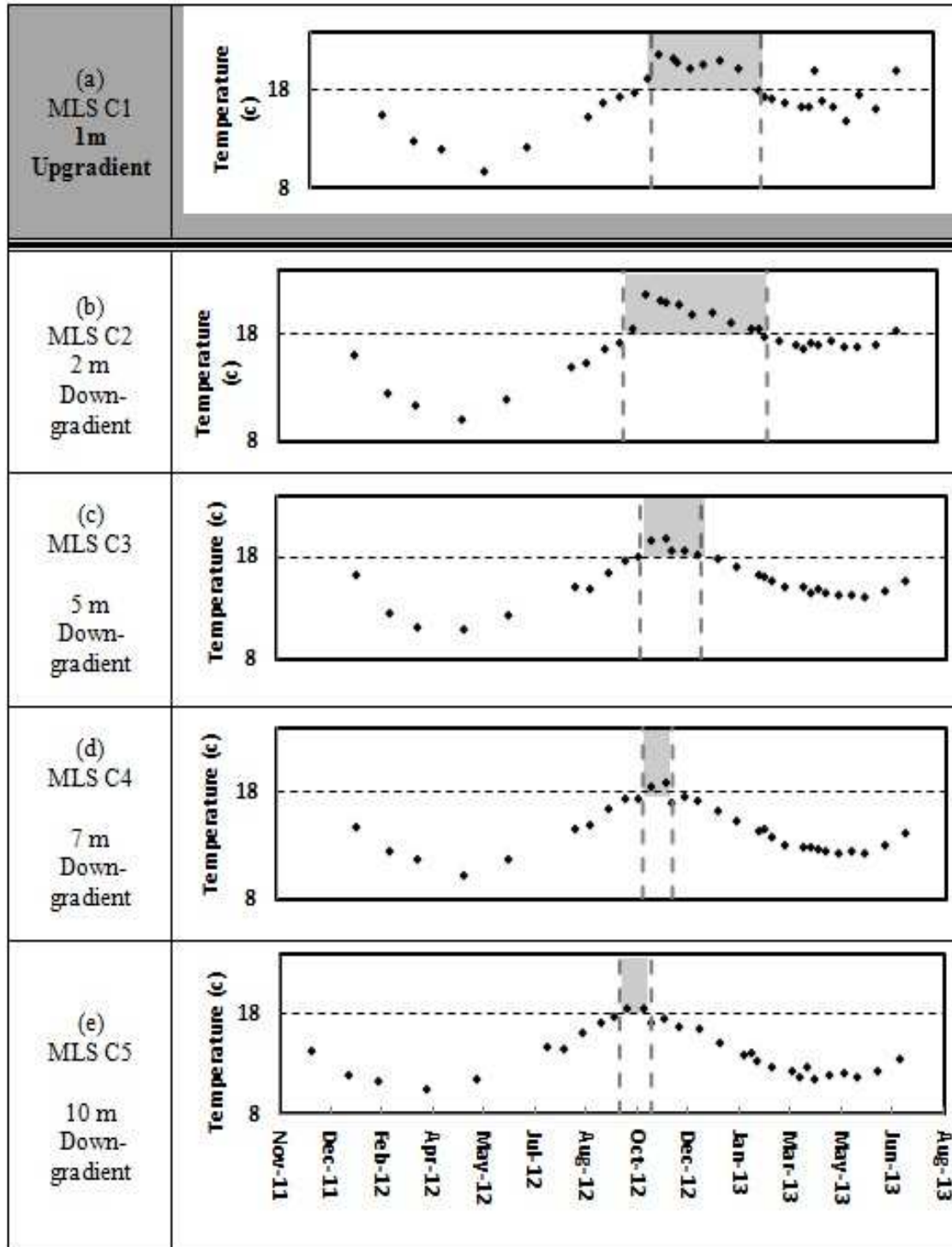


Figure 2.11: Length of the effective season depending up on the position to the heating elements. The temperature changes through the time in five MLS in the main cross-section are demonstrated in this figure. The top graph shows C1 which is at the upgradient of the heating elements. The other four graphs belong to C2, C3, C4, and C5 that are at the downgradient of the heating elements. The gray box in each graph shows the length of the effective season. (After eight months of the heating elements activation)

To show how the effective season changes spatially in the field demonstration a contour map of the effective seasons was created and presented in Figure 2.12. The contour map demonstrates that at the effective season is 40 days in the background MLSs, and also, at the wells that are 7m and 10m away from the heating elements. It, also, shows that the growing in the effective season ranges from 60 days to 200 days depending upon the position to the heating elements. Overall, for the presented heating system design in this paper, the ability of the heating system to increase the length of the effective season can be estimated 5m, and the coverage area is approximately 55m².

2.4.4 Heating System Effects on the Subsurface Heat Movement

Other way to observe the effect of the heating elements on the subsurface temperature is by comparing the temperature contour maps at the same time of the year with heating elements and without heating elements. This is shown in Figure 2.13. The left hand side column shows the temperature isotherms prior to heating (before September 2012). The right hand side column shows the isotherms at the same period of the year when the heating elements were energized (after September 2012). As it is shown, when the heating system was energized, temperatures at the MLSs closer to the heating elements are significantly higher than the temperatures occurred at the same location when the heating system was off. However, temperature at the points 7m to 10m away from the heating elements, when the heating system was energized, was almost at the same temperature that observed on the same location, when the heating system was off. Also, propagation of the heat at subsurface could be interpreted in the right hand side panel by comparing the temperature distribution in different months. By turning on the heating system, the heat starts to propagate through the system very quickly. Graph b.1 shows that, in December, the temperature increased up to 20⁰C, 5m away from the heating system. The same increase in

temperature happens up to just 3m away from the heating system in January (graph b.2). In February, the affected area by the heating elements was even less. This happens due to the starting of the cold season at the saturated zone. During the saturated zone's winter, the heating system must fight against the cold ambient air that goes through the subsurface. Hence, as it can be seen in the graphs b.4 and b.5, in March and May, the temperature at the subsurface decreased in comparison with the previous months. However, it still shows higher temperature related to the previous year that the heating elements were off.

2.4.5 Opportunities to Enhance the Heating System Design

Figure 2.14 shows the power consumption and power cost of the heating system in kw-hr/day and \$/day, respectively. The power unit price was assumed 0.10 \$/kw-hr. The power consumption increases up to 30 kw-hr/day in April due to the effects of the cold ambient air temperature on the subsurface temperature. The power cost during the cold season increases up to 3 \$/day. The power cost can be decreased by adding a gas permeable insulation/heat sink (GPIHS) system to the heating elements and using less electricity energy for the heating elements. Adding the GPIHS layer can enhance the heating system design by prohibiting the excess heat to loss through the soil surface (such as a blanket) and adsorbing the solar radiation (black sheets or black genets).

The idea of using insulation has been shown in the previous works in Alaska and Sub-Antarctica to enhance the bioremediation and natural attenuation. Dellile et al. (2004) showed a permanent annual mean temperature enhancement of 2C by using of plastic sheets in Sub-Antarctica region. Furthermore, Filler et al. (2001) discussed that the TIS design and extension of the effective treatment season in Prudhoe Bay, AK. They demonstrated that for TIS design,

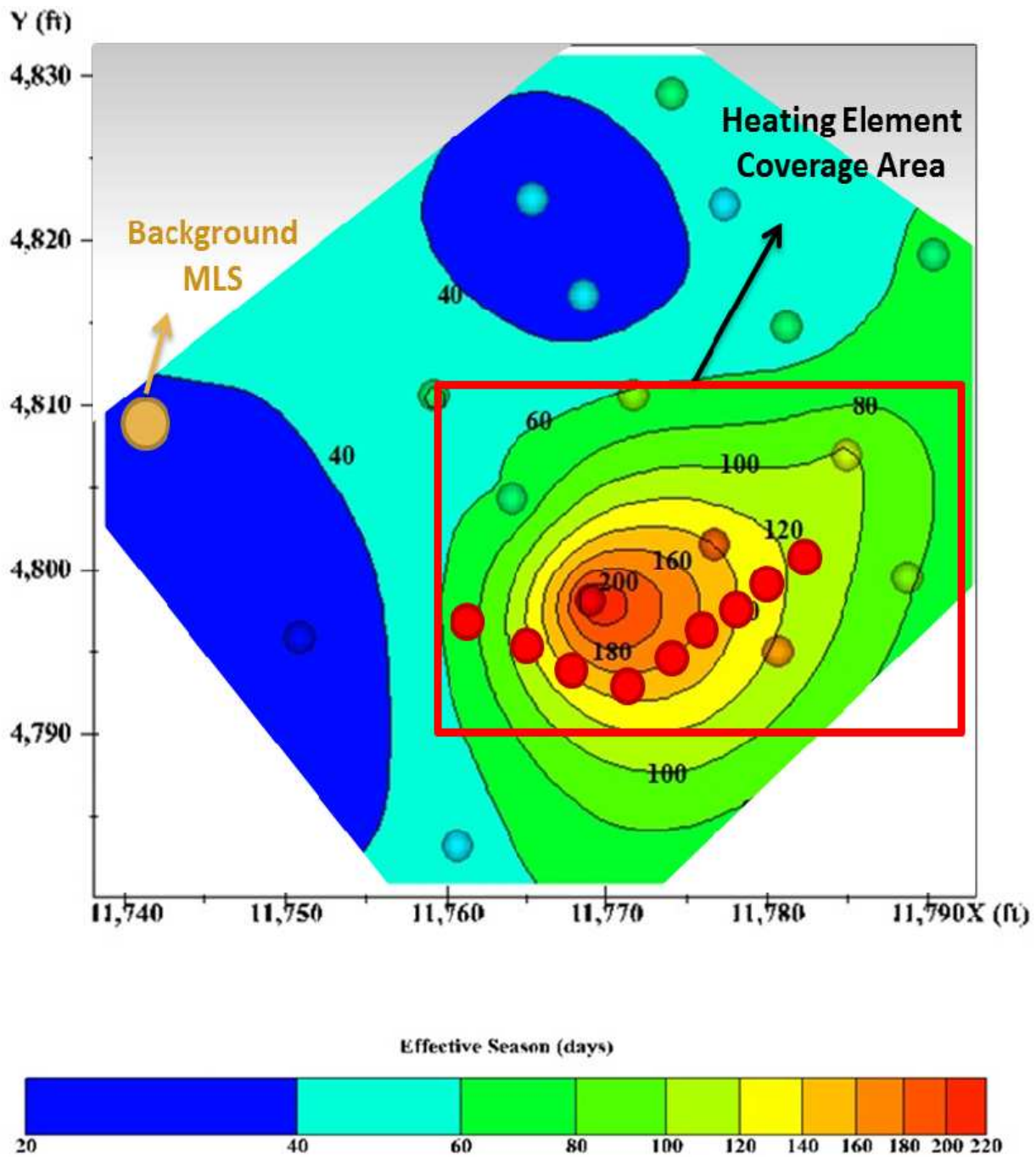


Figure 2.12: Effective season contour map. The length of the effective season at the background wells are 40 days. Coverage area is the area that the heating elements were effective to increase the length of the effective season.

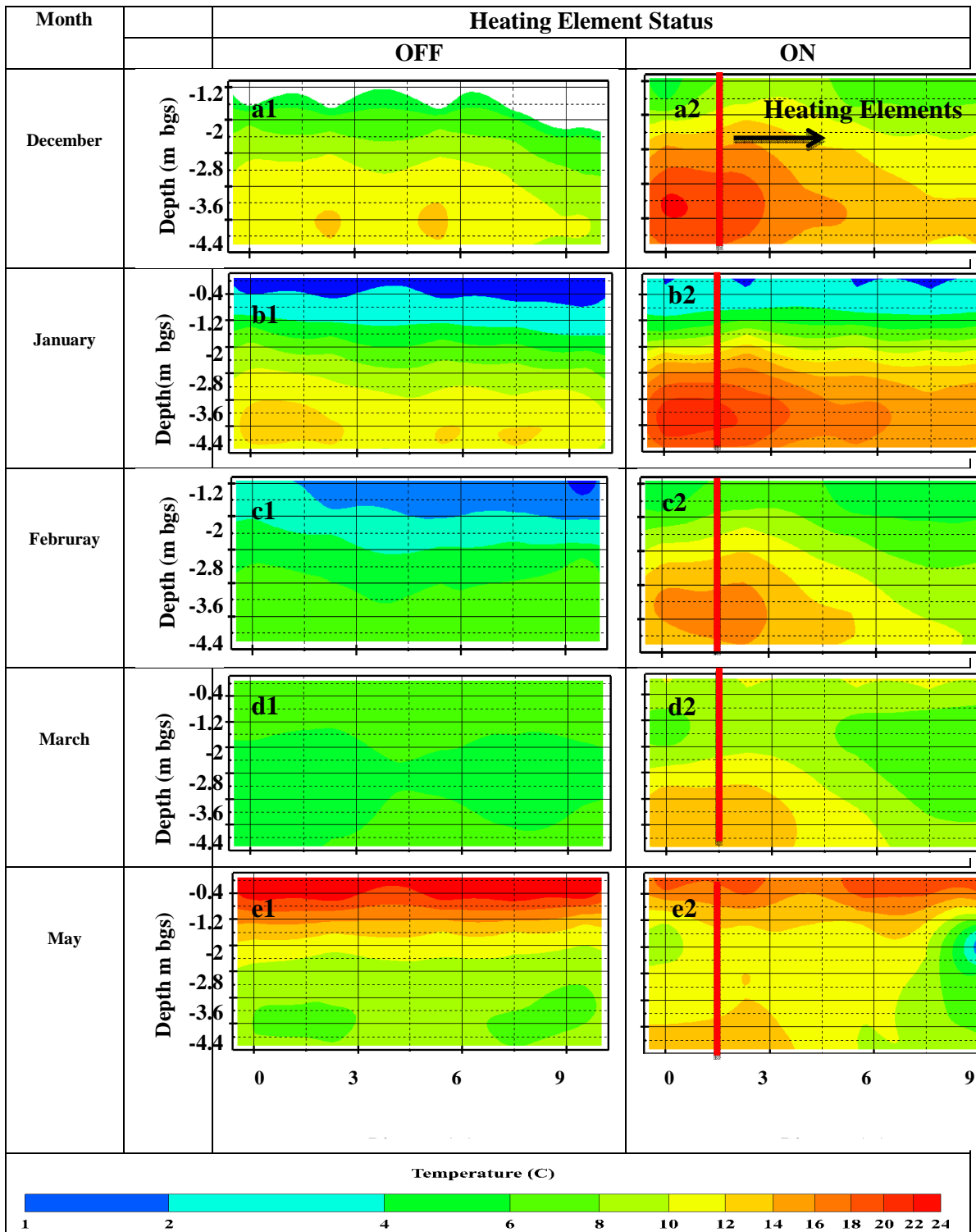


Figure 2.13: Main cross-section temperature isotherms. Left hand side column: shows the temperature isotherms before the activation of the heating elements. Right hand side column: shows the temperature isotherms after the activation of the heating elements. The red bar in the graphs shows the location of the heating elements

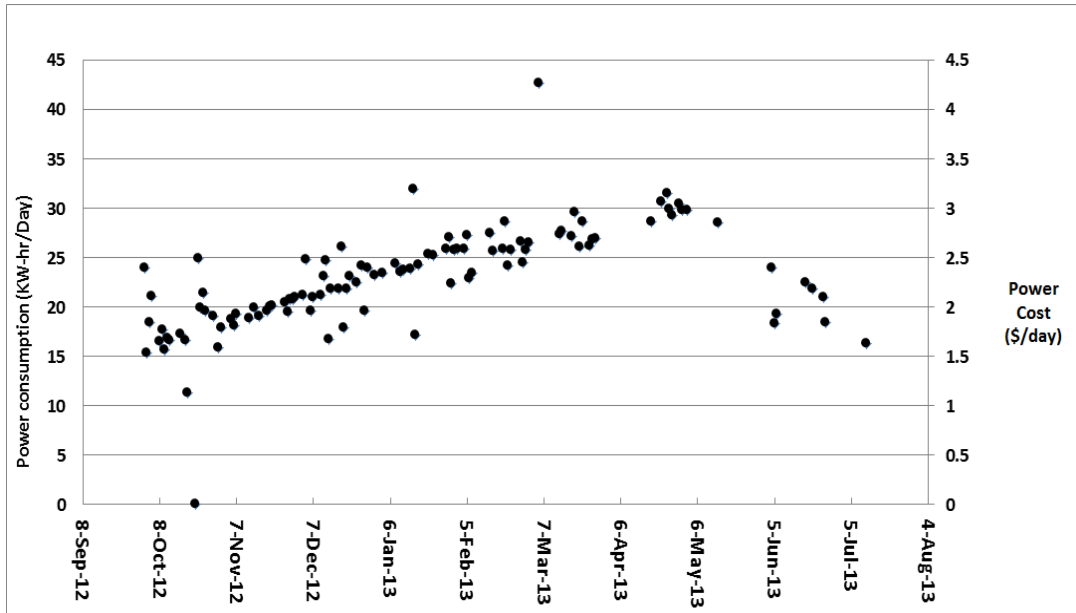


Figure 2.14: Power consumption and power cost for the heating system.

capital cost can be reduced when using a thicker insulation layer in conjunction with increased spacing of heating elements. Periodic active soil warming with TIS has been used at this site to extend the effective season from 2.5 to 6 months during the first year of bioremediation. To contain heat in the biopile during the cold season, 3 in. of R-Gard insulation has been used. The TIS system extended the length of the effective season by just prohibiting the heat loss through the soil surface. On the other hand, the GPIHS system that was tested in current paper can extend the effective season by adsorbing the solar radiation and prohibiting the heat loss through the soil surface.

To test the idea of deploying the GPIHS layer, in November 2012, a portion of the soil in Foothills Campus, Colorado State University, at Fort Collins, CO was covered with a geo net layer (see method section). The temperature data for three months of this experiment are shown in the Figure 2.15. It can be seen that at the beginning of the experiment both the covered soil and uncovered soil are at the same temperature. However, after a while, the temperature at the

covered soil was higher than the one at the uncovered soil. The average temperature difference of the two soils was 4.75°C. Hence, by adding the geo-net to the heating elements, heating system can sustain higher temperatures within the subsurface.

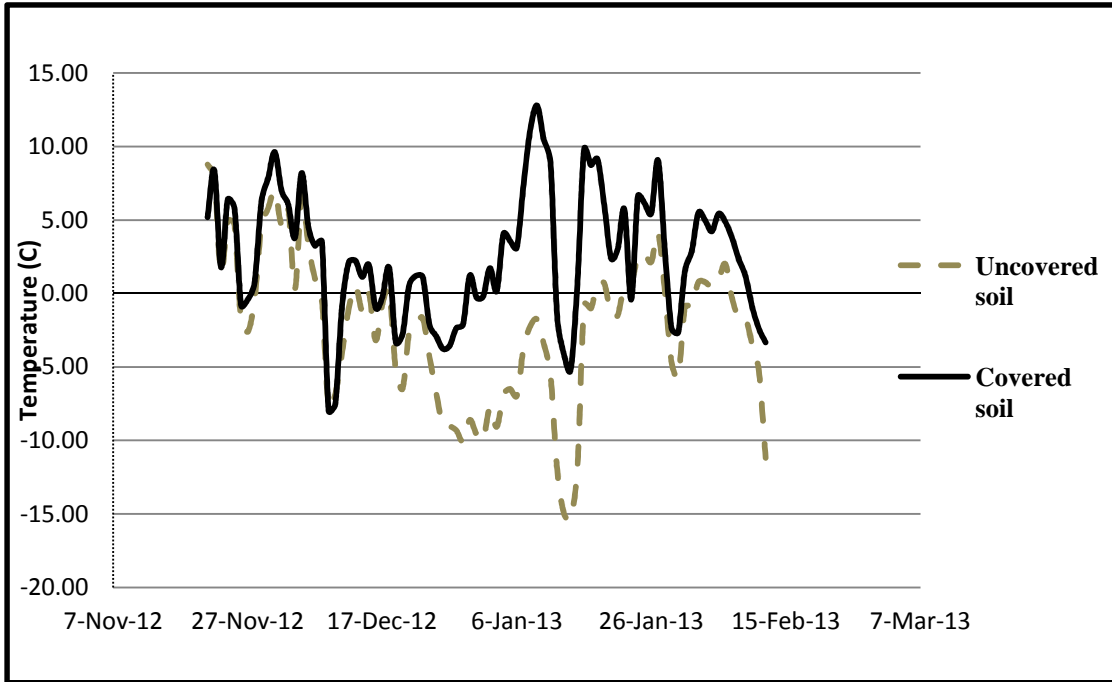


Figure 2.15: Testing an insulation layer. A 1m by 1m geo-net with the thickness of 2.54cm has been anchored to the ground in Foothills Campus, Colorado State University. A continuous data logger such as the one has been used in the refinery deployed 30cm below this mat. Also, another continuous temperature data logger has been deployed 3m away from the geo-net at the same depth below the grade.

2.5 Conclusions

Data collected from December 2011 to December 2012 indicates that in the absence of heating, subsurface temperatures are in the range of 18-30°C for approximately 40 days per year at this field site. Data collected from July 2012 to July 2013 indicates that with heating, conditions can be maintained in the target range for 60 to 200 months per year depending upon proximity to the heat source. A principle challenge is heat loss to the surface in the winter.

Firstly, data that collected from December 2011 to December 2012, at the background wells, demonstrated that temperature is changing between 9°C to 21°C in the saturated zone. Also, in the warm seasons, the shallower points are warmer than the deeper points. On the other hand, in the winter time, the warmer temperature happens at the deeper points. Moreover, the monthly temperature profiles indicate that temperature at the depth beneath the ground lags behind the ambient air temperature. This lag occurs because of the low thermal diffusivity of the saturated sediments.

Next, a new term, effective season, was defined as the period of the year that the temperature is above 18°C in the saturated zone. At this site, the effective season, in the absence of heating, only happens from late Septembers to the end of Octobers (40 days). Data collected from September 2012 to July 2013 indicates that with heating, the length of the effective season grows in a range of 60 days to 200 days depending upon the position to the heating elements. Moreover, the proposed heating system in this paper was successful in increasing the length of the effective season for the area of 55m².

Lastly, minimum and maximum power inputs have been 15 kw-hr/day and 30 kw-hr/day occurring, respectively in October and May. Assuming an energy cost of 0.10 kw-hr, this equates to costs of 1.5 \$/day to 3 \$/day. An independent experiment using Geo-net layer showed that using Gas Permeable Insulation/Heat Sink (GPIHS) system has the potential to enhance the ability of the heating system to sustain temperature beneath the ground surface, and, potentially decrease the power costs. The GPIHS system prohibits the excess heat to loss through the soil surface and also adsorbs solar radiation.

Overall, the results of this study indicate that the period of the year that the subsurface temperature provides suitable conditions for the high LNAPL biodegradation is about 40 days per year. To date data indicated that by using the passive heating sources, the target range can be increased between 60 days to 200 days per year depending upon proximity to the heat source. Lastly, for the future STELA heating system designs, using a GPIHS system is suggested to overcome the heat loss to the surface in the winter and decreasing the power costs.

3. HEAT TRANSPORT MODEL IN SUPPORT OF STELA FIELD DEMONSTRATION

3.1 Synopsis

In recent years, a vision has emerged that passive thermal strategies could enhance natural losses of LNAPL and significantly reduce the longevity of LNAPL. Building on this, a small-scale field demonstration of sustainable thermally enhanced LNAPL attenuation (STELA) has been initiated at a former refinery in Wyoming. The overarching objective of the STELA initiative is to develop a new technology for LNAPLs that is more effective, faster, more sustainable, and/or at lower cost than current options. A primary challenge with evaluation and design of STELA systems is anticipating the long-term performance of STELA system from a thermal prospective. Herein this challenge is met by developing a model, calibrated to field data, which can be used to design a full-scale STELA remedies. Specifically, heat transport is evaluated by coupling MODFLOW and MT3DMS.

The overarching objective of the modeling is to demonstrate methods that can be employed to evaluate and/or design full-scale STELA systems. At 5m downgradient of the heating elements, the developed model predicted 60 days of the effective season in 2012. Also, the simulation results anticipate that by keeping the heating system activated for three years, the effective season will increase each year. At 5m downgradient of the heating system, model results suggested 120 days and 150 days of effective season for 2013 and 2014, respectively as compared to 60 days in the first year. The ability of the model to anticipate the effective season for the next years makes the model a useful tool to design and evaluate the future STELA systems.

Calibration of the model to the field data shows that exothermic reactions associated with LNAPL losses can change the heat distribution at the system. In addition, the simulation results indicate that the losses at the subsurface are 7,500gal/acre/yr. These anticipated loss rates are in consistent with the previous numbers that were calculated by McCoy (2012) (~900-11,000gal/acre/yr.)

3.2 Introduction

As mentioned in Chapter 2, impacts to groundwater, lateral expansion of LNAPL bodies, and impacts to indoor air are primary concerns with LNAPLs, and natural attenuation often deplete petroleum hydrocarbons in the subsurface; however, this depletion occurs at slow rates. The hypothesis that has emerged from Zeman (2012) studies is that sustainable thermal management strategies could enhance natural losses of LNAPL and significantly reduce the longevity of LNAPL, by sustaining temperatures in the range of 18-30 °C.

To test the hypothesis, a field demonstration was initiated at a former refinery to develop a new technology (sustainable thermally enhanced LNAPL attenuation (STELA)) to enhance the biodegradation of LNAPLs. The site is located in Wyoming underlain by the sandy alluvium of the North Platte River. As described in Chapter 2, water level, water temperature, and water quality data were collected through 17 multilevel samplers from November of 2011 to September 2012. In September of 2012, a heating system was energized at the upgradient of the sampling network to deliver heat to sustain subsurface temperature in an LNAPL body. The effects of the heating elements on the subsurface temperature were monitored using 17 multilevel sampling systems for 10 months.

A primary challenge with evaluation and design of STELA systems is anticipating the appropriate spacing of heating elements and necessary energy inputs. Herein this challenge is met by developing a model, calibrated to field data, which can be used to design a full-scale STELA remedies. Specifically, heat transport is evaluated by coupling MODFLOW (Harbaugh 2005) and MT3DMS (Zheng et al. 2010).

The overarching objective of this paper is to demonstrate methods that can be employed to evaluate and/or design full-scale STELA systems. Secondary objectives include developing methods to address temporal temperature variations at grade, and heat generated through degradation of LNAPL. This paper is organized into four sections. The first section provides background information regarding heat transfer in subsurface porous media. Second section outlines methods employed in calibrating the model to field data. Next, results are presented including anticipation of long-term performance of the STELA field demonstration. Lastly, conclusions and recommendations for additional work are documented.

3.3 Background

The following section provides background information regarding heat transfer in subsurface porous media. This includes review of subsurface heat transport numerical models, solute and heat transport analogy, and MT3DMS limitations for the heat transport simulations. This information is foundational to information presented in subsequent discussions regarding methods and results.

3.3.1 Review of Numerical Models for Subsurface Heat Transport

Due to the growing interest in subsurface heat transport (Anderson 2005), different groundwater flow and heat transport codes (Kipp 1997, Pruess 2003, Voss and Provost 2010) have been written to simulate the heat transfer in the porous media (Bravo et al. 2002, Birkholzer et al. 2003, Burow et al. 2005). Since the governing equations for heat transport are mathematically identical to those for solute transport (Vries 1975, Hillel 1982, de Marsily 1986, Narasimhan 1999, Anderson 2005, Kim et al. 2005, Thorne et al. 2006, Zheng 2009), solute transport codes can be used for the heat transport simulations. Among all of the solute transport programs, many references report and evaluate the applications of MT3DMS to simulate thermal transport phenomena in the saturated aquifers (Zheng 2009).

Sethi and Molfetta (2007) used the MT3DMS to model and investigate the origin of a thermal anomaly in the aquifer underneath a municipal landfill in the North of Italy by using the analogy between heat and mass transport in porous media. Hecht-Méndez et al. (2010) evaluated the utility of MT3DMS for shallow geothermal systems by comparing the MT3DMS results with FEFLOW (Diersch 2002) and SEAWAT (Langevin 2008), and their results suggest that MT3DMS can be successfully applied to simulate ground source heat pump (GSHP) systems, and likely other systems with similar temperature ranges and gradients in the saturated porous medium. Ma and Zheng (2009) employed a cross-section model of aquifer-river interactions at the Hanford 300 Area in Washington State as the reference frame to evaluate the impact of fluid density and viscosity in heat transport modeling by comparing the results of MT3DMS (which assume a constant fluid viscosity and density) and SEAWAT (which can exploit variable fluid density and viscosity).

3.3.2 Solute and Heat Transport Analogy

3.3.2.1 Solute Transport Equation

The partial differential equation describing the fate and transport of contaminants of species k in three-dimensional, transient groundwater flow systems solved by MT3DMS as follows (Zheng and Wang 1999):

$$\text{Equation 3.1} \quad R \frac{\partial(\theta C^k)}{\partial t} = \nabla \cdot \left[\theta \left(D_m^k + \alpha \frac{q}{\theta} \right) \cdot \nabla C^k \right] - \nabla \cdot (q C^k) - S$$

Where, the dimensionless retardation factor, R , can be written as:

$$\text{Equation 3.2} \quad R = 1 + \frac{\rho_b K_d^k}{\theta}$$

In the above equations, $\rho_b \left[\frac{M}{L^3} \right]$ is the bulk density, $K_d^k \left[\frac{L^3}{M} \right]$ is the distribution coefficient of species k , $\theta [-]$ is porosity, $C^k \left[\frac{M}{L^3} \right]$ is the concentration of species k , $t [t]$ is time, $D_m^k \left[\frac{L^2}{t} \right]$ is the molecular diffusion coefficient for species k , $\alpha [L]$ is the dispersivity tensor, $q \left[\frac{L}{t} \right]$ is Darcy flux of water, and $S \left[\frac{M}{t L^3} \right]$ represents fluid sources (positive) and sinks (negative). The first term in the right hand side is the hydrodynamic dispersion term, including pure molecular diffusion and mechanical dispersion. The second term describes advection and the third term represents source and sinks. Finally, retardation factor denotes the ratio between the total solute concentration and the mobile assuming concentration given by the distribution of the contaminant in the fluid and solid phases.

3.3.2.2 Fundamentals of Heat Transport Equation in Subsurface Porous Medium

Heat-flow theory in relation to groundwater systems became of the interest since the 1960s and analytical solutions were developed to describe heat transport through the porous medium (Anderson 2005). Carslaw and Jaeger (1959) derived the differential equation of heat conduction in an isotropic solid and in a moving medium. Stallman (1963) derived the basic differential equation for simultaneous transfer of heat and water through the isotropic, homogeneous, and fully saturated porous medium. Bredehoeft and Papadopoulos (1965) developed a one-dimensional analytical solution to describe the vertical steady flow of groundwater and heat through semi-confining layers. Domenico and Palciauskas (1982) presented a two-dimensional solution of heat transport by solving the energy equation for the simultaneous transport of water and heat in a cross-section of a ground water basin. With the advent of numerical models, many investigators turned to numerical solutions of coupled ground water and heat flow models in two and three dimensions (Anderson 2005).

Heat transfer in porous media is governed by three separate mechanisms:

1. Conduction in the solid matrix and fluid phase
2. Convection by the fluid phase
3. Heat exchange between the aqueous and solid phases depending on their temperature difference.

In practice, the assumption is made that the temperature of the solid and the fluid at any point in space become identical almost at once; hence there is only one temperature in the porous medium (de-Marsily 1986).

All that has been said in the subject of the solute transport can be applied to the heat transfer in the porous media. The transport is characterized by:

1. A convection phenomenon similar to advection of solutes and
2. A phenomenon similar to that of diffusion in porous media:
 - a. Pure conduction in the two phases, solid plus liquid, takes the place of molecular diffusion, while
 - b. The heterogeneity of the real velocity gives rise to an equivalent of hydrodynamic dispersion.

The conduction of heat in the solids was analyzed by Fourier in 1822. Fourier name is commonly associated with the linear transport equations which have been used to describe heat conduction. Fourier's equations are mathematically analogous to the diffusion equations (Fick's laws) as well as to Darcy's law for the conduction of fluids in porous media. An analogy can also be drawn between Fourier's equation and Ohm's law for the conduction of electricity. Fourier's law states that the conductive flux of heat in a homogenous body is in the direction of and proportional to the temperature gradient (Hillel 1982). Under the hypothesis of thermal equilibrium between solid and liquid phases (Sethi and Molfetta 2007), the generalized Fourier's law becomes:

Equation 3.3
$$q_h = -k_{T-bulk} \nabla T$$

Where, $q_h \left[\frac{M}{t^3} \right]$ is the thermal flux, the amount of heat conducted across a unit cross-sectional area in unit time, $T [T]$ is temperature, and $k_{T-bulk} \left[\frac{ML}{t^3 T} \right]$ is the bulk thermal conductivity of the aquifer material which accounting the properties of both fluid and solid

phases. Thermal conductivity is defined as the amount of heat transferred through a unit area in unit time under a unit temperature gradient (Hillel 1982).

$$\text{Equation 3.4} \quad k_{T-bulk} = \theta k_{T-fluid} + (1 - \theta)k_{T-solid}$$

Where, $k_{T-fluid} \left[\frac{ML}{t^3 T} \right]$ is the thermal conductivity of the fluid phase and $k_{T-solid} \left[\frac{ML}{t^3 T} \right]$ is the thermal conductivity of the solid phase. *Equation 3.3* is sufficient to describe the heat conduction under the steady state conditions. To account for non-steady conditions we need a second law analogous to the Fick's second law of diffusion. To obtain the second law of heat conduction, the principle of energy conservation in the form of continuity equation is used which states that in the absence of any sources or sinks of heat, the time rate of change in heat content of a volume element of the conducting medium must equal the change of flux with distance:

$$\text{Equation 3.5} \quad \rho_m C_m \frac{\partial T}{\partial t} = -\nabla q_h$$

$\rho_m C_m$ denotes the volumetric heat capacity of the porous medium. The volumetric heat capacity of a soil is defined as the change in heat content of a unit bulk volume of soil per unit change in temperature (Hillel 1982). Volumetric heat capacity can be computed as the weighted arithmetic mean of solid rock and pore fluid (Hecht-Méndez et al. 2010):

$$\text{Equation 3.6} \quad \rho_m C_m = \theta \rho_f C_{p-fluid} + (1 - \theta) \rho_s C_{p-solid}$$

Where $\rho_s \left[\frac{M}{L^3} \right]$ is the density of the solid (mass of the solid divided by the volume of the solid), $\rho_f \left[\frac{M}{L^3} \right]$ is fluid density, $C_{p-solid} \left[\frac{L^2}{t^2 T} \right]$ is the specific heat capacity of the solid,

$C_{p-fluid} \left[\frac{L^2}{t^2 T} \right]$ is the specific heat capacity of the fluid. Combining the *Equation 3.4* and *Equation 3.5*, the second law of heat conduction is obtained:

$$\text{Equation 3.7} \quad \rho_m C_m \frac{\partial T}{\partial t} = \nabla \cdot (k_{T-bulk} \nabla T)$$

Equation 3.7 does not consider the convection part of the heat transport. Considering that the fluid is moving by the velocity of $v \left[\frac{L}{t} \right]$, to calculate the rate at which heat crosses any plane, a convective term ($\theta \rho_f C_{fluid} v T$) of components must be added to the conduction part (Carslaw & Jaegar 1959):

$$\text{Equation 3.8} \quad q_h = -k_{T-bulk} \nabla T + \theta \rho_f C_{fluid} v T$$

There are controversies regarding the importance of thermal dispersion, which is caused by velocity variation within the pore space, to heat transport. For solutes, It has been, historically, assumed that the mechanical dispersion often dominates molecular diffusion. On the other hand, for the heat transport, this is not the case because heat conduction is normally much stronger than thermal dispersion (Langevin et al. 2009). The dominancy of heat conduction over the heat dispersion happens since heat can be conducted through a saturated medium through both the solid phase and liquid phase. For this reason, thermal dispersion is often neglected (Chiasson 1999); however, there are still un-answered questions about the importance of heat dispersion in heterogeneous mediums (Anderson 2005 and Ferguson 2007). To gain the complete form of the heat flow equation, the effects of thermal dispersion can be shown as follows:

$$\text{Equation 3.9} \quad \eta = k_{T-bulk} + \alpha \cdot \theta \rho_f C_{fluid}$$

Equation 3.8 can be completed by adding the thermal dispersion effect and sinks/sources energies ($q_s \rho_f C_{p-fluid} T_s$). In addition, to highlight the similarity with the solute transport equation, heat transport equation can be written as follows (Thorne et al. 2006 and Langevin et al. 2008):

Equation 3.10

$$\left(1 + \frac{1 - \theta}{\theta} \frac{\rho_s}{\rho_f} \frac{C_{p-solid}}{C_{p-fluid}}\right) \frac{\partial(\theta T)}{\partial t} = \nabla \cdot \left[\theta \left(\frac{k_{T-bulk}}{\theta \rho_f C_{p-fluid}} + \alpha \frac{q}{\theta} \right) \cdot \nabla T \right] - \nabla \cdot (qT) - S$$

Where, $q \left[\frac{L}{T} \right]$ is the Darcy flow and $S \left[\frac{T}{t} \right]$ is a heat source or sink.

Comparison of *Equation 3.1* and *Equation 3.10* reveals several important equivalences. The storage terms on the left sides of these equations prefixed with retardation terms. The retardation factor and the distribution factor represented in the solute transport equation which is in regard to solute sorption can be equivalently expressed in the heat transport equation as the heat exchange between the solid and the water. For solute transport, retardation is caused by adsorption of solutes by the aquifer matrix material. While, with the heat transport, retardation is caused by heat transfer between the fluid and solid aquifer matrix and is given as the ratio of the volumetric heat capacity of the porous medium (total phase) and the volumetric heat capacity of the water (mobile phase):

Equation 3.11

$$R_T = \frac{\rho_m C_m}{\theta \rho_f C_{p-fluid}} = 1 + \frac{1 - \theta}{\theta} \frac{\rho_s}{\rho_f} \frac{C_{p-solid}}{C_{p-fluid}}$$

Thermal retardation factor reflects the fact that energy travels through both fluid-filled pores and the rock fabric, and is therefore retarded relative to the fluid velocities (Shook 2001).

MT3DMS can be used to represent thermal retardation by calculating the distribution coefficient for the temperature species as a function of thermal properties. The distribution coefficient is expressed as the ratio between the specific heat capacity of the solids and the volumetric heat capacity of the water:

$$\text{Equation 3.12} \quad K_d^T = \frac{C_{P-solid}}{\rho_f C_{P-fluid}}$$

The new distribution coefficient for heat transport is implemented in MT3DMS in the chemical reaction package. The type of sorption must be set to a linear isotherm in order to keep the temperature exchange rate between the solid and the water constant independently of changes in temperature (Hecht-Méndez et al. 2010).

Moreover, inspection of the *Equation 1* and *Equation 10* demonstrates that the heat conduction is mathematically equivalent to the molecular solute diffusion. To represent the heat conduction with MT3DMS, the thermal diffusivity for the temperature species is calculated as follows:

$$\text{Equation 3.13} \quad D_m^T = \frac{k_{T-bulk}}{\theta \rho C_{P-fluid}}$$

It should be noted that, the thermal diffusivity is of the order of 10^{-2} to 10^{-3} cm^2/s , whereas the molecular diffusion is of the order of 10^{-6} cm^2/s . The larger values for conduction of heat arise partly because heat is transferred through the solid as well as the fluid.

3.3.3 MT3DMS limitations for the heat transport simulation

The intrinsic assumption of MT3DMS is that solute concentrations are sufficiently small so that their effects on the fluid density are negligible. Thus, the use of MT3DMS for the heat transport modeling is based on the assumption that the changes in the fluid density and viscosity induced by the temperature variations are negligible (Zheng 2009). However, temperature has an influence on several physical parameters such as density and viscosity of the water. Temperature can introduce limitations in two main ways:

The hydraulic conductivity depends on density and viscosity of water which are both temperature dependent (Anderson 2005):

Equation 3.14
$$K = kg \frac{\rho}{\mu}$$

Where, $k[L^2]$ is the intrinsic permeability of the soil, $g \left[\frac{L}{t^2} \right]$ is the gravitational acceleration, $\rho \left[\frac{M}{L^3} \right]$ is density, and $\mu \left[\frac{M}{L t} \right]$ is viscosity.

Thus, the first limitation stems from the fact that the temperature variation affects water viscosity and density which effect hydraulic conductivity. However, temperature variations in the shallow subsurface are commonly small, so simulation errors produced from using constant viscosity and density often are small and acceptable (Hecht-Méndez et al. 2010).

Temperature variations can also promote free convection of fluids. The second term on the right hand side of the *Equation 3.10* represents the transport of heat by flowing groundwater, a process known as advection or convection. Free convection refers to the heat which transfers in response to flow driven by temperature-induced density differences, while forced convection

refers to the heat which transfers by the flow driven by any other mechanism. Free convection is thought to occur in areas of high heat flow such as near spreading centers in the ocean but rarely in sedimentary basins. The potential for free convection is often investigated by using the dimensionless Rayleigh number, which is derived by considering the ratio of buoyant forces to viscos forces. The potential for forced convection to perturb the geothermal gradient is quantified by dimensionless Peclet number (the ratio of convection to conduction) (Anderson 2005).

Typically, hydrogeological studies assume that the variation of density and viscosity due to temperature is negligible. Under such circumstances, small thermal gradients in the aquifer can allow for the decoupling of the flow and heat transport equations. However, in some cases that include strong thermal variations, temperature plays an important role in the groundwater flow system (Ma and Zheng 2009), in instance, in the cases of the leachate plumes from landfills or tracer tests, variable density effects should be considered (Simmons 2005).

Thus a question arises that under which conditions the effects of temperature on the fluid density and viscosity can be neglected. Several studies have been carried out to evaluate the effects of temperature variations on the MT3DMS simulations comparing with the SEAWAT. The SEAWAT computer program is a coupled version of MODFLOW and MT3DMS which designed to simulate the variable density ground water flow and transport (Langevin 2009).

Ma and Zheng (2010) compared the MT3DMS and SEAWAT results under the complex field conditions at the Hanford 300A site. They clarified that MT3DMS and SEAWAT results are nearly identical which indicates that the effects of fluid density and viscosity are negligible. They simulate the Hanford 300A site under different scenarios to find the conditions that the density and viscosity variations due to temperature variation are negligible. This study indicated

that the MT3DMS code can be used for heat transport modeling under the assumption of constant fluid density and viscosity when the maximum temperature difference across the flow domain is within 15⁰C (Ma and Zheng 2010).

The thermal energy that introduces to the STELA field demonstration via the heating elements produces temperature variations less than 15⁰C across the domain. Hence, variations in fluid density and viscosity variations are not expected to influence the groundwater flow, and the velocity distribution calculated by MODFLOW can be used with MT3DMS to simulate the heat transport.

The advantages of using MT3DMS over SEAWAT are presented in Ma and Zheng (2010) study. They demonstrated that the computational time for MT3DMS is more than 30% less than for SEAWAT considering variable density and viscosity, when the maximum temperature difference across the flow domain is within 10⁰C. When the maximum temperature difference increases to 15⁰C, the SEAWAT simulation time increases significantly to 225.1% over that required by MT3DMS. Thus, the use of MT3DMS is computationally efficient for heat transport modeling.

Moreover, a major advantage of using MT3DMS for heat transport simulation is that it integrates five different advection solver methods, which are suitable for solving problems in a broad range of hydrogeological and transport conditions. It also allows the user to flexibly enter crucial transport parameters such as diffusivity and dispersivity in form of arrays. Last but not least, as an open source code, it can be modified, extended, and adjusted to specific modeling requirements and individual application cases (Hecht-Méndez et al. 2010).

3.4 Methods

The following section outlines methods employed in calibrating the model to field data and application of the model to anticipate long-term performance of the STELA systems. The first section provides the field description. In the second section, a brief description of the hydrogeology is presented. The third section presented the method for calculation of heat generated through degradation of LNAPL. The fourth section describes the model setup and the boundaries that were used in the solute and heat transport model. The last section outlines the statistical analyses that were used to quantify the effects of degradation of LNAPLs on the heat transport in the subsurface.

3.4.1 Field/Site Description

In November 2011, a field demonstration of the STELA was initiated at a former refinery, located adjacent to the North Platte River in Wyoming. Seventeen multilevel samplers, such as what described by Cherry (1983) and Chapman and Parker (2004), were employed in a 15m (50ft) by 15m (50ft) area to determine the contaminant distribution in the aquifer. The depth that each multilevel sampler is monitoring is 4.2m (14ft) which allows for depth discrete gas (CO_2 , CH_4) and water sampling with a total of six ports; three gas sampling in the vadose zone, at the depths of 1.4m (4ft), 1.8m (6ft), and 2.4m (8ft) below the ground surface (bgs), and three groundwater sampling ports in the saturated zone, at the depths of 3m (10ft), 3.6m (12ft), and 4.2m (14ft) bgs. To evaluate the temperature changes spatially and seasonally, six thermocouples were attached to each multilevel sampler right next to each of the sample ports. the current configuration of the former refinery and the location of STELA demonstration are shown in Figure 3.1.

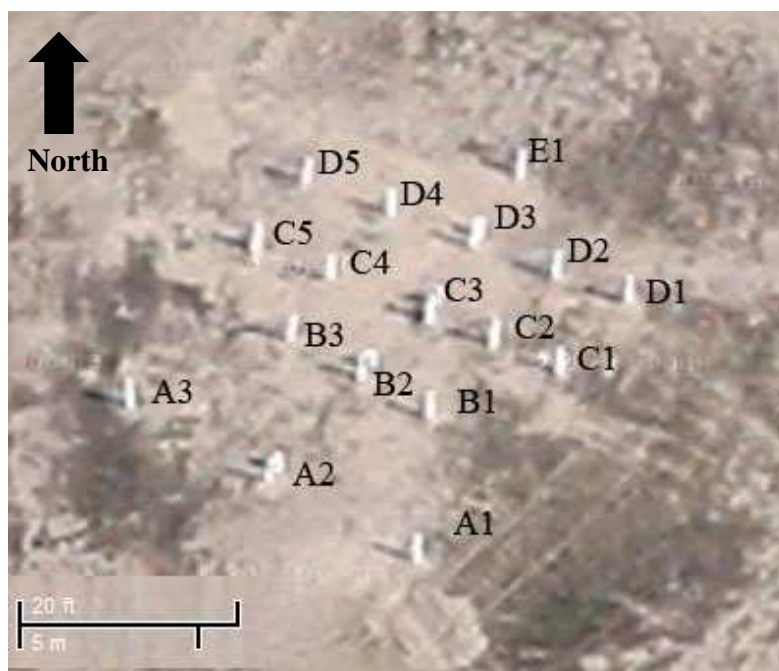
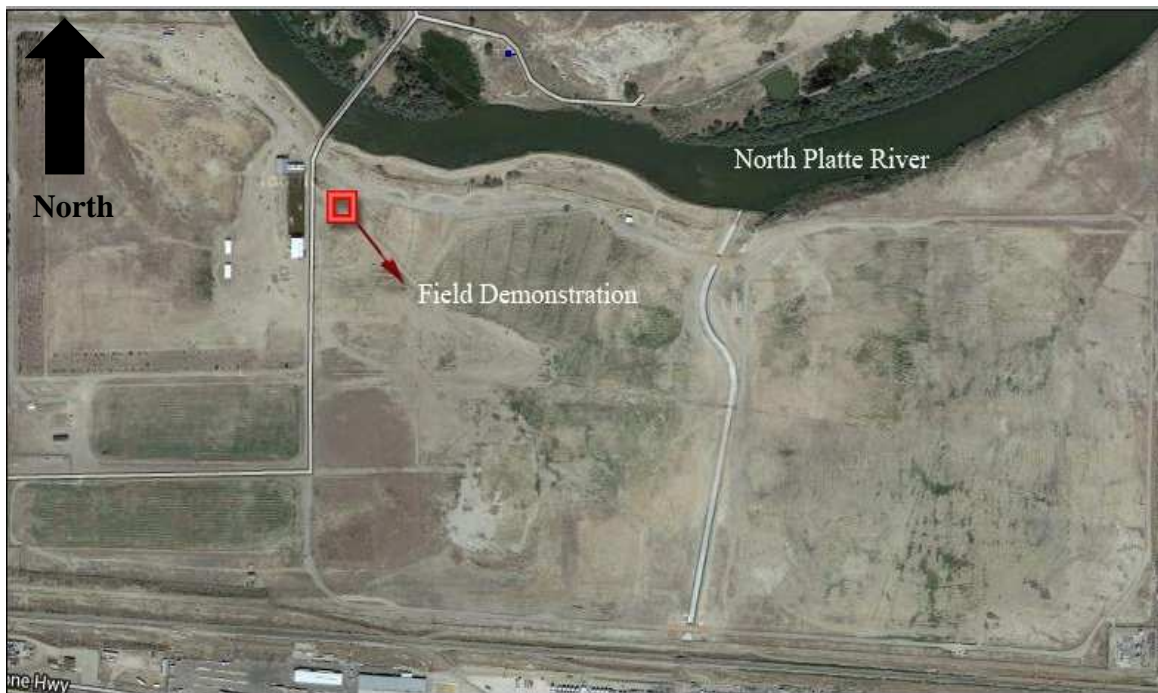


Figure 3.1: Google Earth photo. Top: Current Configuration of the refinery. Bottom: Field Demonstration (Before installation of the heating elements).

In August 2012, ten heating elements were installed along the upgradient edge of the MLS system. Each heating system had a maximum energy input of 200W. The heating elements were distributed in a “Vee” due to the variations in the ground water flow direction. The heating elements are 1m (~3ft) apart. Each heating element consists of a 6m (~20ft) of 16.4w/m (~5w/ft). Arctic submersible heat trace wires (du Alaska Incorporated) wrapped around a 7.62cm (3inches) screen PVC pipe. The heating elements cover 182cm (~6ft) of the saturated zone (8-14ft). Heating elements were energized in September 2012. Figure 3.2 demonstrates the STELA field demonstration layout consisting of both the heating elements and the multilevel samplers. The project time-line is shown in Figure 3.3.

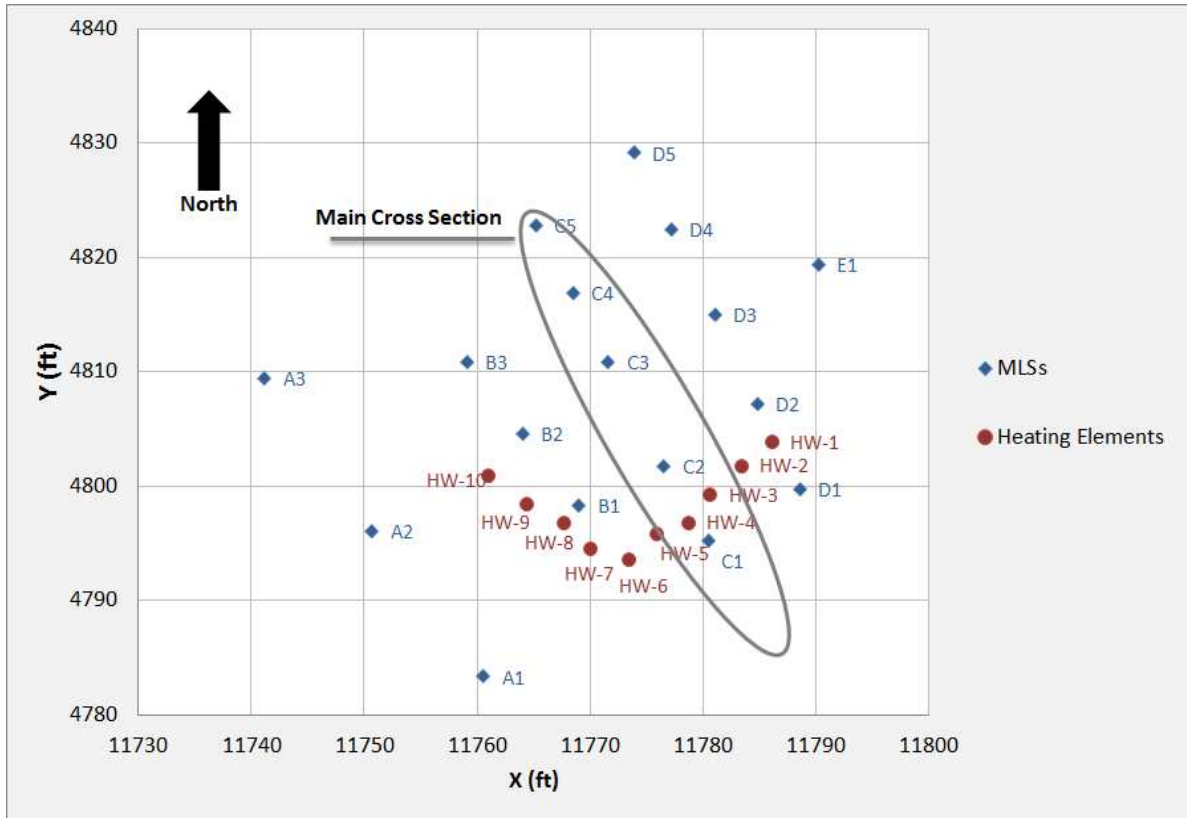


Figure 3.2: STELA field demonstration. In November 2011, seventeen multilevel samplers were installed to monitor the pilot. In September 2012, 10 heating elements employed in two orthogonal lines to deliver heat to the system. The pilot area is 50ft by 50ft.

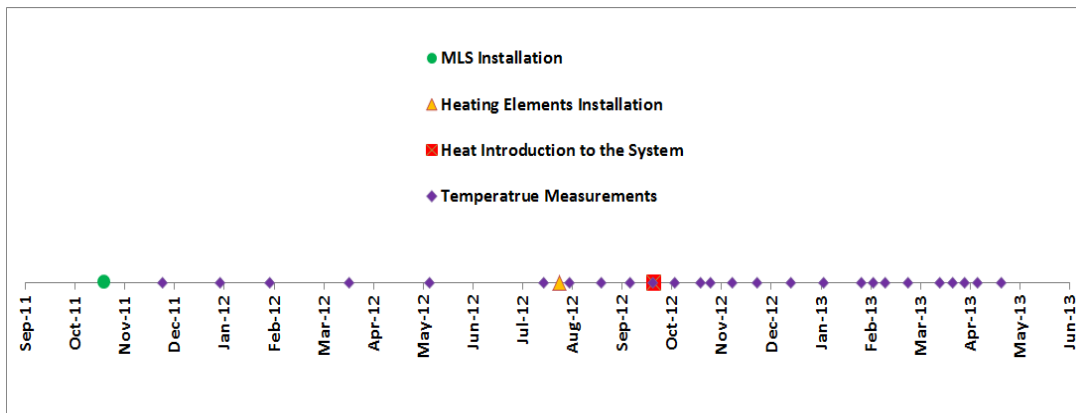


Figure 3.3: STELA Installation and monitoring timeline.

3.4.2 Hydrogeology

During the project, fluctuations in the groundwater flow direction were observed. They are attributed to the seasonal changes and remedial activities that were going on at the site. The groundwater directions varied from the north-northeast and to the northwest (see Figure 2.7). Furthermore, water level was at 3m (9ft) below the ground surface with a seasonal variation of 50cm (1.6ft). Figure 3.4 presents the representative groundwater contour map based on the water level data collected in November 2012. For the purpose of the modeling, the water table was considered at 3m (9ft) below the ground surface and the groundwater flow direction was considered to the North. Soils generally grade from silty to coarse-sand with depth. Figure 3.5 shows the observed soil types in a 3D frame.

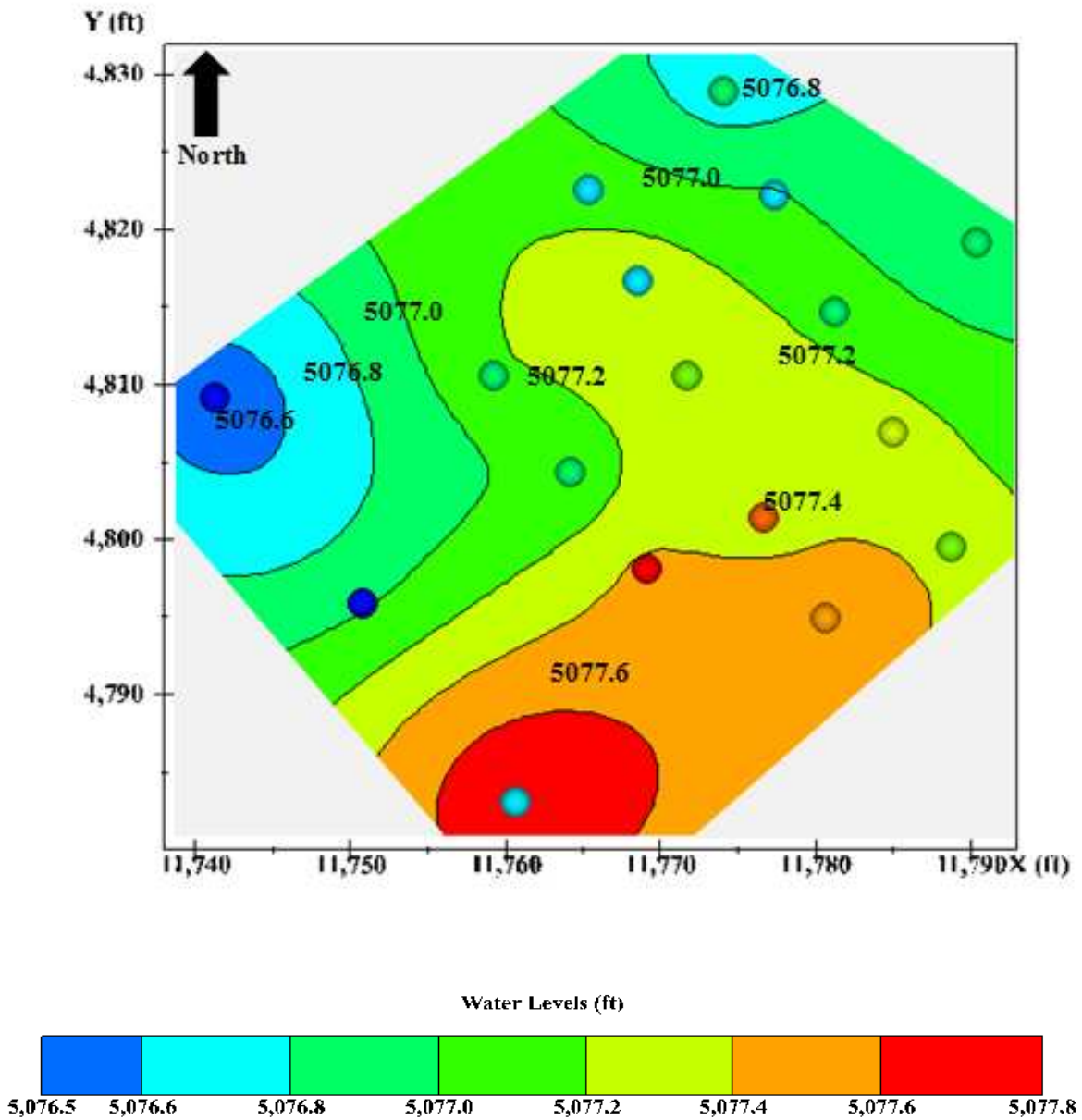


Figure 3.4: Representative Groundwater Contour Map

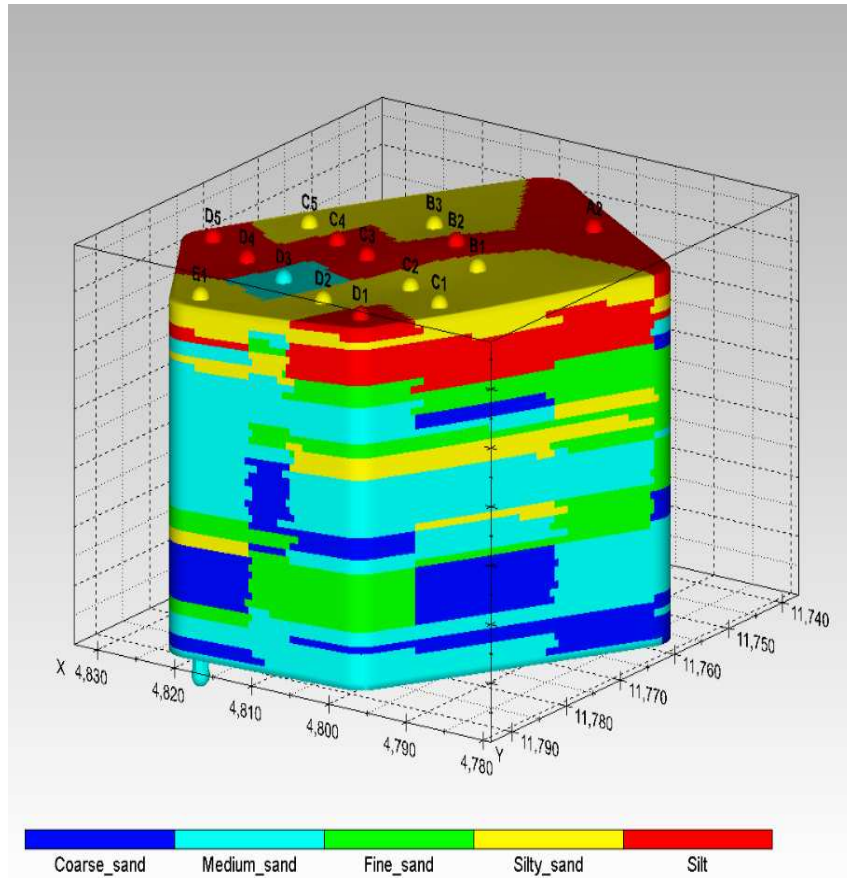
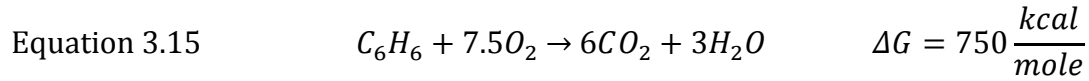


Figure 3.5: Field demonstration reference frame with observed soils.

3.4.3 Natural LNAPL loss rate and energy production correlation

Recent studies by McCoy (2012) suggested that the natural LNAPL losses are heat generating. However, there are controversies over the amount of natural losses at different environments. McCoy studies estimated that the natural LNAPL loss rates range from 800 to 12,000 gal/acre/yr based on data collected from six field sites. Estimates of natural losses of LNAPL reported in current paper and the corresponding thermal energies are calculated using the assumption of benzene (C_6H_6) as the characteristic stoichiometric composition of LNAPL, and an assumed LNAPL density of 0.8 g/ml. Amos et al (2005) illustrated that the mineralization of the LNAPL is a complex process; however, for the simplicity and practicality, the following

equation has been considered as a conceptual mineralization of the benzene assuming that all the benzene is converted to the CO₂ and H₂O, ultimately:



Using the stoichiometry and considering the above assumptions, corresponding energy releases of the LNAPL mineralization can be estimated. One of the objectives of this paper is to verify the effects of the natural LNAPL losses on the subsurface temperature, and to provide an estimation of the natural LNAPL loss rates that occurs at the refinery. To do so, five different scenarios were simulated using the MT3DMS codes. Each scenario considers different LNAPL loss rate occurs at the subsurface. These LNAPL loss rates are as follows: No LNAPL loss rate, 5,000, 7,500, 10,000, and 12,000gal/acre/yr. The corresponding energy releases of each scenario was calculated and shown in Table 3.1. The differences of each scenario and the verification of the best match to the model were quantified by using the statistical methods presented in the next section.

Table 3.1: LNAPL loss rates and corresponding energy releases for each scenario

Scenario	LNAPL loss rate (gal/acre/yr)	Energy Release (KJ/yr in the field demonstration)
1	0	0
2	5,000	2.80E+07
3	7,500	4.20E+07
4	10,000	5.60E+07
5	12,000	6.70E+07

3.4.4 Model Setup

A 3-dimensional domain consists of 56 columns, 56 rows, and 20 layers was used to simulate the heat transport at the subsurface via coupling the MT3DMS and MODFLOW code. The plan view of the gridding is shown in Figure 3.6. The columns width and rows length are 150cm (5ft), and layers thicknesses are 30cm (1ft). However, the width and length of the 50 central cells were tighten to 30cm (1ft) to evaluate the temperature variations more accurately at the field demonstration area.

The simulation was done for 1460 Days (four years starting from January 1st 2011 to December 30th 2014) with time steps of 1 day. The model got to the equilibrium by using back ground conditions in the first year, then gets calibrated using continuous and non-continuous measured temperature in the second year, and finally anticipates temperature trends for the following two years.

The next two subsections describe the groundwater flow and heat transport models including the modeled domains and boundary conditions.

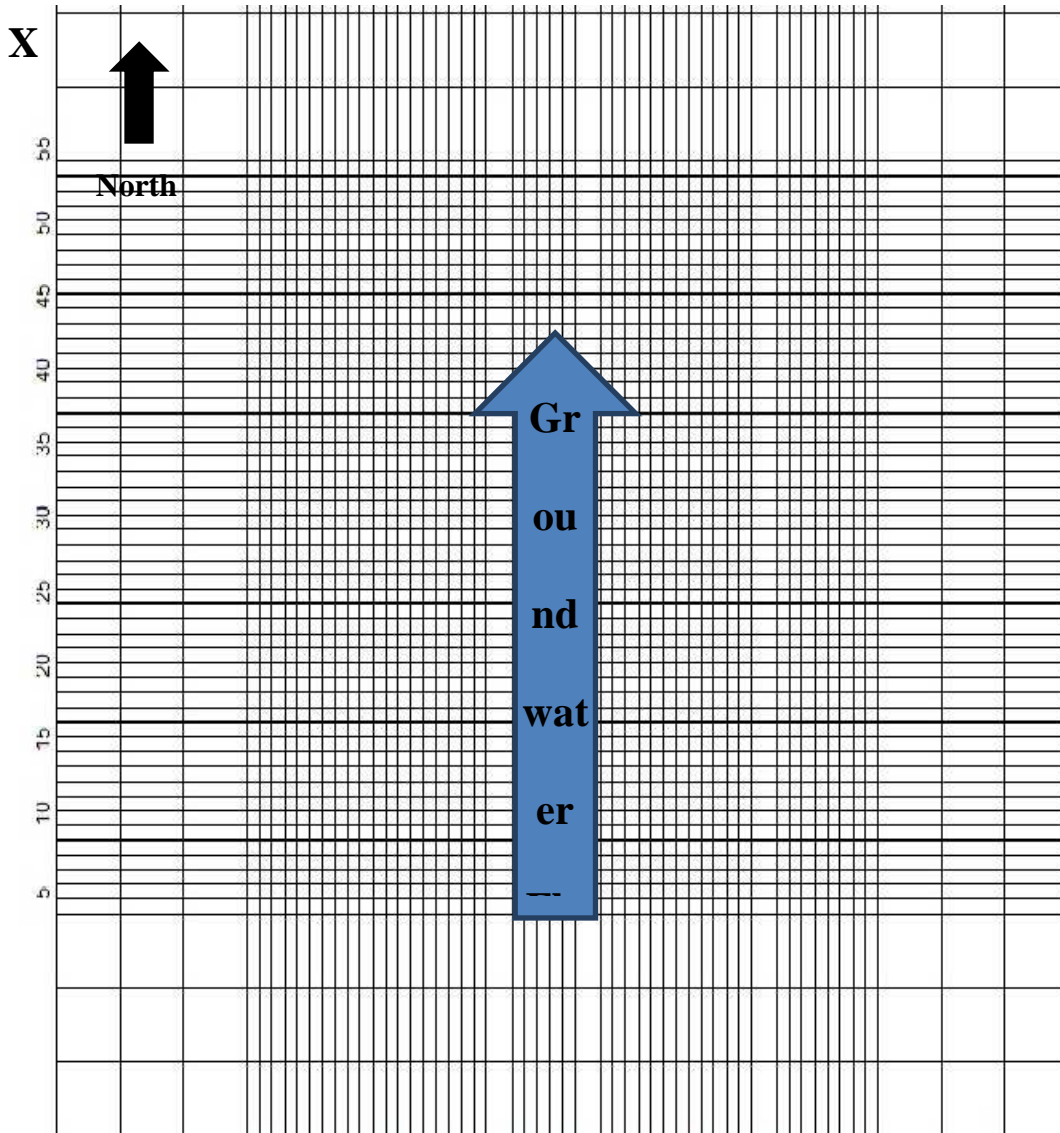


Figure 3.6: Model gridding plan view.

3.4.4.1 Groundwater Flow Model

Y

Groundwater flow was simulated using MODFLOW code. The groundwater flows toward the north and is considered orthogonal to the columns at the seepage velocity of 0.3 m/day (1ft/day). This number is based on best available estimate of hydraulic conductivity, porosity, and hydraulic gradients. To establish the uniform velocity of 0.3 m/day, the South and North boundaries prescribed as constant-head boundaries and arbitrary head values were

assigned to these cells. Also, the West and East boundaries considered as the No-Flow boundaries. Furthermore, the top and bottom boundaries were assumed as the No-Flow boundaries. Figure 3.7 shows the plan view and a typical cross-section of the designed model and the associated boundaries.

The input parameters for the flow model are presented in the Table 3.2. The porosity of the aquifer was chosen 0.3, which is a typical number for quartz deposits. To represent the unsaturated zone in the simulation; the hydraulic conductivity at the 9 top rows was set at very low number (10^{-30} ft/day). Hence, this zone is practically impermeable and no flow occurs (the advective term of heat transfer will be zero) However, due to the diffusivity coefficients, heat flow can happen by diffusion.

Table 3.2: Input parameters for the groundwater flow model (MODFLOW)

ID	Parameter	Symbol	Unit	Unsaturated zone	Saturated zone
1	Hydraulic Conductivity (Horizontal)	Kx	m/day	1.E-30	0.9
2	Hydraulic Conductivity (Vertical)	Kz	m/day	1.E-30	0.9
3	Porosity	θ	-	0.3	

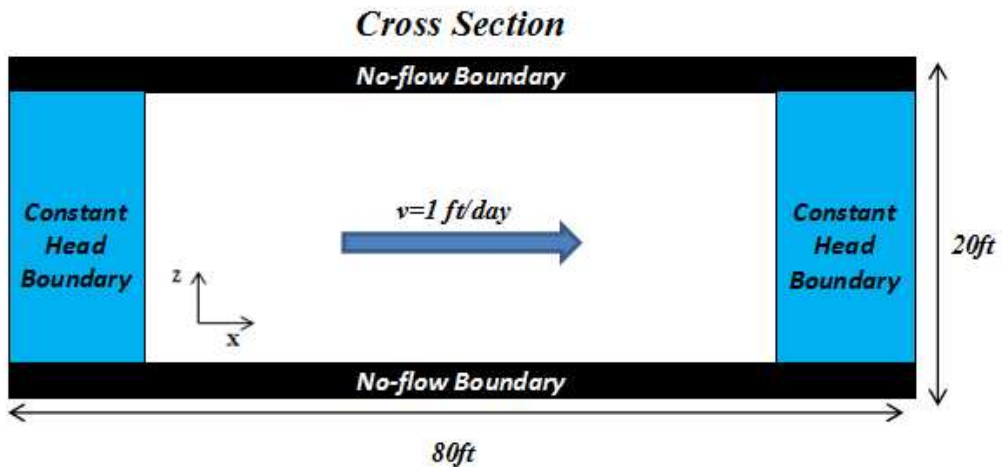
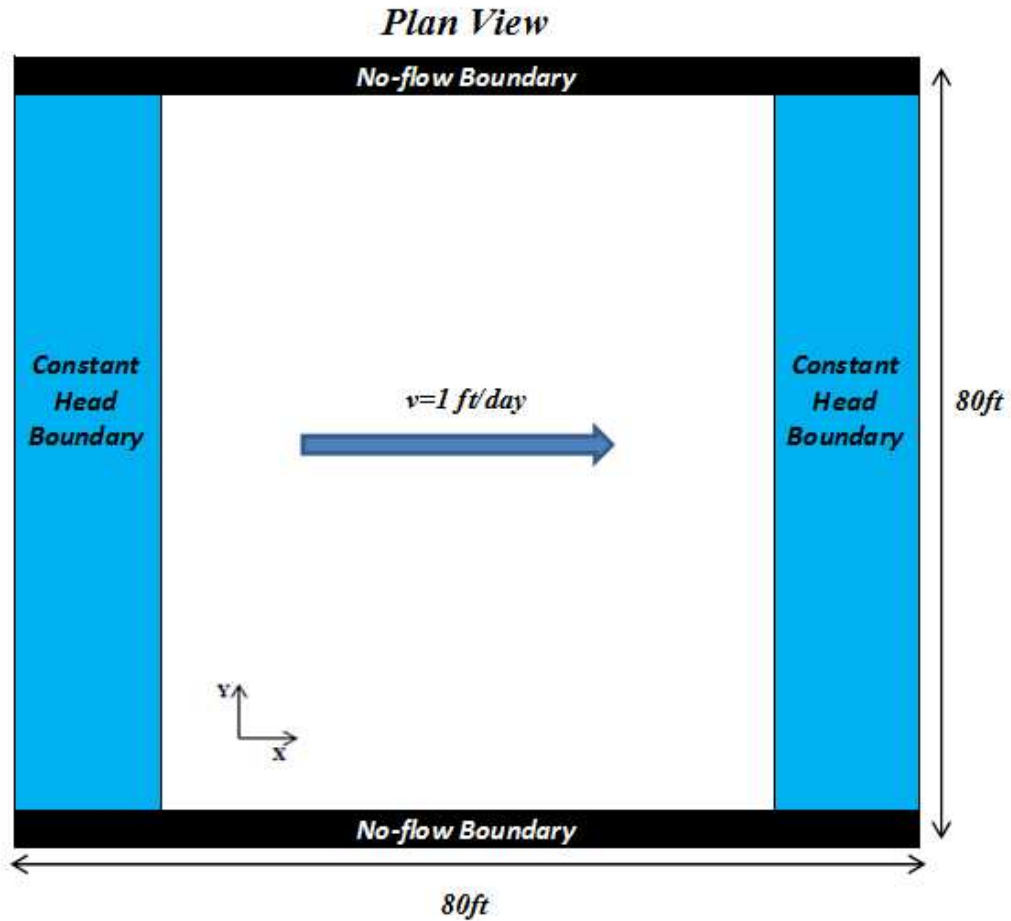


Figure 3.7: MODFLOW boundary conditions. Top: Plan view of the domain with the flow boundary conditions. Bottom: Cross-section of the domain with the flow boundary condition. Arbitrary constant heads at the boundaries was chosen to establish the velocity of 1 ft/day.

3.4.4.2 Heat Transport Model

The Heat transport was simulated using MT3DMS code. For the heat transfer model, the South boundary was prescribed by the specified-temperature at a daily interval and was defined by the measured temperatures in the wells C1 and A1. The North boundary also treated as the specified-temperature at a daily interval and was defined by the measured temperature in Wells A3 and C5. Also, the West and East boundaries assumed as the No-Flow boundary. In addition, the top boundary was prescribed by specified-temperature at a daily interval to represent the surface soil temperature by using ambient air temperature from Casper, Wyoming. Figure 3.9 shows the ambient air temperature changes. Moreover, the bottom layer boundary was defined as the constant temperature boundary, set at 12⁰C. Figure 3.8 presents the plan view and a typical cross-section of the heat transfer model domain with the regarded boundary conditions. Based on McCoy (2012), at depths below 6m (20ft), the temperature is not affected by the seasonal changes and it remains constant at 12⁰C. (McCoy 2012)

It should be noted that the collected ambient air temperature data for the period of January 1st 2011 to December 30th 2012 and the temperature data that were measured at the wells for the period of November 2011 to December 2012 were used to approximate the top boundary temperature for the period of the January 1st 2013 to December 30th 2014 and the sides boundary conditions, respectively. Analysis of three years temperature data records of Casper ambient air temperature from January 1st 2010 to April 30th 2013 revealed a very similar annual pattern in the ambient air temperature.

The input parameters for the heat transport model are listed in Table 3.3. Referred to Langevin (2008), the water and soil density are 1000 Kg/m³ and 2700 Kg/m³, respectively, and

the heat capacity is 4186 J/(Kg K) and 710 J/(Kg K), respectively. Hillel (1982) and de Vries (1975) specified the thermal conductivity of the quartz is 8.8 W/(m K) and the thermal conductivity of water is 0.58 W/(m K). By employing these numbers in *Equation 3.12* and *Equation 3.13*, thermal distribution coefficient and thermal diffusivity were calculated as 0.00017m³/Kg and 0.27m²/day, respectively.

Table 3.3: Input parameters for the heat transport model (MT3DMS)

ID	Parameter	Symbol	Unit	Values
1	Water Density	ρ_f	Kg/m ³	1000
2	Soil Density (Quartz)	ρ_s	Kg/m ³	2700
3	Bulk Density	ρ_b	Kg/ft ³	1900
4	Specific Heat capacity of Soil (Quartz)	C_s	J/Kg/K	710
5	Specific Heat capacity of Fluid (Water)	C_f	J/Kg/K	4186
6	Fluid Thermal Conductivity (Water)	$K_{T\text{-fluid}}$	W/m/K	0.58
7	Soil Thermal Conductivity (Quartz)	$K_{T\text{-solid}}$	W/m/K	5.38
8	Bulk Thermal Conductivity	$K_{T\text{-bulk}}$	W/m/K	3.94
9	Thermal Diffusivity	D_m^T	m ² /day	0.27
10	Thermal Distribution Factor	K_d^T	m ³ /Kg	0.00017

Ten heating elements have been employed in the system at 6 layers orthogonal to the groundwater flow. The heating elements prescribed as the specified temperature boundaries at the constant temperature of 30°C. As mentioned above, the heating elements are located at the depth of 2.7m (~9ft) to 4.2m (~14ft) below the grade, and are thermostatically controlled at 30°C. Thus, at the upgradient of the domain, at each layer from 2.7m to 4.2m below the grade, 10

cells were assigned as the heating elements, and prescribed as the specified temperature boundary with the constant temperature of 30°C. The heating elements energized since September 27th, 2012.

The simulation was done for five different scenarios: the basic scenario considering that LNAPL losses do not generate heat at a significant level that affect the system. The other four scenarios represent the effects of exothermic natural LNAPL losses on the system. Model simulates four different scenarios; LNAPL loss rates of 5,000, 7,500, 10,000, and 12,000gal/acre-yr. Soil core collection at the site showed that the LNAPL zone (the area with the TPH of a 1,000mg/L and higher) is 1.2m (4ft) to 4.0m (13ft) below the ground surface. To introduce the exothermic LNAPL losses to the system, the cells at the layers of 4ft to 13ft below the grade were associated as the heat sources by using the new source and sink term for heat transport in MT3DMS in the sink & Source Mixing Package. As explained in Hecht-Méndez et al., 2010, the type of source set to a mass-loading source (ITYPE0=15).

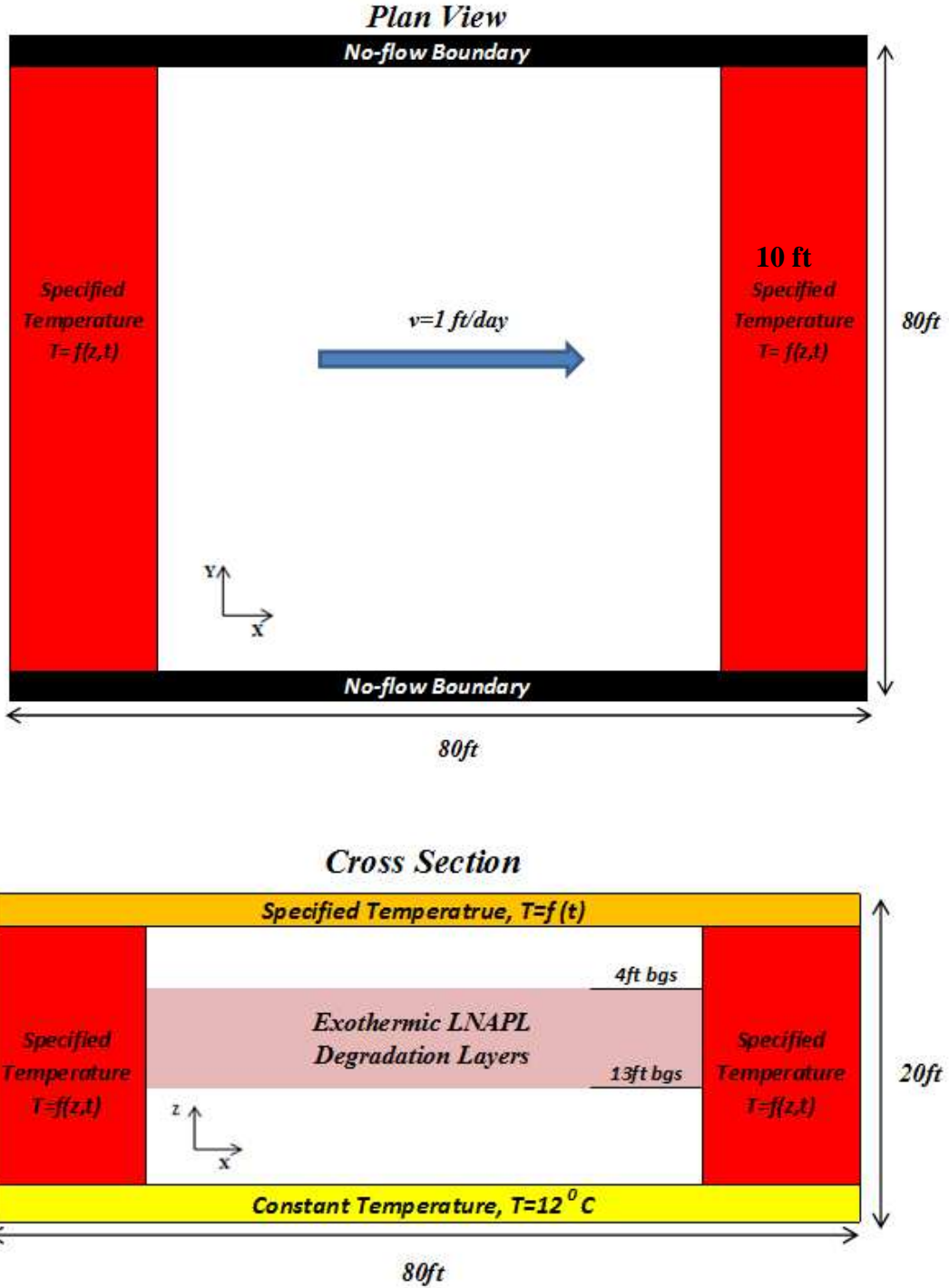


Figure 3.8: MT3DMS boundary conditions. Top: Plan view of the domain with the temperature boundaries. The South boundary was prescribed by the specified-temperature at a daily interval and was interpolated by the measured temperatures in the wells C1 and A1. The North boundary also treated as the specified-temperature at a daily interval and was interpolated by the measured temperature in Wells A3 and C5. Bottom: Cross-section of the domain with temperature boundaries. The top boundary is prescribed by specified temperature using the ambient air temperature at the site. Following McCoy (2012), the bottom temperature boundary is fixed at 12°C .

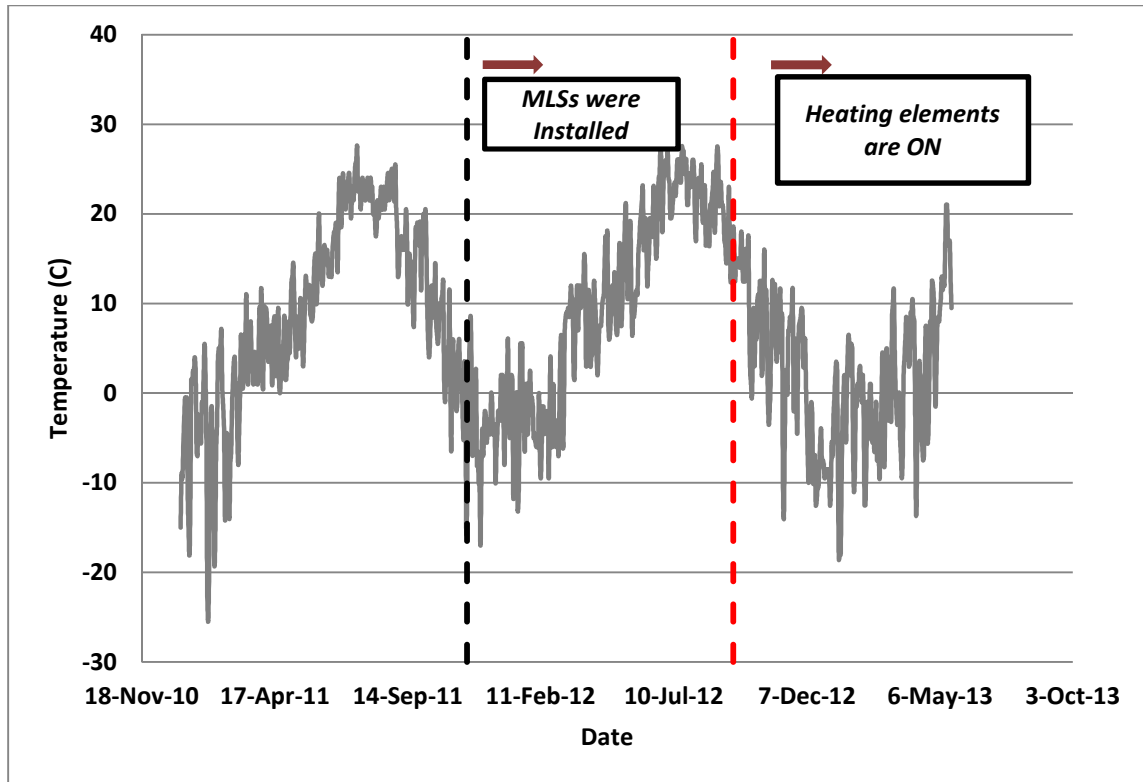


Figure 3.9: Casper ambient air temperature. The top boundary was prescribed by specified-temperature at a daily interval to represent the surface soil temperature by using Casper ambient air temperature.

3.4.5 Quantifying the effects of exothermic biodegradation

Two statistical analyses were used to quantify the differences between the simulations with different LNAPL loss rates. These are the Nash-Sutcliffe efficiency (NSE), and root mean square error (RMSE)-observations standard deviation ratio (RSR). These methods are described in the following sections.

3.4.5.1 Nash-Sutcliffe efficiency (NSE)

The Nash-Sutcliffe efficiency (NSE) analysis or the method of efficiency, which described by Loague and Green (1991) is a normalized statistics that determines the relative

magnitude of the residual variance compared to the measured data variance (Moriassi et al. 2007).

NSE is computed as shown in *Equation 3.16*:

$$\text{Equation 3.16} \quad NSE = 1 - \frac{\sum_{i=1}^n (Y_i^{obs} - Y_i^{sim})^2}{\sum_{i=1}^n (Y_i^{obs} - Y^{mean})^2}$$

where Y_i^{obs} is the i th observation for the constituent being evaluated, Y_i^{sim} is the i th simulated value for the constituent being evaluated, Y^{mean} is the mean of the observed data for the constituent being evaluated, and n is the total number of observations. NSE ranges between $-\infty$ and 1.0, with $NSE=1$ being the optimal value. The performance rating for NSE is provided in *Table 3.2*.

3.4.5.2 RMSE-observations standard deviation ratio (RSR)

Root mean square error (RMSE) is one of the commonly used error index statistics. It is commonly accepted that the lower the RMSE the better the model performance. RSR standardizes RMSE using the observations standard deviation. RSR is calculated as the ratio of the RMSE and the standard deviation of the measured data, as shown in the *Equation 3.17*:

$$\text{Equation 3.17} \quad RSR = \frac{RMSE}{STDEV_{obs}} = \frac{\sqrt{\sum_{i=1}^n (Y_i^{obs} - Y_i^{sim})^2}}{\sqrt{\sum_{i=1}^n (Y_i^{obs} - Y^{mean})^2}}$$

RSR varies from the optimal value of 0, which indicates zero RMSE or residual variation and therefore perfect model simulation, to large positive values. The lower the RSR value, the lower the RMSE value, and the better the model simulation performance (Moriassi et al. 2007). The performance rating of RSR is provided in *Table 3.4*.

Table 3.4: General performance ratings for statistics (Moriassi et al. 2007)

Performance Rating	Statistical Methods	
	NSE	RSR
Very Good	0.75-1	0-0.5
Good	0.65-0.75	0.5-0.6
Satisfactory	0.5-0.65	0.6-0.7
Unsatisfactory	0-0.5	0.7-1

3.5 Results

This section consists of three subsections. The first sub section evaluates the LNAPL losses effects on the subsurface heat flow. The second sub section addresses the temporal temperature variations at the grade. Finally, the last sub section anticipates the long-term performance of the STELA field demonstration.

3.5.1 Evaluation of the LNAPL Losses and Related Effects on the Subsurface Temperature

To show the degree of significance of exothermic LNAPL loss rates on the heat flow at the subsurface, the model was calibrated to the field data and simulations were conducted for five different scenarios. The first scenario assumes that the LNAPL losses do not affect subsurface temperature significantly. In the other four scenarios, LNAPL losses were assumed to be 5,000, 7,500, 10,000, and 12,000gal/acre/yr. The model was calibrated with respect to each of these loss rates.

Estimation of the amount of LNAPL loss rates at the site were done by using the statistical analysis methods that were described, previously. The NSE and RSR values were calculated based on the model simulation results and observed temperatures for all the five

scenarios. The NSE and RSR values for each scenario were compared together to find the best fitting of the simulation results and the observed temperatures. The LNAPL loss rate contributed to the scenario with the best NSE and RSR value was chosen as the estimation of the amount of LNAPL loss rates at the site.

Statistical results are shown in Figure 3.10. *Graph a.* shows the results of NSE analysis. As mentioned in the previous sections, the higher the NSE number the better model fits to the observations, and the NSE numbers above 0.75 (dashed line) shows the favorable match of the simulation results and the observations. It could be seen in the graph that the NSE number for the scenario that consider no losses at the subsurface are below the satisfactory level (NSE number for this scenario is 0.64); however, for the scenarios considering 5,000gal/acre/yr. and 7,500gal/acre/yr., the NSE numbers are above 0.75 (NSE numbers of 0.80 and 0.81, respectively). *Graph b.* shows the results of the RSR analysis for five different scenarios. The lower the RSR numbers the better the model fits to the observations. The RSR values below 0.5 (dashed line) shows the favorable fitting of the simulation results to the field data. The same interpretation that achieved from NSE analysis can be seen from the RSR numbers. The RSR number in the scenario with no LNAPL losses is above the threshold which means that the results are in the unsatisfactory range (The RSR value is 0.65). On the other hand, the RSR numbers for the scenarios considering 5,000gal/acre/yr. and 7,500gal/acre/yr. are below 0.5 and satisfy the RSR analysis criteria (RSR values of 0.45 and 0.44, respectively). Again, considering 5,000 gal/acre/yr. and 7,500gal/acre/yr. LNAPL losses at the site shows a better match of the model results to the field data.

Thus, the calibration to the field data and model simulations demonstrated that the LNAPL losses at the subsurface can change the heat distribution at the system and can affect the

system design. In addition, comparison of four different scenarios with different LNAPL loss rates estimates that the losses at the subsurface are happen at the rates in the range of 5,000gal/acre/yr. to 10,000gal/acre/yr. These anticipated loss rates are in consistent with the previous numbers that were measured by McCoy (2013) in 2012 (~800-12,000gal/acre/yr.)

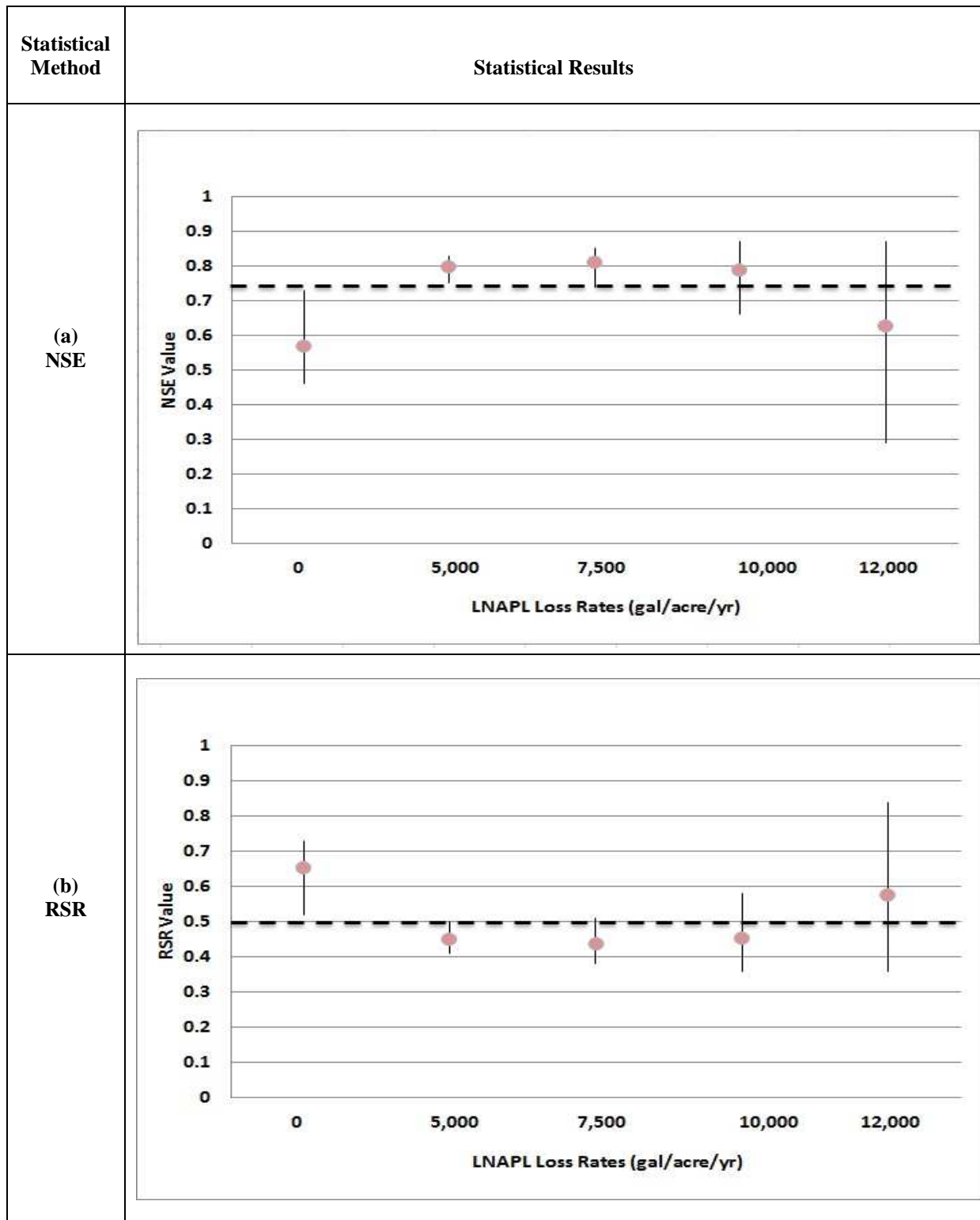


Figure 3.10: Summary of the statistical quantifications (a) NSE. The higher the NSE number, the better the model fits. The NSE numbers above the dashed line shows the favorable match of the simulation results and the observations. (b) RSR. The lower the RSR number, the better the model fits. The RSR numbers below the dashed line shows the favorable match of the simulation results and the observations.

3.5.2 Addressing of temporal temperature variations

Figure 3.11, graphically, compares the simulation temperature contours and the observed temperature contours at the main cross-section that consists of the following wells: C1, C2, C3, C4, and C5. The figures on the left hand side demonstrate the observation isotherms and the ones on the right hand side show the simulation isotherms. The simulation results belong to the scenario considering 7,500gal/acre/yr. LNAPL loss rates. To address how the seasonal changes affect the heat flow, temperature contours were calculated and demonstrated at five different months of the year. In addition, *Graphs d.1, d.2, e.1, and e.2* show the temperature contours at the period of the year that the heating elements were activated. These graphs address the ability of the model to demonstrate the effects of the heating elements on the heating distribution through the subsurface porous medium.

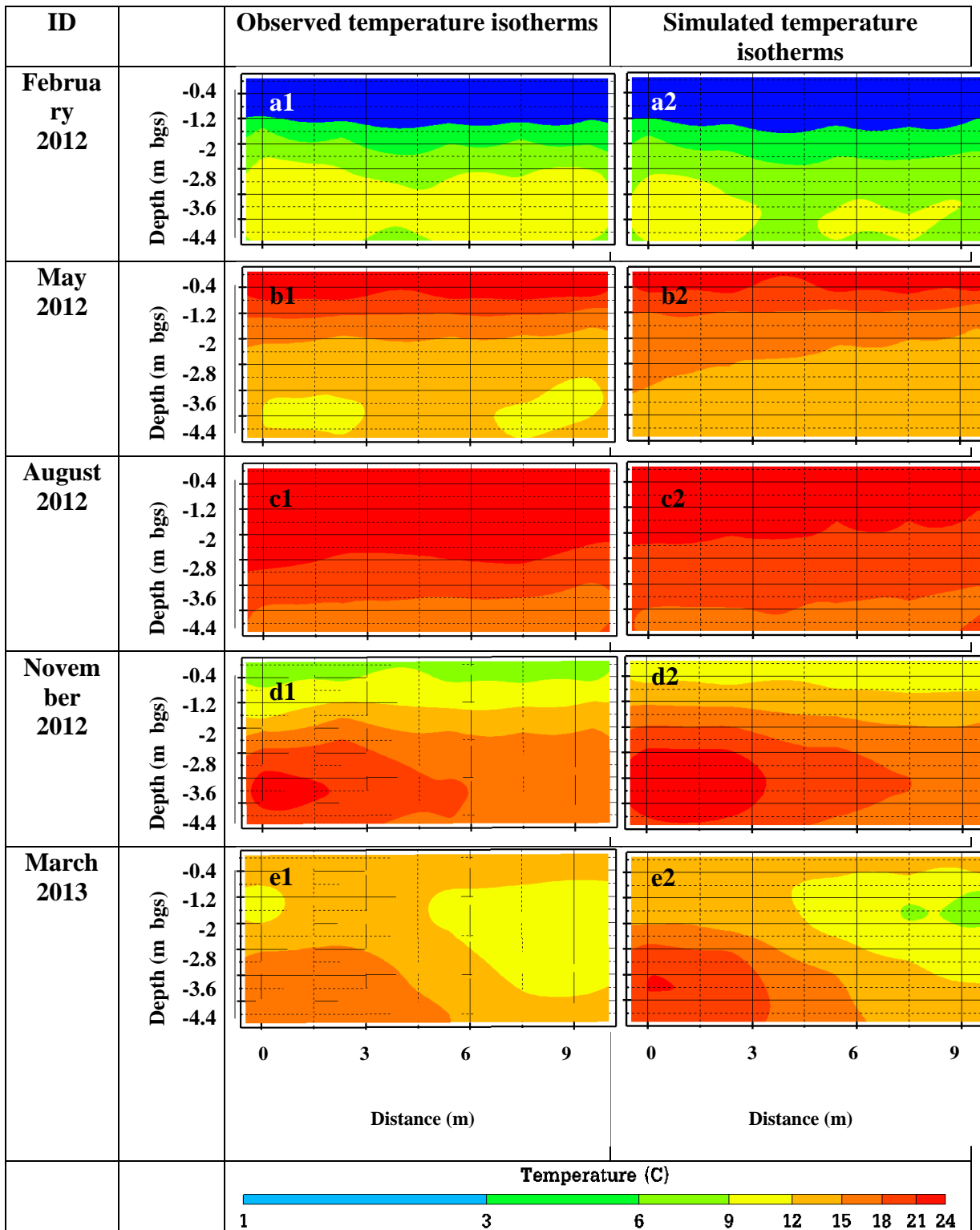


Figure 3.11: Comparison of observed temperature contours and simulation temperature contours. MT3DMS simulation results were chosen at five different times to characterize the seasonal change effects on the heat flow.

Graph a.1 and *a.2* show the temperature isotherms in the February (winter). It can be seen that due to the cold ambient air temperature, the coldest temperature occurs at the shallower depths, while deeper points show higher temperatures. Increasing in subsurface temperature can be seen through the spring and summer, May and August, respectively. In addition, it can be seen that the higher temperatures occur at the shallower depths due to the higher ambient air temperatures in compare with the winter. The temperature isotherms in *Graphs a.1, a.2, b.1, b.2, c.1, and c.2* demonstrate the successful calibration of the model simulations to the field data. As it can be seen in these graphs, although temperature is varying through the depth, it is almost constant at the same depths and alongside the cross-section.

Graphs d.1, d.2, e.1, and e.2 address the ability of the model to show the effect of the heating elements on the subsurface system. In these graphs, the temperature changes can be seen on both of the vertical and horizontal directions. The reason of temperature changes alongside the cross-section includes both the groundwater horizontal movement (advection component of the heat transport) and the diffusion of the heat through the porous medium and the soil grains. However, the vertical changes in the temperature happen mostly because of the diffusion. *Graphs d.1 and d.2* show the temperature isotherms in November 2012 which is two months after the heat was introduced to the system. As it can be seen in the figures, the heat started to propagate through the system. The field data shows that the temperature can be sustain above 18⁰C up to 4.5m downgradient of the heating elements. The simulation anticipated that the heat can be sustained above 18⁰C up to 6m downgradient of the heating elements. *Graphs e.1 and e.2* show the temperature isotherms in March 2013, after 5 months that the heating elements started to introduce heat to the system. Comparing *graphs e.1 and e.2* with *graphs d.1 and d.2* demonstrate that the margins of heat propagation due to the heating elements have been

shortened. The shortening in the heat propagation and lower temperatures in March in compare with the November temperature is due to the cold ambient air temperature. The model was successful to show the shortening in the heat propagation margins; however, the simulation results anticipate higher temperatures than the field data.

3.5.3 Anticipation the long-term performance of the STELA field demonstration

The overarching objective of the STELA is to design a pilot that extends the period of the year that temperature at the saturated zone is above 18C. The period of the year that temperature is above 18C was called “effective season”. To design a successful heating system to sustain the temperature in a target range, anticipating the long-term performance of the heating system is an important challenge. To predict the long-term thermal conditions, the model was simulated for four years, from January 2011 to December 2014. The model gets calibrated by using the observation temperature data from November 2011 to May 2013. Then, the calibrated model was used to predict the temperature variations for the period of April 2013 to December 2014.

The simulated temperature variations and the observed temperature changes for the period of January 2011 to December 2014 are shown in Figure 3.12. This data belongs to Well C3, 5m downgradient of the heating elements, at the depth of 14ft bgs. The effective season are shown by gray shaded boxes in this figure. The black line from the MT3DMS simulation can be compared directly with the dashed line from the observations. Overall, there is a striking similarity between the MT3DMS results and the observation data. The observed temperatures show 60 days of effective season in 2012, started in October to the end of November. The calibrated model successfully demonstrated the same period of the year, as the effective season. The simulation results, also, predicted 120 days of effective season, July to November, in 2013,

and 150 days of effective season, July to December, in 2014. Thus, a growing in the length of the effective season is shown by MT3DMS results. The increasing in the length of the effective season stems from the accumulation of the heat by keeping the heating elements activated for several years. The ability of this model to predict the long-term performance of STELA makes this model a useful method for STELA full-scale design and evaluation.

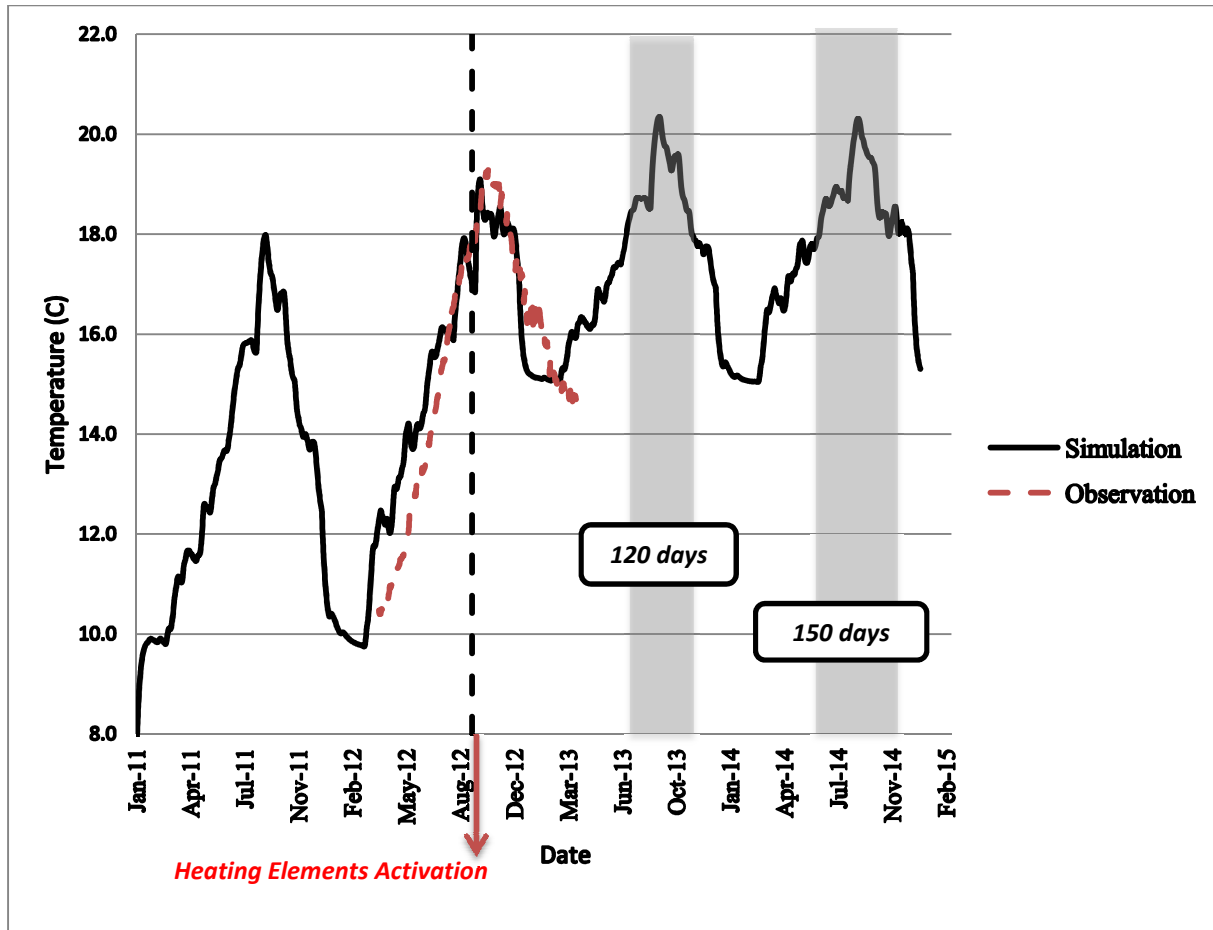


Figure 3.12: MT3DMS simulation results at Well C3-14ft bgs (Prediction of the effective season). The simulation results were calibrated to observed temperature in 2012. At 5m downgradient of the heating elements, the simulation results predict an effective season of 120 days and 150 days in 2013 and 2014, respectively.

3.6 Conclusions

In this paper a heat transport model was developed via coupling the MODFLOW and MT3DMS to support the STELA field demonstration design. The model provides a tool to evaluate and/or design full-scale STELA systems. Moreover, it addresses temporal temperature variations at grade. Furthermore, the model evaluates the effects of the heat that generated through degradation of LNAPL on the heat transport in the subsurface. Lastly, the model anticipates long-term performance of the STELA field demonstration.

The observed data from the field demonstration were consistent with the output of the heat transfer model. Both the model results and field data shows the similar heat propagation pathway due to the heat that introduced to the system via the heating elements. However, the model simulation overestimates the distance that heat can propagate through the subsurface. This could be because of the divergences in the groundwater flow due to the background pumping and drainages on the site.

Moreover, five different scenarios were simulated to clarify the effect of the LNAPL degradation on the heat flow through the system. The statistical analysis on the MT3DMS simulations shows that the LNAPL losses at the subsurface can change the heat distribution at the system. In addition, comparison of these scenarios shows that the losses at the subsurface are in the range of 5,000 to 10,000gal/acre/yr. These anticipated loss rates are in consistent with the previous numbers that were calculated by McCoy (2013) in 2012 (~900-11,000gal/acre/yr.)

Lastly, the developed model, accurately, predicted 60 days of the effective season in 2012. Also, the simulation results anticipate that by keeping the heating system activated for three years, the effective season will increase each year. Model results suggested 120 days and

150 days of effective season for 2013 and 2014, respectively as compared to 60 days in the first year. The ability of the model to anticipate the effective season for the next years makes the model a useful tool to design and evaluate the future STELA systems. Taking advantage of the developed model to design a full-scale STELA field demonstration as a remedy strategy is the purpose of the future works.

4. CONCEPTUAL DESIGN AND COSTS FOR A 1-HECTARE STELA SYSTEM

4.1 Introduction

This section presents a conceptual STELA design. The purpose is to explore the cost of a STELA system at a 1-hectare site in a former refinery in Wyoming. The conceptual site is a 100m by 100m square with depth of 5m. The objective of the STELA design is to accelerate the LNAPL depletion. Table 4.1 summarizes the conceptual site characteristics and designs.

The cost of a remedial technology is one of the key factors in determining its applicability. The remedial technology's cost versus the benefits that it provides will often be a deciding factor in its implementation. The objectives of this section are to provide information on the factors that derive the economics of STELA systems, to provide information that can be used to develop site-specific cost estimates, and to provide a range of cost that can be expected for this technology.

Cost analysis methods follow Simpkin et al. (1998). First of all, a general discussion of the components contributing to STELA remediation system costs is presented. Next, a summary of the costs and options to reduce the costs are addressed. Next, a range of the costs normalized to volume of soil treated, volume of LNAPL removed, and area treated is presented. Lastly, estimated costs for STELA are compared to cost for other LNAPL remediation technologies.

Table 4.1: Site characteristics and system designs for base case.

Site Characteristics	
Type of Site	A former refinery located along the North Platte River, Wyoming. The refinery processed crude oil from local sources into gasoline and diesel. The refinery was decommissioning in the mid 1990's.
Contaminants	Weathered gasoline and diesel
Size of Target Area	1 hectare (approximately 2.5 acres), Square-shaped plot, 100m by 100m.
Hydrogeological Setting	Silt to sand deposit, depth to the groundwater is approximately 3m (9ft).
Target Depth	LNAPL presents from 1m (~3 ft) to 4m (~12 ft) below the ground surface (bgs). Amount of LNAPL in place is 50,000gal/acre (470000 L/hectare)
System Design	
Objective	Near complete depletion of LNAPL
Heating Elements	10 trenches including the heating elements with the length of 100m. The trenches are 10m apart from each other. The heating elements will be employed at the water table.
Energy Source	Line Power will deliver up to 20,000 watts of energy.

4.2 Cost components

The following sections present the basis for key cost components.

4.2.1 Site characterization

Site characterization often will be needed prior to the full-scale implementation of a remedial system. The cost for the site characterization will depend on the amount of information previously obtained and the design requirements. The information that is needed for the site

characterization includes type of site, contaminants, size of target area, hydrogeological setting, and target depth.

This site has been relatively well characterized due to the STELA field demonstration and other remedial methods that are going on. Additional soil borings and monitoring wells will be installed to resolve trenching depth. Soil samples and LNAPL will be collected for laboratory testing from these samples.

4.2.2 Laboratory testing

Site specific laboratory testing must be conducted to select, design, and evaluate a STELA system. The temperature target range for the STELA purposes will be achieved through the microcosm studies. The optimal temperature is site specific and depends on the indigenous microbial community present. For this hypothetical example, the optimal temperature for biodegradation of LNAPL has already been determined based on Zeman's (2012).

4.2.3 Numerical Simulations

Numerical simulations can be helpful in evaluating the potential removal capacity of a full-scale design, in designing a field demonstration, and in designing the full-scale system. The model will be used to aid in the design of the system by providing the timing that need for the system to get to highest performance, the type of the heating elements, the heating elements distribution, and the required energy for the heating system.

For the purpose of this example, a 3-D model will be used to simulate the performance of the STELA system. MODFLOW will be used to model the groundwater flow. MODFLOW via coupling with MT3DMS will be used to model the heat transport at the subsurface porous

medium. The cost for the running the simulation model includes cost of the software, operator time, and computer time.

4.2.4 Field demonstration

Field demonstrations are a necessary component of the STELA systems. The costs for field demonstration can be substantial, partly because of the need to collect sufficient performance data to verify the effectiveness of the system. For this hypothetical site, the field demonstration was described in Chapter 2. Briefly, the field demonstration includes seventeen multilevel samplers. Each multilevel sampler consists of six ports. Three of the ports are in the vadose zone, while three ports are at the saturated zone. Water samples and gas samples were collected through these ports. Also, a thermocouple was attached to each port for the temperature measurements. Furthermore, water levels were measured through the multi-level samplers. In addition, before installing the multilevel samplers, soil cores were collected from all of the wells to determine the baseline contaminant concentrations. To deliver heat to the system, 10 heating elements were deployed in two perpendicular lines. Each heating element is able to deliver up to 200W of energy to the system.

4.2.5 Facility design

It is assumed for this example that the objective of the STELA system is near complete LNAPL depletion.

When the field demonstration is complete and data have been evaluated, the full-scale system can be designed. The type of design required will depend on the complexity of the system, the requirements of the site owner, and the contractual relationship between the owner, designer,

constructor, and operator. Under the traditional approach, the design will typically be performed in several phases. The following are three common design phases:

1. Conceptual or preliminary design (15% design or schematic design)
2. Design Development (30% and 60% design)
3. Construction document preparation (100% design)

The design costs will depend on the complexity and type of design required, for typical civil construction projects, the design may run 6 to 20% of the total construction cost. (Simpkin et al., 1998)

4.2.6 Construction

Numerous components make up a project's construction or capital costs. These components will be project-specific. For STELA projects, they will be the multilevel sampling systems, trenching for heating elements, heating elements installation, Gas Permeable Insulation/Heat Sink (GPIHS) deploying, and general site preparation. In addition to these major costs, other indirect capital costs are typically applied as a percentage of the total of the direct costs. Indirect capital costs are as follow:

1. Mechanical/Electrical installation (20-50%)
2. General requirements (5-10%)
3. Permitting and legal fees (3-5%)
4. Services during construction (5-10%)
5. Operations and maintenance manual preparation (1-4%)
6. Start-up (2-5%)
7. Contingency (10-30%)

4.2.6.1 Trenching and Heating Elements Installation

Figure 4.1 presents the layout of the suggested design. For this example, ten trenches will be employed at the depth of 3m below the ground surface. The trenches are 10m apart from each other. Heating elements will be installed in these trenches. The trenches will be laid out in 10 lines perpendicular to the groundwater flow.

Each heating element consists of Arctic submersible heat trace (du Alaska Incorporated) wrapped around a 3 inches screen PVC pipe. To use the most conduction component of the flow, the soil would be allowed to be in direct touch with the heating elements by allowing the soil to fall on the pipes. Each heating element will be thermostatically controlled by electronic temperature controller in NEMA 4X watertight enclosure. The temperature sensor will be mounted in PVC pipe's interior. To control the real temperature outside of the pipe, screen PVC pipe will be used, so the sensor will be in direct touch with the groundwater flow. The power supply for the heating elements will be provided with the Line Power.

4.2.6.2 Deploying the Gas Permeable Insulation/Heat Sink (GPIHS) system

A layer of geo-net with the thickness of 2.54cm will be covering the site as the GPIHS system. The geo-net will be for several reasons: It is affordable, readily available, gas permeable and the black color of the material is helpful in adsorbing solar radiation

4.2.6.3 Multilevel sampling system installation

A series of monitoring wells also will be constructed on the site. For the purpose of this example 5 additional multilevel samplers are required to monitor the system performance.

Hollow stem auger drilling will be used for the excavation of the holes. Once drilling had reached 5m below the ground surface, three inch ID slotted PVC pipe will be lowered to the bottom of the bore hole. The MLSs will then be placed inside the slotted PVC pipes down the bottom of the bore hole. The area between the MLS and slotted PVC pipe will then be backfilled with the sand to act as a filter pack.

4.2.6.4 Site preparation

Site preparation for this example includes construction of gravel access roads and leveling the ground, installation of utilities to the site (i.e., electrical). Also, for different sites, construction of a temporary building (tent), and installation of temporary site facilities, including office trailers and decontamination facilities might be needed.

4.2.7 Operations, maintenance, and monitoring

Annual O&M and monitoring costs are post-construction costs necessary to ensure the ongoing effectiveness of the project. The O&M and monitoring costs components for STELA are as follows:

1. Labor
2. Temporary site facilities
3. Verification monitoring
4. Power

A contingency also is typically applied to the operations costs to cover unforeseeable additional costs. For this specific example, facilities are already existed at the site.

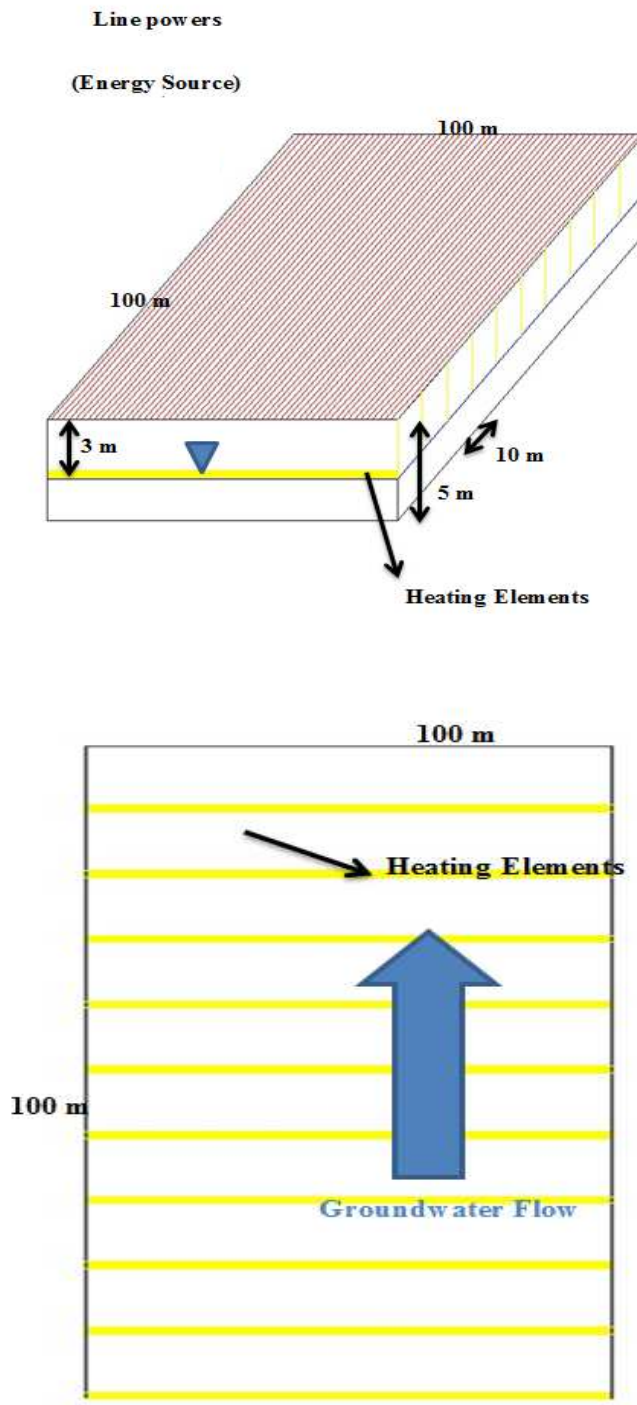


Figure 4.1: Base case design layout. Top: 3D frame. Bottom: Plan view at the water table. (3 meters below the ground surface).

4.3 Results of Cost Analysis

This section presents the results of the cost analysis. This section will help the interested parties to evaluate the applicability of the STEAL as a remedial technology, also to gain an understanding of the costs that may be encountered and the components that affect these costs. The costs presented here take into account the most significant cost components and cost reduction options. The costs were analyzed for 3 different degradation rates. Summary of the degradation rates is presented in Table 4.2.

4.3.1 Most Significant Cost Components

Determination of the most significant components of a STELA system will allow research and development efforts to be focused on reducing these costs. To assist in the evaluation of the most significant components impacting the costs of a STELA system, the costs have been summarized in Table 4.3. The table includes a column with the percentage of the total costs that each key component contributes. For the base case, the primary cost is the heating elements installation. The second significant cost is the operation costs, and the third significant cost that can be reduced is the power cost due to the line power. Figure 4.2 presents the most significant costs for this example.

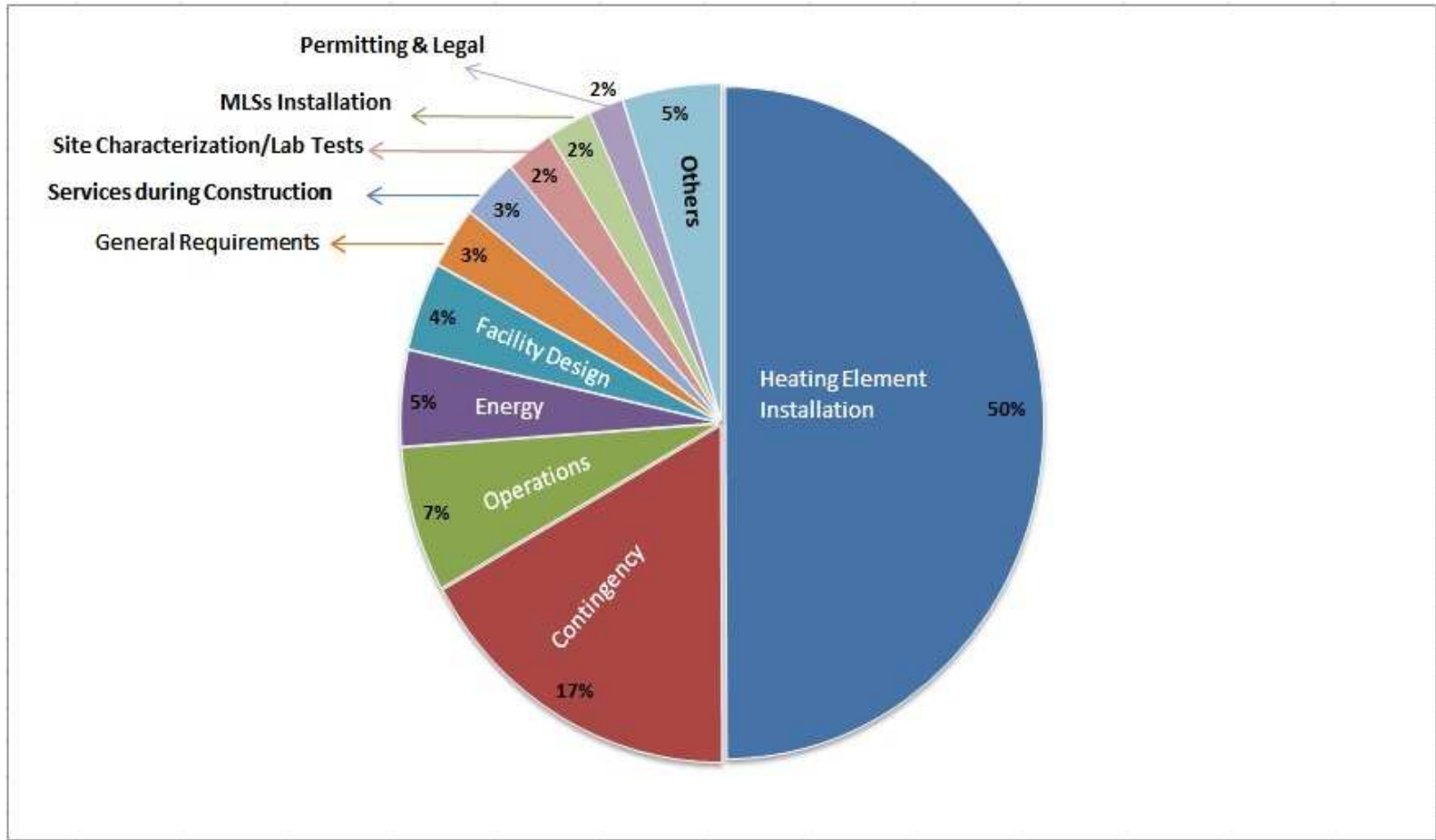


Figure 4.2: Base case most significant costs.

Table 4.2: Summary of the degradation rates at the hypothetical example site.

Description		Comments
Existing Volume of LNAPL in the Pilot (gal/acre)	50,000	Based on soil core samplings during the field demonstration.
Apparent Degradation Rate (gal/acre/yr)	5,000	Triplicate Data (McCoy 2012)- the appropriate thermal conditions exists just 1 month a year.
Degradation Rate Considering the Enhancement Factor (gal/acre/yr)	20,000	Based on Zeman's Microcosm Study (2012), the enhancement factor in degradation rate is 4.0 if the appropriate thermal conditions exist through the year.

Degradation Rate Description	Anticipated Degradation Rates (gal/acre/yr)	Time for Complete Removal (years)	
Minimum Degradation Rate	7,727	7.0	If heating system leads to 3 months of the effective season
Average Degradation Rate	10,455	5.0	If heating system leads to 5 months of the effective season
Maximum Degradation Rate	14,545	4.0	If heating system leads to 8 months of the effective season

Table 4.3: Cost analysis summary-Base Case (Case 1)

Description	Cost (\$)	Percent of Total
Additional Site Characterization and Laboratory Testing	12,625	2.4
Numerical Simulation	4,000	0.8
Field Demonstration	0	0.0
Facility Design	22,058	4.2
Subtotal	38,683	7.4
Construction		
Site Preparation	7,000	1.3
Heating Elements Installation	260,000	50.0
Installation of the Monitoring Samplers	11,750	2.3
Mechanical and Electrical Installation	0	0.0
Site Survey	1,500	0.3
General Requirements	15,213	2.9
Permitting & Legal	9,128	1.8
Services during construction	15,213	2.9
O&M Manual Preparation	3,043	0.6
Start-up	6,085	1.2
Contingency	88,233	17.0
Subtotal	441,163	80.2
Demolition	4,412	0.8
0.8		
Operations		
Labor	19,000	3.7
Site Facilities	0	0.0
Verification Monitoring	10,000	1.9
Power (Energy)	24,000	4.6
Contingency	7,250	1.4
Subtotal	36,250	11.6
Total Project Cost	520,507	100.0

4.3.2 Cost Reduction Options

From Table 4.3, it appears that the total cost of STELA could be reduced by sustaining the target temperature using more efficient heating system, and by using a more efficient energy source. Options for reducing the costs of remediation at this site were evaluated and compared

using the cost spreadsheets. The results are summarized in Table 4.4. Details on these cost-reducing options can be found in the spreadsheets in Appendix A.

The base case (Case 1) system that used for this example included ten rows of heating elements, with 10m spacing. Line power was used as the energy source. The costs for the system could be reduced by using the Photo Voltaic (PV) as the energy source instead of line power. Case 2 in Table 4.4 presents remediation costs with using the PV.

Also, to reduce the heating elements installation costs, the spacing of the trenches could be increased. To deliver the same amount of energy to the system, a GPIHS membrane must be added to the system as an insulation layer. Cost 3 in Table 4.4 shows the system that has seven rows of the heating elements, and is covered by a GPIHS membrane.

From this analysis, it is clear that reducing the cost of the energy sources by using Photo Voltaic (PV) instead of the line powers is not critical to reducing the costs of the STELA system. Thus, not only is using the PV environmentally friendly, but also it is affordable. In addition, using a GPIHS membrane as an insulation layer appears to be inefficient, although it reduces the trenching costs. As it is shown in Table 4.4, the capital cost was increased by \$45,000 to cover the cost of the additional GPIHS membrane.

Table 4.4: Summary of sensitivity analysis.

Degradation Rates	Case	Description	Capital Cost	O&M Annual Cost	Total Project Cost (Present Worth)
	1	1-hectare site-base case	464,276	209,756	674,032
Minimum Degradation Rate	2	1-hectare using Photo Voltaic (PV)	484,257	209,756	694,013
	3	1-hectare using GPIHS	510,386	209,756	720,142
Average Degradation Rate	1	1-hectare site-base case	464,276	156,944	621,220
	2	1-hectare using Photo Voltaic (PV)	484,257	156,944	641,201
	3	1-hectare using GPIHS	510,386	156,944	667,330
Maximum Degradation Rate	1	1-hectare site-base case	464,276	128,541	592,817
	2	1-hectare using Photo Voltaic (PV)	484,257	128,541	612,798
	3	1-hectare using GPIHS	510,386	128,541	638,927

4.4. Range of Cost Estimates

Because there is little available information on full-scale applications of STELA, so that estimates, rather than exact costs, must be discussed. Costs are reported per unit volume of porous medium treated, per unit of LNAPL recovered, and per unit area of site. When comparing costs between sites or between technologies, care should be taken to express costs on a similar basis.

Table 4.5 summarizes the cost estimates, normalized to common units so that the costs can be compared. The total cost ranges between \$590,000 to \$720,000 per hectare, \$11.9 to \$14.4 per cubic meter of treated soil, and \$1.3 to \$1.5 per liter of LNAPL removed depends on

the energy source, heating system and the degradation rate. The costs range, normalized to common units, can also be compared in Figure 4.3.

Table 4.5: Cost estimate summary (Unit Costs)

Degradation Rates	Case	Description	Per Area Cost		Per Volume Impacted soil		Per LNAPL Removed	
			\$/Hect	\$/Acre	\$/m ³	\$/yd ³	\$/L	\$/gal
Minimum Degradation Rate	1	1-hectare site-base case	674,032	272,888	13.5	10.3	1.4	5.5
	2	1-hectare using Photo Voltaic (PV)	694,013	280,977	13.9	10.6	1.5	5.6
	3	1-hectare with GPIHS	720,142	291,556	14.4	11.0	1.5	5.8
Average Degradation Rate	1	1-hectare site-base case	621,220	251,506	12.4	9.5	1.3	5.0
	2	1-hectare using Photo Voltaic (PV)	641,201	259,595	12.8	9.8	1.4	5.2
	3	1-hectare with GPIHS	667,330	270,174	13.3	10.2	1.4	5.4
Maximum Degradation Rate	1	1-hectare site-base case	592,817	240,007	11.9	9.1	1.3	4.8
	2	1-hectare using Photo Voltaic (PV)	612,798	248,096	12.3	9.4	1.3	5.0
	3	1-hectare with GPIHS	638,927	258,675	12.8	9.8	1.4	5.2

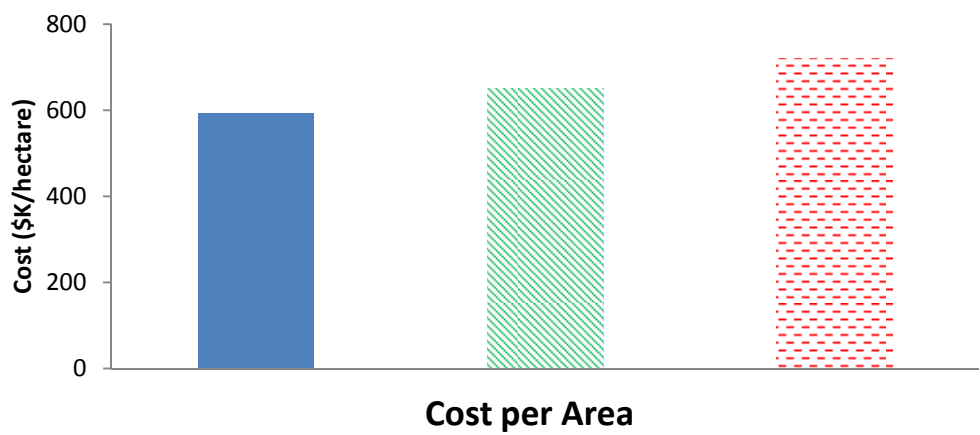
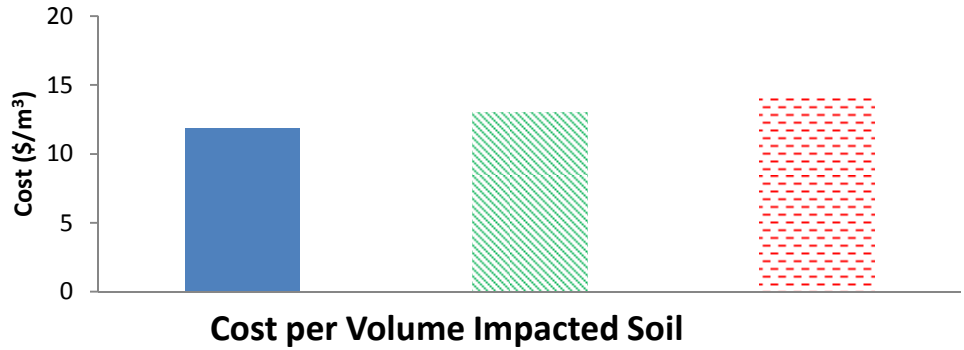
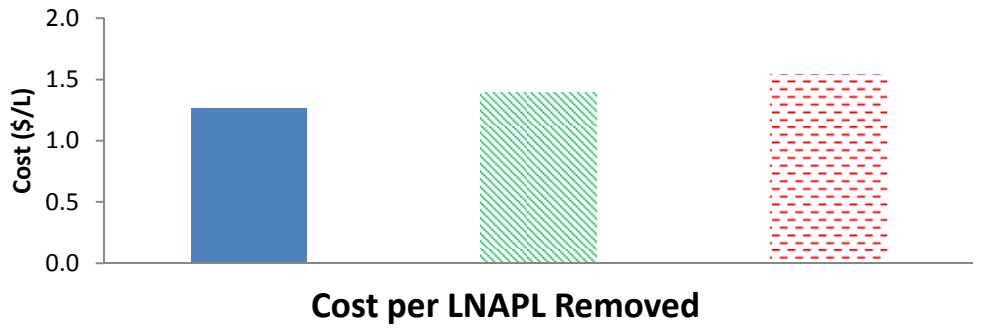
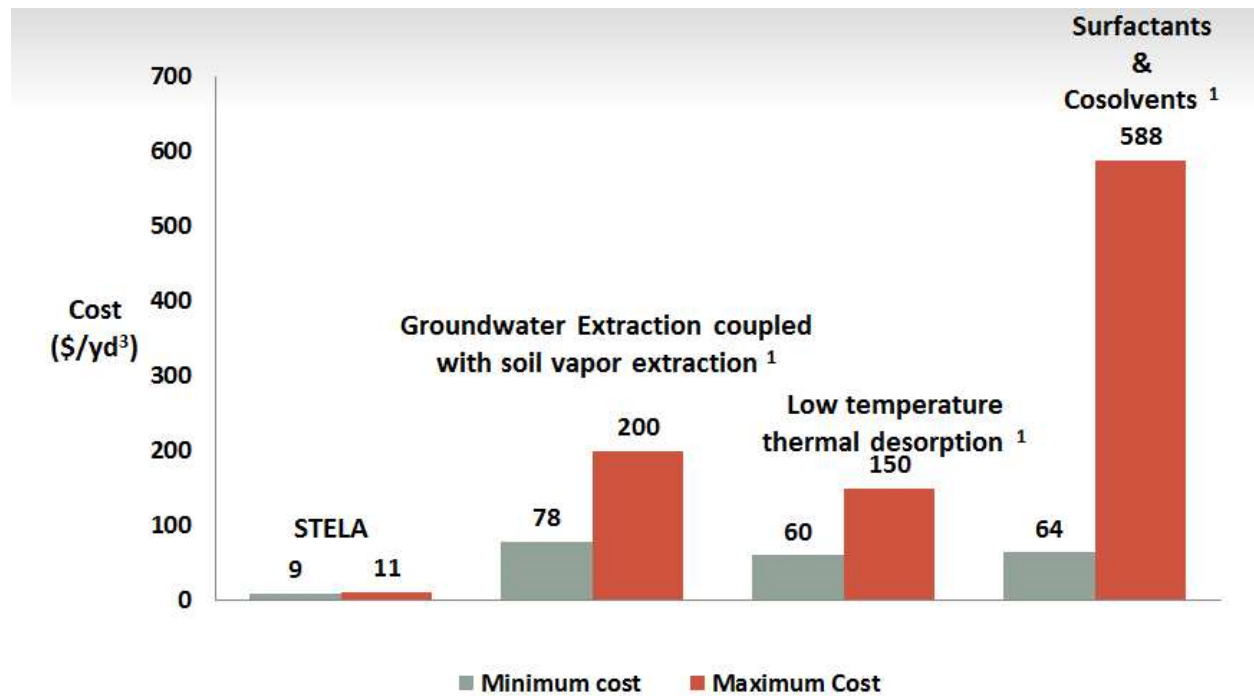


Figure 4.3: Summary of the cost normalized to volume of soil treated, volume of LNAPL removed, and area treated.

4.5 Comparison of STELA costs and other LNAPL Remedial Technologies

In summary, cost of this magnitude support the hypothesis that STELA has the potential to have cost that is lower than other common LNAPL options. For example, Simpkin et al. (1999) reported the costs of surfactants/cosolvents flushing system in the range of \$64 to \$588 per cubic yard. They, also, reported \$78 to \$200 per cubic yard and \$60 to \$150 per cubic yard for the groundwater extraction coupled with soil vapor extraction and low temperature thermal desorption, respectively. Figure 4.4 presents range of cost estimates for STELA and range of costs for the mentioned technologies.



¹Simpkin et al. 1999

Figure 4.4: Comparison of STELA and other LNAPL remedial technologies.

5. THESIS CONCLUSIONS

The primary objective of this thesis was to collect data needed to document thermal aspects of STELA including cost and performance. Moreover, by coupling MT3DMS with MODFLOW, a heat transfer model has been developed. A key value of the modeling effort is advancing methods that can be used to design full-scale systems. Lastly, a hypothetical STELA design was presented to explore the cost of a STELA system at a typical site in a former refinery.

Firstly, Data collected from December 2011 to December 2012 indicates that in the absence of heating, temperature is changing between 9°C to 21°C in the saturated zone and is in the range of 18-30°C for 40 days per year. Data collected from September 2012 to July 2013 indicates that with heating, conditions can be maintained in the target range for 60 to 200 days per year depending upon proximity to the heat source.

Minimum and maximum power inputs have been 15 kw-hr/day and 30 kw-hr/day occurring, respectively in October and May. Assuming an energy cost of 0.10 kw-hr, this equates to costs of 1.5 \$/day to 3 \$/day. An independent experiment using Geo-net layer showed that using Gas Permeable Insulation/Heat Sink (GPIHS) system has the potential to enhance the ability of the heating system to sustain temperature beneath the ground surface, and, potentially decrease the power costs. The GPIHS system prohibits the excess heat to loss through the soil surface and also adsorbs solar radiation.

Moreover, a heat transport model was developed via coupling the MODFLOW and MT3DMS to support the STELA field demonstration design. The model provides a tool to evaluate and/or design full-scale STELA systems. In addition, it addresses temporal temperature variations at grade. Also, the model pointed out the effects of the heat that generated through

degradation of LNAPL on the heat transport in the subsurface. The model suggested that the LNAPL losses at the subsurface are in the range of 5,000 to 10,000gal/acre/yr.

At 5m downgradient of the heating elements, the developed model, accurately, predicted 60 days of the effective season in 2012. Also, the simulation results anticipate that by keeping the heating system activated for three years, the effective season will increase each year. At 5m downgradient of the heating elements, model results suggested 120 days and 150 days of effective season for 2013 and 2014, respectively as compared to 60 days in the first year. The ability of the model to anticipate the effective season for the next years makes the model a useful tool to design and evaluate the future STELA systems. Taking advantage of the developed model to design a full-scale STELA field demonstration as a remedy strategy is the purpose of the future works.

Lastly, a conceptual STELA design was presented in the last chapter to explore the cost of a STELA system at a 1-hectare site in a former refinery in Wyoming. The cost analysis study indicated that the primary cost is the heating elements installation. The second significant cost is the operation costs, and the third significant cost that can be reduced is the energy source. The cost estimates normalized to common units indicated that the total cost ranges between \$590,000 to \$720,000 per hectare, \$11.9 to \$14.4 per cubic meter of treated soil, and \$1.3 to \$1.5 liter of LNAPL removed depends on the energy source, heating system and the degradation rate. Cost of this magnitude support the hypothesis that STELA has the potential to have cost that is lower than other options employed for LNAPL remediation.

6. FUTURE WORKS

Work conducted to date supports the hypothesis that STELA has the potential to be more effective, lower cost, and more sustainable than current remedies for LNAPL sites. Research directed at the evaluation and improvement of thermally enhanced for subsurface remediation is ongoing at Center for Contaminant Hydrology at Colorado State University. The next few years will likely bring with them many advancements and innovations. Listed below are several areas of investigation that will require attention:

Heating system design: the heating system that was used in STELA field demonstration is not necessarily the most efficient, environmentally friendly and cost effective method to sustain the temperature at the subsurface. Attention will require for improving methods to deliver heat to the subsurface.

In this thesis, an introductory evaluation of the impact of adding a GPIHS system as an improving component to the heating system was done. Further research needs to be conducted to analyze the long-term impacts of using the GPIHS system. Other ways to improve the heating system design is to use different shapes of the heating elements (trenches instead of the vertical elements), to change the spacing and distribution of the heating elements, and to deploy geothermal heating loops instead of the heat traces.

In addition, this thesis recommends using of the line powers as the energy source. Line powers are well known for being a clean source of energy. In current STELA field demonstration, line power was used to input electrical energy to the system. Line powers are generally less expensive than the line powers. However, the cost analysis that was done in

chapter 5 shows that using the line powers is not significantly more cost effective than the line powers.

Numerical heat transfer model: The heat transfer model that developed and presented in this thesis can be useful in anticipating the long-term performance of STELA field demonstrations and full-scale designs. This numerical model was simulated via coupling MT3DMS and MODFLOW and is applicable for the sites with the temperature variations of less than 15⁰C through the system. Using SEAWAT as the heat transport model is recommended for higher ranges of temperature variations. Also, better techniques must be used to address heat generated through reaction as a function of temperature.

Other Contaminants: In this thesis, thermally enhanced attenuation of LNAPLs was evaluated and described. Evaluation of the applicability of thermally enhanced attenuation for a variety of environmental contaminants (e.g. chlorinated solvents) is recommended.

REFERENCES

- Amos, R. T., & Mayer, K. U. (2005). Investigating the role of gas bubble formation and entrapment in contaminated aquifers: Reactive transport modelling. *Journal of contaminant hydrology*, 87(1-2), 123-154.
- Anderson, M. P. (2005). Heat as a ground water tracer. *Ground water*, 43(6), 951-968.
- Baedecker, M. J., Cozzarelli, I. M., Eganhouse, R. P., Siegel, D. I., & Bennett, P. C. (1993). Crude oil in a shallow sand and gravel aquifer—III. Biogeochemical reactions and mass balance modeling in anoxic groundwater. *Applied Geochemistry*, 8(6), 569-586.
- Baedecker, M. J., Eganhouse, R. P., Bekins, B. A., & Delin, G. N. (2011). Loss of volatile hydrocarbons from an LNAPL oil source. *Journal of contaminant hydrology*, 126(3), 140-152.
- Birkholzer, J. T., Mukhopadhyay, S., & Tsang, Y. W. (2004). Modeling seepage into heated waste emplacement tunnels in unsaturated fractured rock. *Vadose Zone Journal*, 3(3), 819-836.
- Bravo, H. R., Jiang, F., & Hunt, R. J. (2002). Using groundwater temperature data to constrain parameter estimation in a groundwater flow model of a wetland system. *Water Resources Research*, 38(8), 1153.
- Bredehoeft, J. D., & Papaopulos, I. S. (1965). Rates of vertical groundwater movement estimated from the Earth's thermal profile. *Water Resources Research*, 1(2), 325-328.
- Burow, K. R., Constantz, J., & Fujii, R. (2005). Heat as a tracer to estimate dissolved organic carbon flux from a restored wetland. *Ground Water*, 43(4), 545-556.
- Carslaw, H. S., & Jaeger, J. C. (1959). *Conduction of Heat in Solids* (paperback).

Chapman, S. W., & Parker, B. L. (2005). Plume persistence due to aquitard back diffusion following dense nonaqueous phase liquid source removal or isolation. *Water Resources Research*, 41(12), W12411.

Charbeneau, R. J., & Chiang, C. Y. (1995). Estimation of Free-Hydrocarbon Recovery from Dual-Pump Systems. *Groundwater*, 33(4), 627-634.

Cherry, J. A., Gillham, R. W., Anderson, E. G., & Johnson, P. E. (1983). Migration of contaminants in groundwater at a landfill: A case study: 2. Groundwater monitoring devices. *Journal of Hydrology*, 63(1), 31-49.

Chiasson, A. D., Rees, S. J., & Spitler, J. D. (2000). *A preliminary assessment of the effects of groundwater flow on closed-loop ground source heat pump systems*. Oklahoma State Univ., Stillwater, OK (US).

Conant, B. (2004). Delineating and quantifying ground water discharge zones using streambed temperatures. *Groundwater*, 42(2), 243-257.

Cozzarelli, I. M., Bekins, B. A., Baedecker, M. J., Aiken, G. R., Eganhouse, R. P., & Tuccillo, M. E. (2001). Progression of natural attenuation processes at a crude-oil spill site: I. Geochemical evolution of the plume. *Journal of Contaminant Hydrology*, 53(3), 369-385.

Cozzarelli, I. M., Bekins, B. A., Eganhouse, R. P., Warren, E., & Essaid, H. I. (2010). In situ measurements of volatile aromatic hydrocarbon biodegradation rates in groundwater. *Journal of contaminant hydrology*, 111(1), 48-64.

Coulon, F., Pelletier, E., Gourhant, L., & Delille, D. (2005). Effects of nutrient and temperature on degradation of petroleum hydrocarbons in contaminated sub-Antarctic soil. *Chemosphere*, 58(10), 1439-1448.

Coulon, F., McKew, B. A., Osborn, A. M., McGenity, T. J., & Timmis, K. N. (2007). Effects of temperature and biostimulation on oil-degrading microbial communities in temperate estuarine waters. *Environmental microbiology*, 9(1), 177-186.

De Marsily, G. (1986). *Quantitative hydrogeology*. Paris School of Mines, Fontainebleau.

Delille, D., Coulon, F., & Pelletier, E. (2004). Effects of temperature warming during a bioremediation study of natural and nutrient-amended hydrocarbon-contaminated sub-Antarctic soils. *Cold Regions Science and Technology*, 40(1), 61-70.

Einarson, M. D., & Cherry, J. A. (2002). A new multilevel ground water monitoring system using multichannel tubing. *Ground Water Monitoring & Remediation*, 22(4), 52-65.

Einarson, M. D. (2006). Multilevel ground-water monitoring. *Practical Handbook of Environmental Site Characterization and Ground-Water Monitoring*, 808-848.

Fels, J. B. (1999). Source-identification investigations of petroleum contaminated groundwater in the Missouri Ozarks. *Engineering geology*, 52(1), 3-13.

Ferguson, G. (2007). Heterogeneity and thermal modeling of ground water. *Ground water*, 45(4), 485-490.

Filler, D. M., & Carlson, R. F. (2000). Thermal insulation systems for bioremediation in cold regions. *Journal of cold regions engineering*, 14(3), 119-129.

- Filler, D. M., Lindstrom, J. E., Braddock, J. F., Johnson, R. A., & Nickalaski, R. (2001). Integral biopile components for successful bioremediation in the Arctic. *Cold regions science and technology*, 32(2), 143-156.
- Guilbeault, M. A., Parker, B. L., & Cherry, J. A. (2005). Mass and flux distributions from DNAPL zones in sandy aquifers. *Ground Water*, 43(1), 70-86.
- Harbaugh, A. W. (2005). *MODFLOW-2005, the US Geological Survey modular ground-water model: The ground-water flow process*. Reston, Virginia: US Geological Survey.
- Heath, R. C. (1983). *Basic ground-water hydrology* (Vol. 2220). US Geological Survey.
- Hecht-Méndez, J., Molina-Giraldo, N., Blum, P., & Bayer, P. (2010). Evaluating MT3DMS for heat transport simulation of closed geothermal systems. *Ground water*, 48(5), 741-756.
- Hillel, D. (1982). *Introduction to soil physics* (Vol. 364). New York: Academic press.
- Huntley, D., & Beckett, G. D. (2002). Persistence of LNAPL sources: Relationship between risk reduction and LNAPL recovery. *Journal of Contaminant Hydrology*, 59(1), 3-26.
- Irianni Renno, M. (2013). Biogeochemical characterization of a LNAPL body in support of STELA. (Master of Science thesis, Colorado State University)
- Johnson, P., Lundegard, P., & Liu, Z. (2006). Source Zone Natural Attenuation at Petroleum Hydrocarbon Spill Sites—I: Site-Specific Assessment Approach. *Ground Water Monitoring & Remediation*, 26(4), 82-92.
- Kamp, G. V. D., Luba, L. D., Cherry, J. A., & Maathuis, H. (1994). Field study of a long and very narrow contaminant plume. *Ground Water*, 32(6), 1008-1016.

Kim, J., & Corapcioglu, M. Y. (2003). Modeling dissolution and volatilization of LNAPL sources migrating on the groundwater table. *Journal of contaminant hydrology*, 65(1), 137-158.

Kim, J., Park, Y., & Harmon, T. C. (2005). Real-time model parameter estimation for analyzing transport in porous media. *Ground Water Monitoring & Remediation*, 25(2), 78-86.

Kipp Jr, K. L. (1997). Guide to the Revised Heat and Solute Transport Simulator: HST3D Version 2.

Langevin, C. D., Thorne, D. T., Dausman, A. M., Sukop, M. C., & Guo, W. (2008). SEAWAT version 4: A computer program for simulation of Multi-Species Solute and Heat Transport. Techniques and Methods Book 6, Chapter A22. US Department of the Interior. *US Geological Survey*.

Langevin, C. D., Dausman, A. M., & Sukop, M. C. (2010). Solute and heat transport model of the Henry and Hilleke laboratory experiment. *Ground Water*, 48(5), 757-770.

Lapham, W. W. (1989). Use of temperature profiles beneath streams to determine rates of vertical ground-water flow and vertical hydraulic conductivity. *Available from Books and Open Files Report Section USGS Box 25425, Denver, CO 80225. USGS Water-Supply Paper 2337, 1989. 35 p, 32 fig, 6 tab, 25 ref.*

Leahy, J. G., & Colwell, R. R. (1990). Microbial degradation of hydrocarbons in the environment. *Microbiological reviews*, 54(3), 305-315.

Lowe, D. F., Oubre, C. L., Ward, C. H., & Simpkin, T. J. (1999). *Surfactants and cosolvents for NAPL remediation: A technology practices manual* (Vol. 1). CRC Press LLC.

- Lundegard, P. D., & Johnson, P. C. (2006). Source zone natural attenuation at petroleum hydrocarbon spill sites—II: application to a former oil field. *Ground Water Monitoring & Remediation*, 26(4), 93-106.
- Ma, R., & Zheng, C. (2010). Effects of density and viscosity in modeling heat as a groundwater tracer. *Ground water*, 48(3), 380-389.
- MacFarlane, D. S., Cherry, J. A., Gillham, R. W., & Sudicky, E. A. (1983). Migration of contaminants in groundwater at a landfill: A case study: 1. Groundwater flow and plume delineation. *Journal of Hydrology*, 63(1), 1-29.
- Mahler, N., Sale, T., & Lyverse, M. (2012). A mass balance approach to resolving LNAPL stability. *Ground Water*, 50(6), 861-871.
- McCoy, K. M. (2012). RESOLVING NATURAL LOSSES OF LNAPL USING CO2 TRAPS (Master of Science thesis, Colorado State University).
- Margesin, R., & Schinner, F. (2001). Biodegradation and bioremediation of hydrocarbons in extreme environments. *Applied microbiology and biotechnology*, 56(5-6), 650-663.
- Mercer, J. W., & Cohen, R. M. (1990). A review of immiscible fluids in the subsurface: Properties, models, characterization and remediation. *Journal of Contaminant Hydrology*, 6(2), 107-163.
- Mohn, W. W., & Stewart, G. R. (2000). Limiting factors for hydrocarbon biodegradation at low temperature in Arctic soils. *Soil Biology and Biochemistry*, 32(8), 1161-1172.

Moriasi, D. N., Arnold, J. G., Van Liew, M. W., Bingner, R. L., Harmel, R. D., & Veith, T. L. (2007). Model evaluation guidelines for systematic quantification of accuracy in watershed simulations. *Transactions of the ASABE*, 50(3), 885-900.

Morway, E. D., Niswonger, R. G., Langevin, C. D., Bailey, R. T., & Healy, R. W. (2012). Modeling Variably Saturated Subsurface Solute Transport with MODFLOW-UZF and MT3DMS. *Ground Water*.

Mulkins-Phillips, G. J., & Stewart, J. E. (1974). Effect of environmental parameters on bacterial degradation of bunker C oil, crude oils, and hydrocarbons. *Applied microbiology*, 28(6), 915-922.

Narasimhan, T. N. (1999). Fourier's heat conduction equation: History, influence, and connections. *Reviews of Geophysics*, 37(1), 151-172.

Newell, C. J., Acree, S. D., Ross, R. R., & Scott, G. H. (2012). Light Nonaqueous Phase Liquids, EPA Technical Support Project Issue Papers.

Nielsen, D. (2006). *Practical handbook of environmental site characterization and ground-water monitoring*. CRC press.

Perfumo, A., Banat, I. M., Marchant, R., & Vezzulli, L. (2007). Thermally enhanced approaches for bioremediation of hydrocarbon-contaminated soils. *Chemosphere*, 66(1), 179-184.

Pitkin, S. E., Cherry, J. A., Ingleton, R. A., & Broholm, M. (1999). Field demonstrations using the Waterloo ground water profiler. *Ground Water Monitoring & Remediation*, 19(2), 122-131.

Pruess, K. (2004). The TOUGH codes—A family of simulation tools for multiphase flow and transport processes in permeable media. *Vadose Zone Journal*, 3(3), 738-746.

Reinhard, M., Barker, J. F., & Goodman, N. L. (1984). Occurrence and distribution of organic chemicals in two landfill leachate plumes. *Environmental science & technology*, 18(12), 953-961.

Robertson, W. D., Cherry, J. A., & Sudicky, E. A. (1991). Ground-water contamination from two small septic systems on sand aquifers. *Ground water*, 29(1), 82-92.

Ronen, D., Magaritz, M., & Levy, I. (1987). An in situ multilevel sampler for preventive monitoring and study of hydrochemical profiles in aquifers. *Ground water monitoring & remediation*, 7(4), 69-74.

Sale, T. (2003). Answers to frequently asked questions about managing risk at LNAPL sites. *Soil and Groundwater Research Bulletin*, (18).

Sethi, R., & Molfetta, A. D. (2007). Heat transport modeling in an aquifer downgradient a municipal solid waste landfill in Italy. *American Journal of Environmental Sciences*, 3(3), 106-110.

Shook, G. M. (2001). Predicting thermal breakthrough in heterogeneous media from tracer tests. *Geothermics*, 30(6), 573-589.

Simmons, C. T. (2005). Variable density groundwater flow: From current challenges to future possibilities. *Hydrogeology Journal*, 13(1), 116-119.

Simpkin, T. J. (1999). Surfactants and cosolvents for NAPL remediation: A technology practices manual (Vol. 1). D. F. Lowe, C. L. Oubre, & C. H. Ward (Eds.). CRC Press.

Stallman, R. W. (1963). Computation of ground-water velocity from temperature data. *US Geol. Surv. Water Supply Pap, 1544*, 36-46.

Thorne, D., Langevin, C. D., & Sukop, M. C. (2006). Addition of simultaneous heat and solute transport and variable fluid viscosity to SEAWAT. *Computers & geosciences, 32*(10), 1758-1768.

Vries, D. D., & Afgan, N. H. (1975). *Heat and mass transfer in the biosphere. 1. Transfer processes in the plant environment*. Scripta Book Co..

Witt, M. E., Klecka, G. M., Lutz, E. J., Ei, T. A., Grosso, N. R., & Chapelle, F. H. (2002). Natural attenuation of chlorinated solvents at Area 6, Dover Air Force Base: groundwater biogeochemistry. *Journal of contaminant hydrology, 57*(1), 61-80.

Zeman, N. R. (2012). THERMALLY ENHANCED BIOREMEDIATION OF LNAPL. (Master of Science thesis, Colorado State University)

Zheng, C., & Wang, P. P. (1999). *MT3DMS: A modular three-dimensional multispecies transport model for simulation of advection, dispersion, and chemical reactions of contaminants in groundwater systems; documentation and user's guide*. ALABAMA UNIV UNIVERSITY.

Zheng, C. (2009). Recent developments and future directions for MT3DMS and related transport codes. *Ground Water, 47*(5), 620-625.

Zheng, C., Weaver, J., & Tonkin, M. (2010). MT3DMS, a modular three-dimensional multispecies transport model—user guide to the hydrocarbon spill source (HSS) package. *Athens, Georgia: Prepared under contract to the US Environmental Protection Agency.*

Zheng, C., Hill, M. C., Cao, G., & Ma, R. (2012). MT 3 DMS: Model use, calibration, and validation. *Transactions of the ASABE*, 55(4), 1549-1559.

APPENDIX A: HYPOTHTICAL SITE COST STUDIES/ COST WORKSHEET

Description	Qty	Unit	Unit Cost	Total cost	Comments	Percent of Total	
Capital Costs							
Additional Site Characterization and Laboratory Testing							
Soil borings	0			0	Relying on the existing data	0.0	
Installation of Monitoring Wells	0			0	Use existing monitoring wells at the site	0.0	
Initial GW Testing	0			0	Use existing data	0.0	
Initial LNAPL Testing							
	Borings	25	each	250	6,250	20m centers	1.2
	Piezometers	25	each	75	1,875		0.4
	TPH Analysis	5	each	100	500	20 percent of total	0.1
Lab Tests, Work Plan, and Report	40	hr	100	4,000		0.8	
Microcosm Study	0			0	Based on Zeman (2012)	0.0	

Subtotal				12,625		
Numerical Simulation						
Model Simulations	40	hr	100	4,000		0.8
Subtotal				4,000		
Field Demonstration						
Installation of Monitoring Wells	0			0	Already conducted	0.0
Installation of Heating Elements	0			0	Already conducted	0.0
Analysis of produced fluids and gases	0			0	Already conducted	0.0
Soil Boings	0			0	Already conducted	0.0
Analysis of soils	0			0	Already conducted	0.0
Field Demonstration Labor	0			0	Already conducted	0.0
Field Demonstration Work Plan and Report	0			0	Already conducted	0.0
Subtotal				0		
Facility Design						

Design	5%			441,163	22,058	Percentage is based on total construction costs (including Gen. Requirements & Contingency)	4.2
Subtotal Construction					22,058		
Site Preparation							
Gravel Access Road and site grading	1	hectare		2,000	2,000		0.4
Temporary Building (Tent)	0				0	A building already exists	0.0
Utilities Installation							0.0
Electricity	1	hectare		5,000	5,000		1.0
Heating Elements Installation							
Trenching	1000	m		100	100,000		19.2
Heat traces	1000	m		150	150,000		28.8
Wrapping the Heat Traces	1000	m		10	10,000	hose, wrapping	1.9
Backfilling the trenches	0				0	covered by installation	0.0

Energy Source	Thermostats	0			0	Covered by heat trace	0.0
	Line powers	2000 0	w	1	20,000	Power based on pilot, in the pilot it is 200w/m. Line power costs is 1\$/w	3.8
	Wirings	1	lump sum	4,000	4,000		0.8
	Batteries	0			0	direct use of power as it produces	0.0
	Energy Control System	0			0	direct use of power as it produces	0.0
Installation of the Monitoring Samplers	MLS	5	each	2,000	10,000		1.9
	Data Loggers	5	each	100	500		0.1
	Drilling the wells	5	each	250	1,250		0.2
Mechanical and Electrical Installation	0			0	covered above	0.0	
Site Survey	1	day	1,500	1,500		0.3	
Subtotal					304,250		
General Requirements	5%			304,250	15,213		2.9
Permitting & Legal	3%			304,250	9,128		1.8

				50		
Services during construction	5%		304,250	15,213		2.9
O&M Manual Preparation	1%		304,250	3,043		0.6
Start-up	2%		304,250	6,085		1.2
Subtotal				352,930		
Contingency	25%		352,930	88,233		17.0
Total -Construction Capital Costs				441,163		
Demolition	1.0%		441,163	4,412		0.8
Salvage Value	0			0		0.0

Annual Operations/Maintenance and Monitoring Costs

Labor						
Operators	200	hr	45	9,000	1 operator, 4hr a week	1.7
Maintenance Technician	0			0	covered by the operator	0.0
Engineer	100	hr	100	10,000	1 engineer, 2hr a week	1.9
Temporary Site Facilities						
Office Trailer	0			0	Using existing facilities	0.0

Portable Toilet	0		0	Using existing facilities	0.0
Decontamination Facilities	0		0	Using existing facilities	0.0
Maintenance Materials	0		0		0.0
Verification Monitoring	1	lump sum	10,000		1.9
Subtotal			29,000		
Contingency	2		29,000		
	5		0	7,250	1.4
	%				
Total-Annual Operations/Maintenance and Monitoring Costs				36,250	
Total-Operations/Maintenance and Monitoring Costs	1	yr	36,250	36,250	
			0		
Total Cost				520,507	100.0